Neural circuits dynamics underlying Fourier motion detection and the alternation in perceptive visual states in the zebrafish larva

Auriane Duchemin

Sorbonne Université

Ecole doctorale Cerveau-Cognition-Comportement

Institut de Biologie de l'Ecole Normale Supérieure

Neural circuits dynamics underlying Fourier motion detection and the alternation of perceptive visual states in the zebrafish larva

Par **Auriane Duchemin**

Thèse de doctorat de Neurosciences

Dirigée par **Germán Sumbre**

Présentée et soutenue publiquement le 07 février 2022

Devant un jury composé de :

Melody Ying-Yu HUANG, University Hospital Zürich	Rapportrice
Michael ORGER, Champalimaud Center for the Unknown, Lisbon	Rapporteur
Aristides ARRENBERG, Universität Tübingen	Examinateur
Georges DEBREGEAS, Sorbonne Université	Examinateur
Elim HONG, Sorbonne Université	Examinatrice
Germán SUMBRE, Institut de Biologie de l'ENS	Directeur de thèse

Abstract

In the presence of moving visual stimuli, the majority of animals follow the Fourier motion energy (luminance), independently of other stimulus features (edges, contrast, etc). While the behavioral response to Fourier motion has been studied in the past, how Fourier motion is represented and processed by sensory brain areas remains elusive. During the first part of my PhD, I investigated how visual moving stimuli with or without the first Fourier component (square-wave signal or missing fundamental signal) are represented in the main visual regions of the zebrafish brain.

Usually these moving visual stimuli are non-ambiguous, resulting in just one correct interpretation of the stimulus. However, manipulation of the power of the first Fourier component can in theory generate two potential motion percepts (motion to the left or to the right). This leads to a behavioral alternation between two opposite behavioral outputs. For the second part of my work I studied the circuit processes and mechanisms underlying the alternation between these behavioral states.

For the first part, I monitored the larva's optokinetic response (OKR) induced by square-wave and missing-fundamental signals. Then, I used two-photon microscopy and GCaMP6f transgenic zebrafish larvae to monitor neuronal circuit dynamics in the optic tectum and the pretectum (the two main visual centers in teleost fish) in response to the different visual stimuli. I observed that both the optic tectum and the pretectum circuits responded to the square-wave gratings. However, only the pretectum responded specifically to the direction of the missing-fundamental signal. In addition, a group of neurons in the pretectum responded to the direction of the behavioral output (OKR), independently of the type of stimulus presented. These results suggest that the optic tectum responds to the different features of the stimulus (e.g. contrast, spatial frequency, direction, etc.), but does not respond to the direction of motion if the motion information contained in the stimulus is not coherent (e.g. the luminance moving in one direction and the second-order components like edges and contrast moving in the opposite direction). On the other hand, the pretectum mainly responds to the motion of the stimulus based on the Fourier energy.

For the second part of my PhD, I modified the square-wave stimulus to create an ambiguous motion stimulus: a square-wave stimulus with attenuated fundamental frequency. This stimulus displayed ambiguous Fourier energy direction of motion. I tested different percentages for the fundamental frequency and discovered that with 10% of the fundamental frequency left in the stimulus, the larvae showed alternations between the two behavioral states (periods of successive eye pursuits vs. periods of spontaneous eye rotations). These results suggest that during the presentation of this ambiguous stimulus the larvae alternate between periods of perceptive and non-perceptive states. I then studied the neural basis of these alternation of behavioral states. Using whole-brain Ca^{2+}

imaging I obtained preliminary results showing particular neuronal assemblies capable of decoding the alternations between behavioral states. The best assemblies displayed a few mistakes during the decoding, that were different between assemblies, suggesting that each assembly was encoding a different information. The circuit and the successive activation of multiple assemblies thus seem to create the alternation rather than a single assembly. Moreover, the specificity of the decoder to determine the upcoming switch was very good, therefore there seems to be some information in the neural activity that is specific to this alternation. Principal components analysis also suggests that the average activity of the assemblies around the switches is not the main information extracted by the decoder, but rather that it uses the activity of subgroups of neurons inside the assemblies. This work is a first step to shed light on the mechanisms by which several brain states can alternate with each other to bias sensory perception.

Acknowledgements

First of all, I would like to thank Germán for having taken me in the lab, for having been available and helpful whenever I needed, and for letting me explain science to kids from time to time. Also, many many thanks to the best team in the universe: Martin, Ale, Faadil, Emi, Diego, Virginie, Sarah, Chiara, Enrique, Ehud, as well as Astou and past members Ruggero, Thomas, Adrien, Jonathan and Ani. I am very grateful for having done my PhD with such great people. I won't forget either the SPIBENS team, with which I learned a lot and had awesome moments, thank you all!

En dehors du labo, je souhaiterais remercier toustes les copaines qui ont partagé ces 5 dernières années avec moi, en particulier Chloé, Célestine, Papours, Charlie, Béber, Talbot, Nop, Laeti, Tatouille et Camille (Eksta <3), ainsi que les bios avec qui j'ai hâte de repartir en weekend, et la team d'Ici c'est Paris qui a rendu l'année 2021 géniale malgré les confinements et autres joyeusetés du moment.

Enfin, merci à ma famille d'être toujours là, toujours géniale, et merci à Rémy d'être tous les jours à mes cotés, de ne jamais douter de moi même quand ça m'arrive et d'améliorer tous les petits moments du quotidien.

My PhD would not have been the same without you all!

(I also thank Pink Floyd and The Alan Parsons Project for helping me writing the manuscript.)

Contents

List of Figures

Nomenclature

dpf	days post-fertilization
F1	fundamental frequency of the Fourier signal
hpf	hours post-fertilization
MAE	Motion aftereffect
OKR	Optokinetic Response
OMR	Optomotor Response
PC	Principal Component
PCA	Principal Component Analysis
ROI	Region of interest
SPIM	Selective Plane Illumination Microscopy

1

Introduction

Contact with the external world relies on sensory receptors which transmit information to the brain. The brain then needs to process it, extract the most relevant information and generate the adequate motor behaviors. This integration of the sensory information can be modulated by the brain's internal state. Thus, perception does not necessarily represents the physical properties of the detected objects but an interpretation of it that the brain is constantly updating. This is evident when perceiving optical illusions. These illusions arise from adaptive properties considered as side effects of certain brain computations, and therefore are useful tools for neuroscience and cognitive researchers to elucidate the mechanisms underlying perception. The optical illusions have been studied since the early nineteenth century, and can be defined as errors in perception: when the perception of stimuli deviates from their physical characteristics [Wade, 2018]. In some cases, sensory illusions can occur in the absence of errors. For example, when sensory information is ambiguous, leading to two or more correct interpretations of the same stimulus. This phenomenon is called bistability (or multistability in the case of more than two interpretations).

The perceptual bistability emerges due to the impossibility of the brain to process simultaneously the different percepts of an ambiguous figure. Therefore, just one of the percepts can be consciously perceived at a given time. These percepts will compete between each other generating unstable perception and resulting in spontaneous switches

between the different percepts. How and why these switches in perception appear still remains elusive. For my thesis, I tried to shed light on the mechanisms underlying these alternations in perception, using the zebrafish model.

In this introduction, I will first explain briefly general principles about visual perception, including historical studies and motion perception, and more specifically the spontaneous alternations in perception in humans and other animal species. I will then describe the zebrafish model, argue why it provides numerous advantages for the study, and go into more details about what is already known about visual processing and visuomotor behavior of the larva.

1.1 Visual perception

Vision is the perception of the external world from light radiation that reaches the eye. However, this raw information needs to be processed by the brain to recognize objects, analyze situations and react in the appropriate manner. The internal states of the brain can influence the sensory perception. For example concentration: when the mind is focused on a certain task, we can be completely blind to other stimuli, that in other circumstances we would have seen. The eyes will get the light information but the brain will dismiss it as not necessary for the task we are doing and thus the information will never be perceived in a conscious manner. This phenomenon of inattentional blindness has been shown notably by Simons and Chabris in 1999 in a experiment where viewers were asked to count the number of basketball passes between people in a team. In the middle of the video, a person wearing a gorilla costume was crossing the frame, and about half of the viewers did not see it, because they were too focused on the counting [Simons and Chabris, 1999]. Other examples of internal states that can alter the perception are stress, hunger, lack of sleep, etc.

The first written essays about visual perception were elaborated by Aristotle more than 2300 years ago. Aristotle proposed that the eye would take the form of the object and send a 'percept', i.e. an impression, via the blood vessels to the sensus communis, located in the heart. According to his theory, the sensus communis is then the one that discriminates between the different percepts and interprets them [Aristotle, 1984]. In 1604, Johannes Kepler provided the first theory of the retinal image. He applied the laws of light refraction that were known at the time and showed that the path of light in the eye ends as an inverted image on the retina. In the late 19th century, Hermann Munk proved that damages to the occipital cortex in monkeys was associated with blindness. None of them had access to the activity of the brain, and it is only in recent years that it

became technically possible to investigate experimentally the neurobiological mechanisms underlying visual perception.

A large part of the studies to understand visual perception has then focused on stimulation and recordings of the induced neuronal responses. For example, Ungerleider and Mishkin in 1983 developed their famous theory of two distinct streams (ventral and dorsal) in the primate cortical visual system, using a mixture of behavioral, anatomical and electrophysiological techniques [Mishkin et al., 1983]. According to their model, starting from the primary visual cortex in the occipital lobe, there is a ventral pathway that is involved in object recognition and a separated dorsal pathway for the spatial location of the same object.

As it emanates from Mishkin's work and other studies, the brain's visual system is functionally specialised: different networks control different aspects of vision (color, movement, location, etc). Perception thus involves the activation of neuronal networks that break up the physical properties of the visual scene to later on reintegrate all the information pieces into a unified conscious visual percept. The ability to study neuronal activity at the whole-brain level, or at least entire regions at a time, with single-cell resolution, is therefore necessary to study the network mechanisms underlying visual perception.

An alternative and singular approach for studying visual perception has been the use of visual illusions. Visual illusions can induce perception in the absence of a physical external stimulus. It thus allows for the dissociation between neural activity associated with sensory detection from that associated with sensory perception. An example of such illusions is the Checkershadow illusion, published by Edward H. Adelson in 1995 (see Figure 1.1) [Adelson, 1995].

This illusion displays a checker board with light gray and dark gray squares, with an object on top that is creating a shadow that darkens some part of the board. The squares

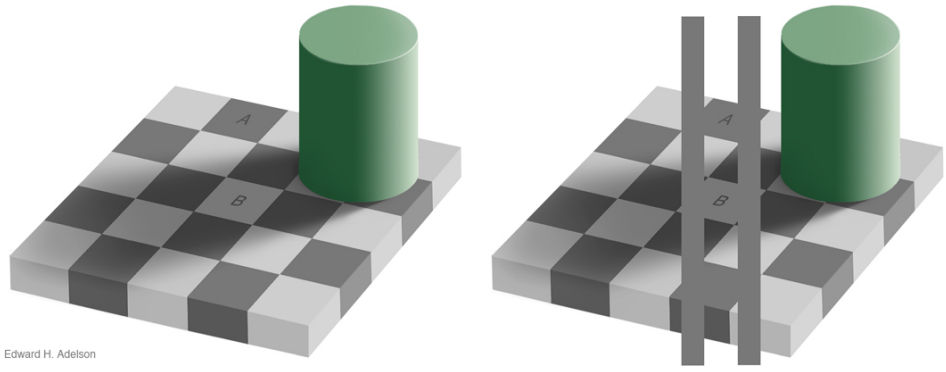

Figure 1.1: **The Checkershadow illusion.** The left panel is the illusion as it was published in 1995 by Edward H. Adelson. The squares marked as A and B are the exact same color, as can be seen on the right panel. Image retrieved from http://persci.mit.edu/gallery/checkershadow

marked with A and B are of the exact same shade of gray, but we are totally unable to see it. Here, the physical characteristics of the squares differ from the perception we get from them, and it helps us understand the mechanisms used by the brain. There are two types of explanation for this illusion. First, the brain tends to enhance contrast. Thus, as the "light gray" B square is surrounded by darker squares, we see it lighter than the "dark gray" A square that is surrounded by light squares. The second explanation is that there is top-down assumptions that play a role, because the brain is primed to recognize a checker board as an alternation of black and white squares so it will enhance this perception. The brain is also primed to interpret the shadow in the image, thus making the shade of square B appear brighter than it physically is. The relative shade of gray rather than the absolute brightness is important for the interpretation of the image, and that is indeed what the brain enhances.

1.1.1 Motion perception

Motion perception is the process of inferring the direction and speed of an object based on visual inputs. In the retina, there is already a local computation of directionality. In mammals, this information is then sent by several retinal ganglion cells (RGCs) to the primary visual cortex V1 via the lateral geniculate nucleus (LGN) of the thalamus (thalamocortical pathway). The RGCs also send the directionality information to the superior colliculus in mammals, or the optic tectum (homologous to the superior colliculus) in non-mammalian vertebrates (subcortical pathway). In V1, the majority of cells are direction selective and/or orientation selective, which means that the neurons will typically respond to a pattern with an edge in a certain orientation moving in a particular direction. From V1, neurons project to two primary pathways (corresponding to the ventral and dorsal streams of Ungerleider and Mishkin [Mishkin et al., 1983]). Projections to the temporal cortex contribute to the recognition of objects and projections to the parietal cortex process visual motion. More precisely, direction-selective neurons from V1 project to the middle temporal (MT or V5) region and from there to the MST area (middle superior temporal cortex). The majority of the cells in these two areas are also direction selective, but with larger receptive fields than those observed in primary visual areas [Grzywacz and Merwine, 2003].

All along this main motion processing pathway there is cross-talk with other subcortical and cortical areas, to take into account the context in which a stimulus was presented. For example, the analysis of the scene is not the same if an individual is moving through an environment or if the environment moves around a static individual, even though the information arriving at its eyes can look very similar. The information from the muscular, vestibular, and other proprioreceptive systems and efferent copies is

integrated with the motion information in the brain to produce coherent behavior and perception.

Although in mammals the retino-thalamic pathway represents the main visual route, the retina also projects to other brain regions. For example, in the case of Milena Canning, who suffered from strokes that destroyed her occipital cortex, losing the visual cortex left her clinically blind. However, after some time, she realized that she was still able to perceive consciously the moving objects, even if she didn't see anything else around. The research team that studied her case showed that even though her primary visual cortex has been seriously damaged, her MT area was preserved, and some pathways must therefore exists between her retina and MT area without going through V1 [Arcaro et al., 2019].

In addition to this cortical pathway, the retina also projects to the superior colliculus and the pulvinar nucleus. Azzopardi and Hock [Azzopardi and Hock, 2011] argue that the retinogeniculate pathway through V1 is involved mostly for feature-based motion detection, and that this retinocollicular pathway is more involved in detecting motion energy. In this paper, they studied blindsight patients that have an impaired retinogeniculate pathway in one hemisphere but an intact retinocollicular pathway (in the same hemisphere). The intact retinocollicular pathway allowed them to still unconsciously discriminate motion direction in their blind hemifield. They used an adaptation of an illusion called the reverse-phi motion (see next paragraph), that allowed them to cue two opposite directions at the same time, either from the motion energy or from the change in stimulus shape. The patients chose the shape direction when it was presented to their intact visual field and the motion energy direction when presented to their blind field.

Phi and reverse-phi motion

The phi motion consists of the sequential appearance of the same image at neighboring spatial positions: even without a continuous movement of the image we perceive a movement in the direction of the new image. The reverse-phi consists also of sequential images of close spatial location, but the contrast of the images is reversed between each frame [Anstis, 1970]. The contrast-reversal introduces Fourier components (i.e. motion energy) that move in the reverse direction. In this case the direction of motion appears to be reversed. The reverse-phi motion phenomenon has been shown to elicit this effect also in primates [Krekelberg and Albright, 2005], in drosophila [Tuthill et al., 2011] and in zebrafish [Orger et al., 2000]. We can note that these last two species do not have a cortex, so this proves that the cortical pathway is not necessary for this illusion to be perceived.

Fourier motion

Several studies have shown that visual apparent motion mainly follows the Fourier components of the stimulus. When a pure square wave is decomposed into its Fourier components only the odd harmonics emerge: the fundamental and the third, fifth, seventh, etc. harmonics, such that they have respectively amplitudes of one-third, one-fifth, one-seventh, etc. of the amplitude of the fundamental frequency. Similar as using the reverse-phi, it is possible to create a stimulus that has a Fourier motion energy going in opposite direction to the other features (contrast, edges, textures, etc.): the missing-fundamental stimulus (sometimes called fluted-square-wave), that is a square-wave with its fundamental frequency subtracted (see Figure 1.2) [Adelson and Bergen, 1985, Chen et al., 2005].

When creating a movement by shifting the frames by a quarter-wavelength steps (compared to the original square wave), the third harmonic moves forwards by three-quarters of its own wavelength, in other words it appears to move backwards by one-quarter of its wavelength (see Figure 1.3 for a visual explanation). As the third harmonic is also the strongest Fourier component in the missing-fundamental stimulus, the latter should appear to move backwards as well, even though the rest of the features move forwards, if the visual apparent motion is processed using the Fourier components. It is

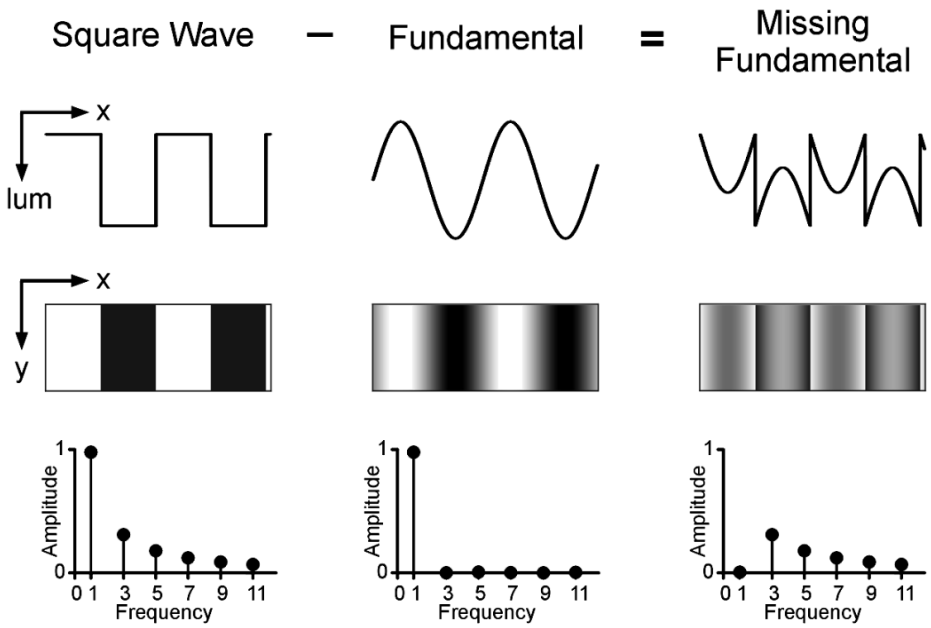

Figure 1.2: **Missing fundamental stimulus.** The missing fundamental stimulus (third column) corresponds to the fundamental (second column) being subtracted from the square wave (first column). **(First Row)** Plot of the luminance as a function of spatial position. **(Second Row)** Visual appearance of the three stimuli. **(Third Row)** Amplitude of the harmonics that can be found in each stimulus, corresponding to their Fourier spectrum. From [Chen et al., 2005].

indeed the case, at least for the very first moments of perception in humans. This was tested by Chen *et al.* and Sheliga *et al.* using the initial ocular following responses in humans [Chen et al., 2005, Sheliga et al., 2005]. The effect is also present in monkeys [Miura et al., 2006] and in mice [Sugita et al., 2012]. In zebrafish, the effect is not limited to the initial ocular following responses: when the missing-fundamental stimulus is presented to larvae, they constantly follow the direction of the Fourier energy and not the one of the other features [Orger et al., 2000]. More information on zebrafish visual perception can be found in section 1.2.2.

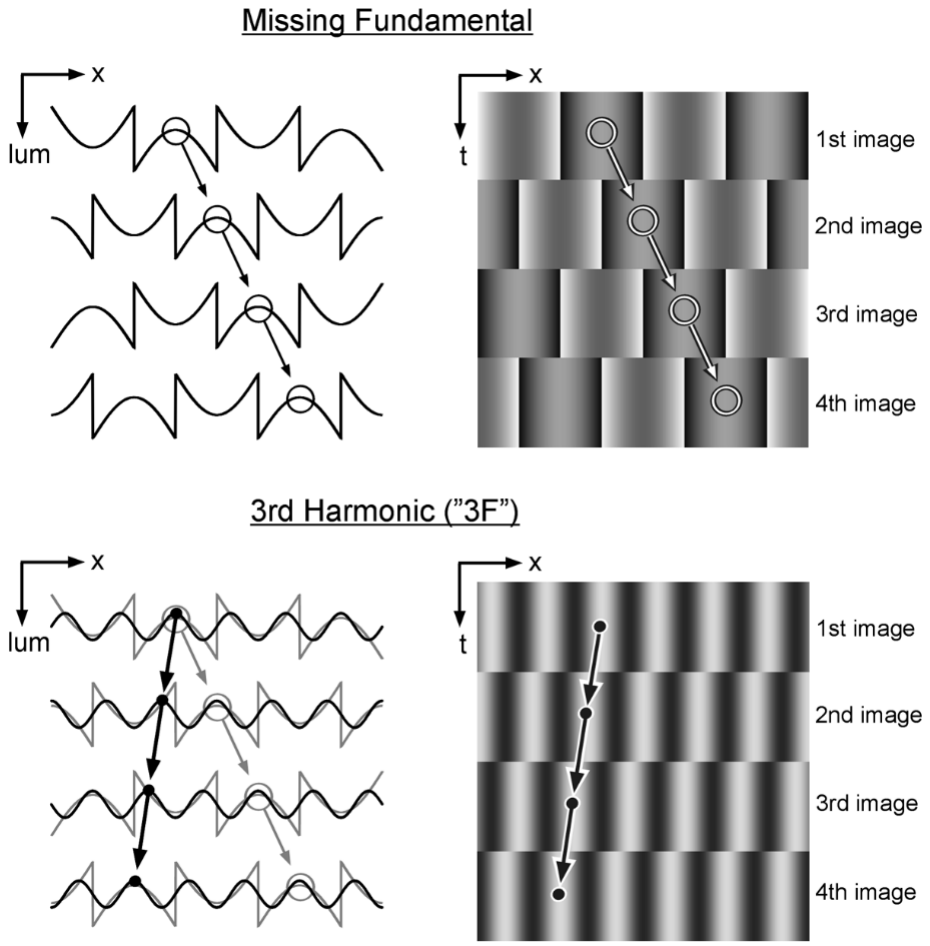

Figure 1.3: **Opposite apparent motion for the missing fundamental stimulus. (Top)** From top to bottom, 4 successive time frames shifted to the right by one-quarter wavelength for the missing fundamental stimulus (circles and arrows). The plot on the left shows the luminance profile , with the circles and arrows showing the same point in the profile across time, moving to the right. The plot on the right displays the visual appearance of the 4 time points. **(Bottom)** Same plots, but for the 3rd harmonic alone. Between each frame the profile steps three-quarters of its wavelength to the right, which cannot be distinguished from one-quarter of its wavelength to the left, as shown by the black dots and arrows. Our brain assumes that the nearest image makes more sense, so we perceive this motion to the left. From [Chen et al., 2005].

1.1.2 Perceptual switches and visual bistability

The human brain is capable of perceiving only a single percept of a given stimulus at a given moment. This property does not affect perception, as most of the objects have a single interpretation. However, some objects are ambiguous, leading to more than a single interpretation, and visual bistability.

Historical facts

Ambiguous figures have been known for a long time and a lot have been created. Some examples are shown in Figure 1.4. The majority of the references from this section can be found in the book "The Oxford Compendium of visual illusions" [Shapiro and Todorovic, 2017].

There is evidence found in Pompeii that already two thousand years ago some mosaic or tiles patterns of cubes that can change visual perception, giving the impression of depth, were used as floor decoration (Figure 1.4.A). But the phenomenon started to be studied in the psychological domain during the 19th century, with for example Louis Albert Necker that published his "diagram of a reversing rhomboid" (today known as the Necker cube, see Figure 1.4.B) in 1832, after having observed perceptual reversals in engravings of crystals. In the Necker cube we do not know which face of the cube is in front, and thus the cube can be perceived as seen from above or from below. It is interesting to note that we always immediately perceive the cube as a 3D image and to really perceive just the 2D drawing (some square, triangles and trapezoids) is a very hard task. A lot of studies were also made by Edgar Rubin, notably with his vase and faces illusion (1915, Figure 1.4.C) where we don't know what is the background and what is the object, so there is a figure-ground alternation in perception. In this first three examples, the ambiguities are dependent on the lost dimension of the pictures' depth, that creates uncertainty and fluctuation in apparent depth.

Other ambiguities can arise just from the drawing, when there is not enough details for the viewer to choose from the two possible interpretations. That is the case for example in the Duck/Rabbit ambiguous figure (Figure 1.4.D), as well as the young/old woman (Figure 1.4.E). The first author of the duck-rabbit image is not known: it was published in a German magazine (the Fliegender Blätter) in October 1892. It was then reproduced and discussed by Jastrow in 1900, thanks to whom it became more widely known. For the young-old woman image, the oldest drawing has been found as a 1888 German postcard. It was then simplified by Hill in 1915 that published it under the title "My Wife and My Mother-in-Law". This version of the image was popularized in research by Edwin Boring in 1930.

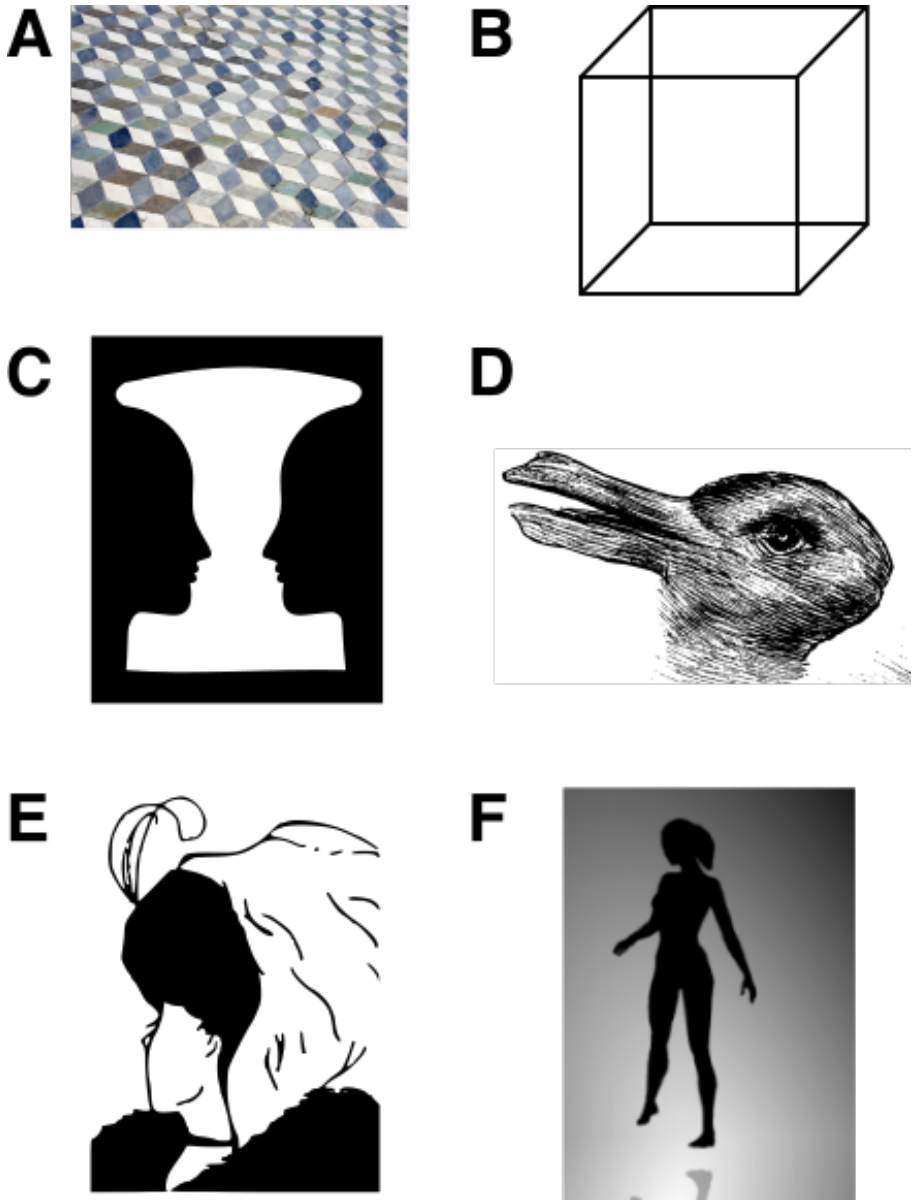

Figure 1.4: **Visual bistability examples.** Here are six different examples of visually ambiguous figures. **(A)** A tiled floor from Pompeii, where the cubes can be seen alternatively hollow or protruding from the ground. **(B)** The Necker Cube, which can be seen from above or from below. **(C)** An example of Rubin's vase-faces, if we see the background in white we perceive two faces, and when the background is black we see a vase. **(D)** The Duck/Rabbit figure, with the rabbit looking to the right and the duck looking to the left. **(E)** The young/old woman figure, where the nose of the old woman corresponds to the chin of the young one. **(F)** The Kayahara dancing silhouette, when the silhouette spins we perceive it alternatively turning clockwise or counterclockwise.

The ambiguity can also happen in moving objects, as the Kayahara Silhouette illusion proves (2003, Figure 1.4.F). This illusion is a spinning image of a woman, where we see only the silhouette of the woman without any indication of the depth. Thus if someone perceive that she has the right leg towards the viewer, someone else can perceive that this leg is the left leg and is going away from the viewer. Depending on this perception,

when the silhouette turns, we can perceive it as turning clockwise or counterclockwise, generating a switch in the perception (switching from one percept to the other). This ambiguous stimulus belongs to the class of depth-ambiguous reversible figures, and the effect is amplified by the spinning movement.

A last class of perceptual switch is the binocular rivalry. Sir Charles Wheatstone was the first in 1832 to study this phenomenon using his newly invented stereoscope for stimulating independently the two eyes. This is indeed the basis of the binocular rivalry: having two completely different images coming to the two eyes. If the two images cannot be combined by the brain to recreate a meaningful scene, human perception will focus and perceive one of the two images, completely ignoring the other one. At one point (usually a few seconds) it will switch to the other one and the perception will then pop back and forth between the two images.

The perceptual switches coming from all these ambiguous figures have been studied in humans, have been modeled, and there are even some studies in animal models.

Studies in humans

Using fMRI, EEG or MEG techniques, it has been shown that many different regions in the human brain were associated with the perceptual reversals during visual bistability (for a review see [Martínez and Parra, 2018]). The frontal and parietal cortices are involved in solving the ambiguity and defining and stabilizing the percept. For the perceptual stabilization, another area that seems to play an important role is the intraparietal sulcus, while the upper parietal lobes are involved in the regulation between alternation and stabilization processes. The regions involved in the switch between percepts also depend on the type of ambiguity present in the stimulus. It has been shown for example that the right fusiform gyrus is involved for the figure-ground reversals (like Rubin's vase-faces for example) but not really for the other types of ambiguous images. For the bistable images where the reversals change their meaning (like the duck-rabbit or the young-old woman), the areas of the ventral stream are the most involved, which makes sense as they are the regions that process the recognition of objects. Finally, for the ambiguities linked with perspective or movement (like the Necker cube or Kayahara's dancing silhouette) the regions concerned are the visual areas related to movement and the extrastriate visual cortex.

The generic theoretical model to explain visual bistability consists of two neural populations representing the two alternating percepts (see Figure 1.5). These antagonist populations are activated by the sensory inputs and are connected by mutual inhibition. The population that is the most active "wins" (in a winner-takes-all fashion) and is the only one highly active while the other is suppressed. The winning population will then

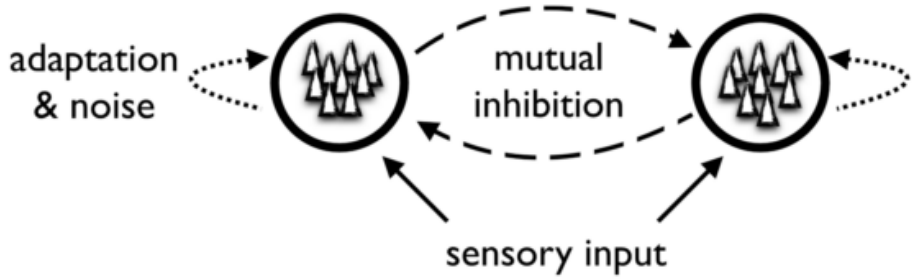

Figure 1.5: **Generic model of bistability.** Two stimulus-sensitive populations mutually inhibiting each other compete for being the active one. Noise and adaptation stochastically lead to an alternation between the two populations. From [Scocchia et al., 2014]

undergo adaptation, the neuronal fatigue being due either to slow after-hyperpolarizing currents or to short-term depression of excitatory synaptic connections [Scocchia et al., 2014]. At some point, the adaptation process and the noise that is present from the rest of the brain will add up to the second population taking over the first.

We can understand and adapt this model for two strategies: the bottom-up approach where the majority of the switching process is due to stimulus-selective neural populations in visual cortex and endogenous brain dynamics, that slow down or speed up the adaptation process ; or the top-down approach that goes with the idea that the general brain state (attention, prior knowledge, state of mind, etc) will be the "command" (the noise added to the model), initiated by brain areas that integrate sensory and non-sensory information to coordinate a diversity of behaviors, and will effectively be the major cause of reversals.

Going with the bottom-up strategy, van Loon *et al.* showed that higher concentrations of GABA in the visual cortex induces slower perceptual dynamics (less switches and longer periods of stabilization), and they obtained the same result by administrating lorazepam, a benzodiazepine that enhances the action of GABA-A receptors in the brain [Van Loon et al., 2013]. It was also shown that some neuronal activity in the primary visual cortex correlates with the perceptual state of observers [Polonsky et al., 2000].

On the other hand, several studies suggest that top-down mechanisms influence the perceptual switching rate. Indeed, it has been shown that both stable (clinical condition, genetics, prior knowledge, etc) and transient (attentional or emotional state, voluntary control, etc) states of the individual have a role in the perceptual switching dynamics [Scocchia et al., 2014]. Clinical conditions such as bipolar disorder, obsessive-compulsive disorder, major depression and schizophrenia has been shown to alter the perceptual reversal rates, at least during binocular rivalry [Ye et al., 2019]. In autism spectrum disorder patients [Intaitė et al., 2019] and aging adults with no particular clinical condition [Kondo and Kochiyama, 2018], the dynamics are also altered. The effect of top-down

prior or context information is also evident for meaningful-content ambiguous images (like the duck-rabbit). For example, if the image moves from left to right, the perception will mostly be of the object that is facing to the right (and vice-versa) [Bernstein and Cooper, 1997]. Voluntary control of the perceptual switch has been shown to affect more the binocular rivalry than the other types of ambiguities [Dieter et al., 2016], and in those it has more effect on meaning-content images than perspective reversals [Scocchia et al., 2014].

Overall, both bottom-up ("low-level") and top-down ("high-level") processes seem to work together, as was reviewed by Sterzer *et al.* [Sterzer et al., 2009], the high-level being actively involved in interpreting the sensory inputs, but without the low-level they would not have enough information to do so. Moreno-Bote *et al.* developed a model in which the noise is necessary for the switches to occur [Moreno-Bote et al., 2007].

Studies in animal models

External recording techniques, such as fMRI or EEG, are the only ones accessible to study the brain activity of humans. They are very useful and can lead to discoveries about general regions of the brain, but it is impossible to have a very precise spatial location. The use of animal models allows the use of electrophysiology techniques with single-cell resolution and direct voltage measurements.

The studies on visual bistability that were made on animal models were done mostly on monkeys. Researchers used structure-from-motion cylinders: dots in the shape of a 3D cylinder that move coherently to give the impression of a rotating cylinder, and as there is no information on depth, both directions of motion are equally probable. Using this approach, it was shown that MT neurons contributed to the perceptual choice [Dodd et al., 2001], and that there are also inter-neuronal correlations at longer time scales that indicates top-down influences on the MT neurons [Wasmuht et al., 2019]. Using binocular rivalry, Leopold and Logothetis found that the fraction of neurons that answer to the reversals is changing according to the brain region: only a small fraction of cells in V1 and V2 were correlated to the perceptual switches, while it was a much higher fractions of the cells from the extrastriate cortex regions V4, MT and MST [Leopold and Logothetis, 1996]. In contrast, neurons from the LGN (thalamus) show no correlation with the reversals. It thus seems that both top-down and bottom-up strategies also exist in the monkey's brain.

Bistable perception was also proven to exist in mice, using a visual stimulus consisting of plaids made of superposition of moving gratings. Looking at this plaid, humans perceive either individual components movements (transparent motion) or a general pattern, adding up the two gratings (coherent motion). The eye movement responses observed in

mice can be followed by using an infrared camera and calculating the distance between the pupil and the reflection of the light on the surface of the cornea. When confronted with the plaid, mice perceive alternatively both the transparent and coherent motion. The perception is not only generated by subcortical areas, as lesions to V1 alter the perceptual switching rates [Palagina et al., 2017].

The electrophysiological recordings are helpful for seeing with high temporal and spatial precision, but it fails to shed light on the dynamics of large neuronal circuits leading to the perceptual switch. To address this question, it will be necessary to record large portions of the brain with single-cell resolution.

1.2 The zebrafish model

The zebrafish *Danio rerio* is a tropical teleost fish of the Cyprinidae family (freshwater fish) that owes his name to the horizontal blue stripes that run along its body (see Figure 1.6.B). It was first identified in 1822 during a trip in India by Francis Hamilton, a Scottish botanist and zoologist [Hamilton, 1822]. In the wild, they live in rice fields, shallow streams or ponds in Nepal, India, Pakistan, Bangladesh and possibly Myanmar [Parichy, 2015] (see Figure 1.6.A). They usually live in clear water but can also cope with turbid waters (in particular after raining). They are found across a large range of environmental conditions (temperatures, pH or salinity can vary greatly between the different places they live in). It is a gregarious species that usually form shoals of tens of individuals (see Figure 1.6.C). They eat mostly insects larvae and plankton and grow up to approximately 4 cm.

1.2.1 Advantages of using zebrafish as an experimental model

The zebrafish has long been a hobby fish before becoming a research model in the laboratory. The same characteristics made it attractive for both uses: mostly its tolerance of a broad range of environmental conditions and the ease and relative inexpensiveness with which large numbers of individuals can be bred and maintained in captivity [Harper and Lawrence, 2010]. Landmarks studies in the 1980s and early 1990s, involving large-scale genetic screens, produced thousands of developmental mutants that allowed major discoveries in the field of developmental biology [Streisinger et al., 1981, Chakrabarti et al., 1983, Grunwald and Streisinger, 1992]. It is not absurd that the developmental studies were the ones that started using this model: the external development of transparent eggs, that can be obtained all year round in large quantities (around 200 to 300 eggs

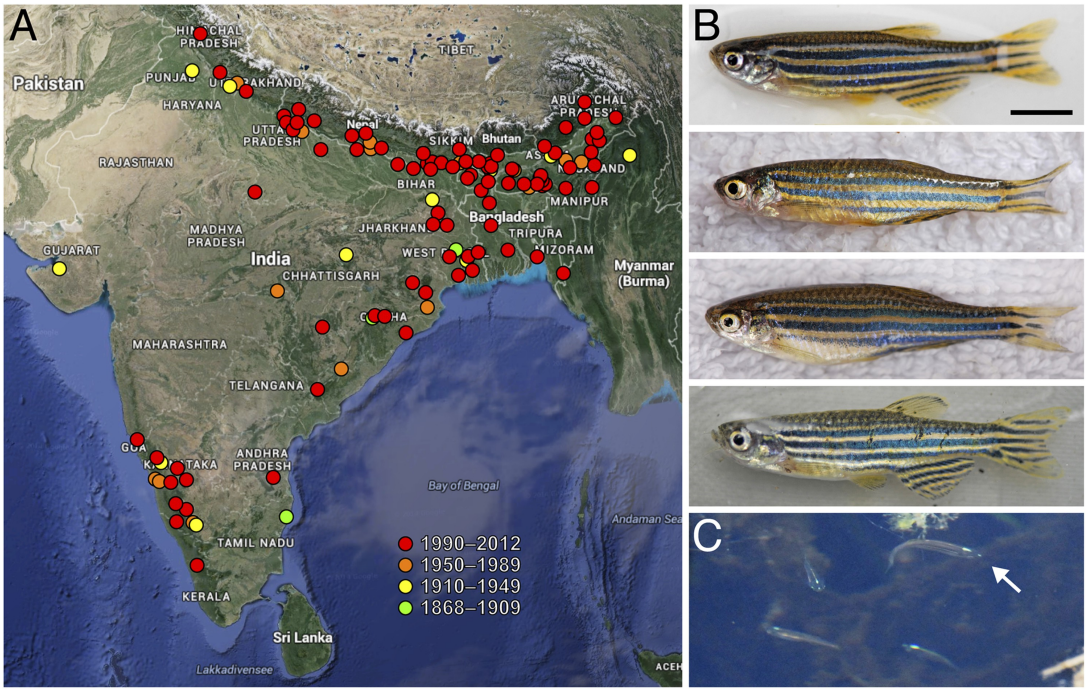

Figure 1.6: **Geographical range of zebrafish. (A)** Sites where zebrafish have been reported between 1868 and 2012. **(B)** Zebrafish from northeastern India. The upper two fish are males and the lower two fish are females. Scale bar: 5 mm. **(C)** A group of fish, with a single fish pointed out by the arrow. From [Parichy, 2015]

per week per female) is ideal for this kind of research. Moreover, it has been shown that approximately 70% of the human genes have at least one zebrafish orthologue and 84% of genes known to be associated with human disease have a zebrafish counterpart [Howe et al., 2013]. The numerous advantages of this fish and the development of many mutant and transgenic lines over the years led to the extension of its use to other fields of research beyond developmental biology, including human health and disease, evolution or neuroscience.

Zebrafish has also advantages for research in neuroscience in general, and for my PhD project in particular. The zebrafish larva hatches at around 3 days post-fertilization (dpf) and then does not have the nutritive support of the yolk sac anymore: it needs to catch prey and avoid predators to survive. These behaviors are mainly guided by the visual system. It was shown that when they reach the age of 5 dpf their visuomotor function was similar to those observed in adults [Easter and Nicola, 1997]. See Figure 1.7 for a picture of the larva at 6 dpf. This fast development of functional sensory systems in general, and vision in particular, and the large repertoire of motor behaviors [Friedrich et al., 2010, Portugues

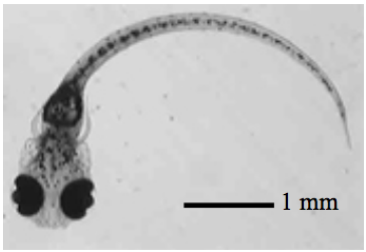

Figure 1.7: **Zebrafish larva at 6 dpf**

and Engert, 2009] are a good advantage for my PhD project. Furthermore, the use of *nacre* zebrafish lines that lacks melanophores is ideal for imaging techniques in intact larvae through its transparent skin and skull at the larval stage [Lister et al., 1999]. The larval brain at 5 dpf is less than 0.5 mm thick and 1.5mm long, making virtually all neurons accessible. Moreover, at the larval stage (before scales are formed and before the functional development of the gills), the respiration is mainly performed by osmosis through the skin, enabling us to immobilize the larva in low-melting agarose for a long period of time without damage. All those reasons and the wide range of available zebrafish mutants (especially GCaMP-expressing lines) enable the use of calcium imaging on this model to monitor the dynamics of large neuronal networks with single-cell resolution, in an intact non-anaesthetized, non-paralyzed behaving vertebrate [Panier et al., 2013, Romano et al., 2015, Pérez-Schuster et al., 2016].

As in the general vertebrate brain, the main excitatory and inhibitory neurotransmitters of the zebrafish are respectively glutamate and GABA, and there are also serotoninergic, dopaminergic, cholinergic, norepinephrinergic neurons. The gross architecture of many brain areas, e.g., retina, olfactory bulb, cerebellum and spinal cord, and their main projection pathways are similar to those of other vertebrate classes [Friedrich et al., 2010]. The optic tectum receives inputs from different brain regions and responds to multiple sensory modalities [Thompson et al., 2016], as its mammalian counterpart, the superior colliculus. It was believed before that first-order motion (motion of an object that differs in luminance from its background) was processed even without a cortex but that second-order motion (motion in which the moving contour is defined by contrast, texture, flicker, or some other quality that does not result in an increase in luminance or motion energy) necessitates a cortex to be perceived: actually zebrafish behaviorally respond to both first-order and second-order motion [Orger et al., 2000]. Thus this motion does not necessarily requires the cortex or in fish, it is processed by the optic tectum rather than the fore brain. Even with some differences in the architecture of the brain, the zebrafish has been shown to elicit a comparable behavior to humans when confronted with illusory motion [Gori et al., 2014], with motion after-effect [Pérez-Schuster et al., 2016] or with Fourier motion [Orger et al., 2000].

1.2.2 Zebrafish visual perception

The visual system of the zebrafish is composed of the retina and several brain centers: the optic tectum, pretectum and thalamus that respond to different features of the visual stimulus. During visually driven behavior, many more areas are active, like the motor centers in the hindbrain, the cerebellum and some populations in the diencephalon among others [Bollmann, 2019].

The retina

The zebrafish retina is very similar to the mammalian retina in terms of structure and type of cells, with five canonical retinal neuron classes: photoreceptor, horizontal cell, bipolar cell, amacrine cell, and ganglion cells (RGCs), organized in three nuclear layers, separated by two plexiform (synaptic) layers. The outer retina contains rod photoreceptors and four types of cone photoreceptors, including an ultraviolet-sensitive cone type, mostly present in the acute zone [Zhou et al., 2020]. Hence, zebrafish are tetrachromats and extend their visual range into the ultraviolet. The sensitivity to UV light most probably evolved due to the reflection of UV-light by the zooplankton. According to the cellular organization of the retina, the visual information is split into several parallel representations that are transmitted to subpopulations of bipolar and ganglion cells. Visual features such as luminance and contrast, color and stimulus size, and visual motion direction are already extracted in the retina and encoded in the spiking activity of different types of RGCs [Bollmann, 2019]. For example, the retina contains RGCs that are orientation- or direction-selective. When both dendritic morphology and central projections are taken into account, it seems that more than 50 RGCs morphological types exist, suggesting a large number of parallel computations already in the retina [Robles et al., 2014, Yonehara and Roska, 2014]. The information is then transferred to the brain through the axons of the RGCs that form the optic nerve which projects to 10 different arborization fields (AF) within the diencephalon and mesencephalon in the larva's brain (see Figure 1.8). The largest arborization field (AF10) is the neuropil of the optic tectum, the highest and largest zebrafish visual center. There are nine other arborization fields that are nearly all contralateral (almost complete optic chiasm), with only one of them (AF1) being bilateral, projecting to the hypothalamus [Burrill and Easter, 1994].

The optic tectum

The optic tectum is the main visual center of zebrafish (see Figure 1.9 for its location in the brain). It is involved in receiving multiple sensory inputs and processing them to integrate all information and generate adequate motor behaviors [Thompson et al., 2016], via its projections to the hindbrain motor centers. It is homologous to the superior colliculus in mammals, which is known to be involved in the detection of small prey-like objects to generate goal-directed behaviors (eye and head orienting movements). The optic tectum is mainly composed of a large number of GABAergic and glutamatergic neurons (similar proportions) and a smaller number of cholinergic neurons.

The projections from the retina (AF10, see Figure 1.8.B) are retinotopic and non-overlapping in the tectum: axons from neighbouring regions of the retina terminate at neighbouring positions in the tectum and frontal images activate a more rostral part of the

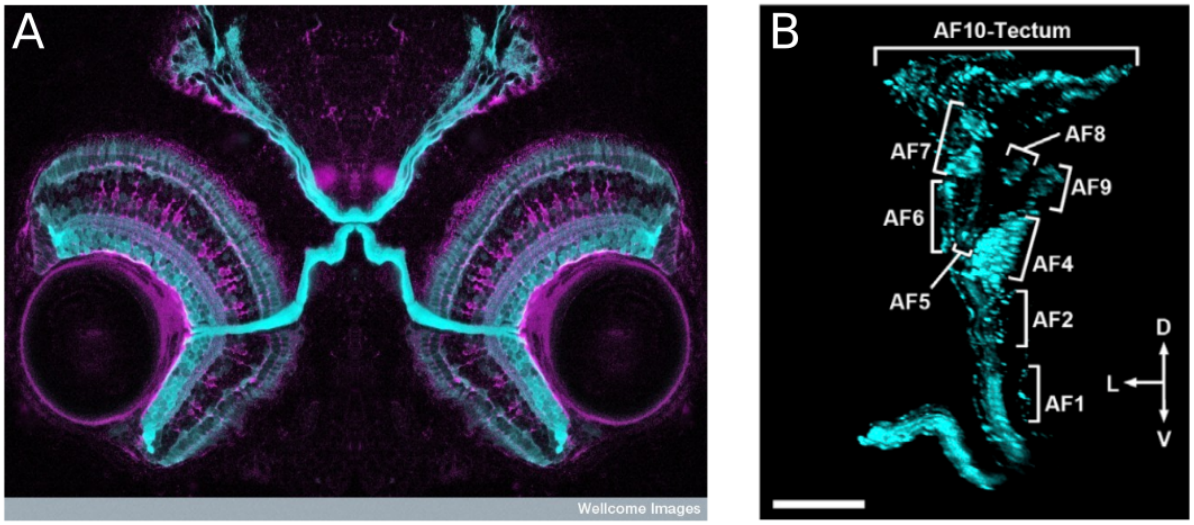

Figure 1.8: **Projection of the retina into the larva brain. (A)** Confocal image showing the retina and the projections to the brain in a 4 dpf zebrafish larva. Both the retinal ganglion cell layers and photoreceptor cell layers are shown in cyan. The glial cells are shown in purple. The optic nerve (cyan) transmits information from the eye to the brain. Image from Kara Cerveny and Steve Wilson (http://www.cellimagelibrary.org/images/39022). **(B)** The 10 arborization fields made by RGC axons in a 6dpf larva. AF3 is located in a plane behind AF2 in this view. The scale bar represents 50 μm. Image from [Robles et al., 2014].

tectum while temporal images are coded more caudally [Stuermer et al., 1990, Romano et al., 2015]. Light spots presented in different regions along the visual field of the larvae activate compact groups of neurons in the optic tectum, with the nasal to temporal hemifields mapped in the contralateral rostro-caudal tectal axis, creating a functional retinotopic map [Romano et al., 2015]. Robles *et al.* also demonstrated that sublaminae of the tectum receive inputs from different combinations of RGC axons, that correlate with different functional properties [Robles et al., 2013]. The laminar organization of retinal afferents thus seems to create a structural framework for the integration of visual inputs to the tectum. In fact, the whole tectal network is a multilayered structure, each with different functional roles. For example, superficial layers of the tectal neuropil contain more small-size-selective retinal inputs (prey-like stimuli), while large-size-selective inputs (predator-like stimuli) are more frequently observed in deeper layers [Preuss et al., 2014]. Similarly, different preferred directions are represented in different sublaminae of the tectum, which are innervated by specific cell types [Gabriel et al., 2012]. Direction and orientation selectivity are already present in the RGC inputs, but are not treated the same way in the tectum. First, RGCs coding for the trajectory of motion (direction) target the more superficial layers of the tectum while RGCs carrying orientation information project to deeper layers [Nikolaou et al., 2012]. Moreover, the same orientation-selective populations are found in the tectum and the retina, but there is an emergent population of direction-selective neurons in the tectum that does not exist in the RGC inputs [Hunter

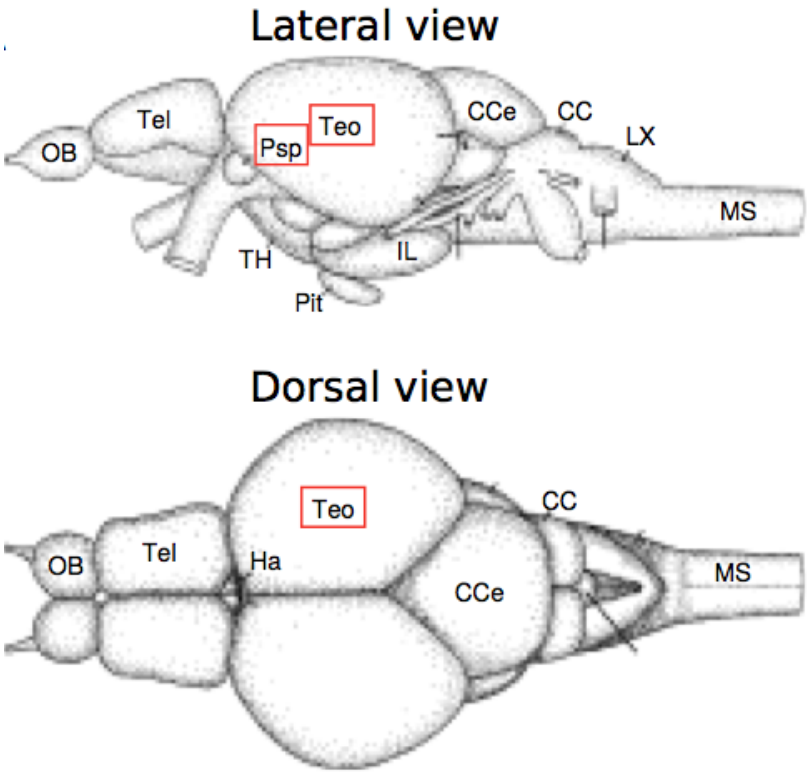

Figure 1.9: **Lateral and dorsal views of the zebrafish brain.** The optic tectum and the pretectum are framed in red. CC, cerebellar crest; CCe, cerebellar corpus; Ha, habenula; IL, inferior lobe of hypothalamus; LX, vagal lobe; MS, spinal cord; OB, olfactory bulb; Pit, pituitary; Psp, parvocellular superficial pretectal nucleus; Tel, telencephalon; Teo, tectum opticum; TH, tuberal hypothalamus. From [Wullimann et al., 1996].

et al., 2013]. Therefore, the direction selectivity, contrary to the orientation selectivity, is established in the tectum as well as at the retinal level. This emergent direction selectivity is certainly created by local inhibitory circuits, because it was demonstrated that the excitatory inputs show little selectivity to the preferred direction, while the inhibitory inputs display a lot of selectivity for the null direction [Grama and Engert, 2012]. Along the same lines, the deeper layers of the tectum are tuned to small visual stimuli while GABAergic interneurons in the superficial layers (SINs) are tuned to large visual stimuli. The latter acts as a size-recognition filter inhibiting the response to large stimuli in other tectal layers [Del Bene et al., 2010].

Apart from the projections from the retina, the optic tectum receives direct or indirect inputs from all sensory organs, the opposite tectal hemisphere, and other brain regions such as the telencephalon, nucleus isthmi, among others.

The ongoing spontaneous activity of the optic tectum is organized in neuronal assemblies composed of highly correlated neurons. These neuronal assemblies are spatially organized reflecting the functional retinotopic map, they are tuned to biologically relevant visual stimuli (e.g., prey), and their activation predicted orienting tail movements.

Moreover, the neuronal assemblies show attractor-like dynamics (all-or-none activations and winner-takes-all dynamics), characteristics that could improve prey-detection in cluttering or low-contrast environments. This suggests that the functional connectivity of the optic tectum is adapted for its functional role [Romano et al., 2015].

Along the same lines, it was also shown that neurons in the more rostral parts of the tectal retinotopic map better respond to larger objects than those in areas of the retinotopic map representing the lateral field of view (during prey-capture prey will cover a larger size of the retina as the larva gets closer to it) [Förster et al., 2020].

The involvement of the optic tectum in prey capture was also supported by ablations studies, showing that tectal ablation significantly affects prey capture of paramecia [Gahtan, 2005]. Moreover, a population of glutamatergic tectal interneurons, tuned to small-size stimuli, was proven to be required for approach towards small objects [Barker and Baier, 2015]. The adaptation of the optic tectum to prey capture is thus undeniable. Other visuomotor behaviors such as the optomotor response (see next section 1.2.3) are mainly controlled by the pretectum. Indeed, Wang *et al.* has shown that the tectum preferentially extracts size-specific stimuli in the upper nasal visual field (corresponding to prey capture), while the pretectum represents larger (wide-field) stimuli in the lower visual field (adapted for optic flow processing) [Wang et al., 2020].

The pretectum

The pretectum is situated in the caudal diencephalon, ventral to the optic tectum (see location on Figure 1.9). It is involved in optic flow processing and sends information for appropriate motor behaviors associated with optic flow, such as the optokinetic and optomotor responses (OKR and OMR, see next section 1.2.3). It can thus be considered as homologous to the accessory optic system in mammals [Matsuda et al., 2021], that is the region involved in optokinetic nystagmus and visual-vestibular interaction in mammals. It receives inputs from the retina, optic tectum, cerebellum, telencephalon and nucleus isthmi and it sends outputs to the optic tectum, torus longitudinalis, cerebellum, hypothalamus and tegmentum. Both hemispheres of the pretectum are also connected together via the posterior commissure, which allow transfer of monocular information within the pretectum. Indeed, ablation of this commissure abolishes binocular integration of the pretectal information [Naumann et al., 2016].

The pretectum is organized in multiple nuclei that are highly specialized in their functions, according to their differences in connections [Yáñez et al., 2018]. The direction-selective RGCs project to the pretectum via the arborization field 5 (AF5, see Figure 1.8.B) and meet pretectal neurons with simple tuning to monocular optic flow. It has been shown that the direction-selective RGCs respond directionally to glider stimuli and that

the information is further refined and integrated in the pretectum to construct a behavior-ready visual representation [Yildizoglu et al., 2020]. Translation-selective neurons are intermingled with the direction-selective cells but do not receive retinal inputs, meaning that they respond to the same direction of motion coming from both eyes [Kramer et al., 2019]. So far, four bilateral pairs of clusters have been described by Kubo *et al.*, that process horizontal whole-field motion and can distinguish between translational (both eyes give the same direction of motion) and rotational (the direction of motion is opposite for the two eyes) optic flow [Kubo et al., 2014]. Coherently with this discovery, it has been shown that the pretectum is highly involved in the generation of optomotor and optokinetic behaviors (see next section 1.2.3). However, it should be noted that the pretectum has at least two functional regions, one that is responsive to optic flow (RGCs projecting via AF5) and a more rostral one that is innervated by the AF7 and is involved in prey detection [Semmelhack et al., 2014]. This region is retinotopic and innervated by the temporal retina, which creates a high-resolution representation of the anterior visual field, usually where prey is located at the final stage of a prey-capture behavior [Robles et al., 2014].

1.2.3 Zebrafish visuo-motor behaviors

During development, the first visuo-motor behavior to emerge is the visual startle response: a sudden decrease in brightness (interpreted as threat) leads to an escape response. This behavior emerges between 68 to 79 hours post-fertilization (hpf) (approximately 3 dpf), right after the retinal ganglion cells (RGCs) reach the tectal neuropil and the first synaptic connections are formed [Easter and Nicola, 1996]. A little later (between 73 to 80 hpf), the optokinetic response (OKR) appears. This is the earliest visual behavior requiring pattern vision and directionality [Easter and Nicola, 1996, Easter and Nicola, 1997]. Slightly after, the optomotor response (OMR) and positive phototaxis (larva's attraction to the lighter areas) develop. See Figure 1.10 for a schematic view of the optokinetic and optomotor responses.

Both the OKR and the OMR serve to compensate for self-motion and stabilize the external world on the retina. The OMR consists in tail-flip bouts generating swimming in the direction of perceived movement. This behavior enables the larva not to be swept away by the current and stay in the same region of the stream using the apparent motion of the visual cues present in the riverbed. The OKR is due to the presentation of coherently moving objects in a large region of the larva's visual field that evokes slow eye rotations (pursuits) in the direction of perceived movement followed by rapid saccades in the opposite direction to reset the eyes' position [Portugues and Engert, 2009]. Because

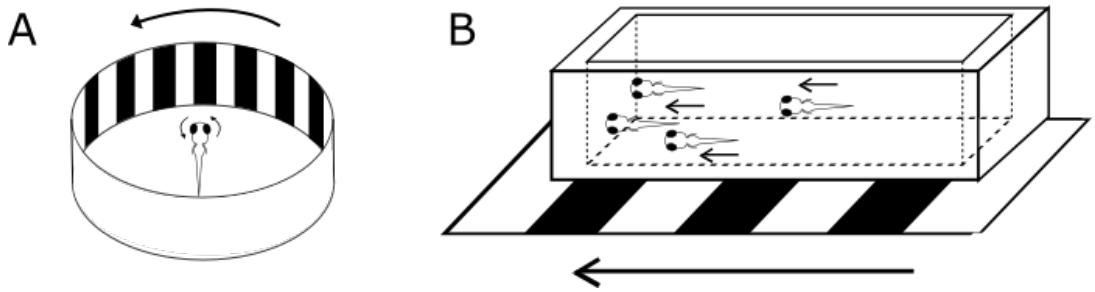

Figure 1.10: **OKR and OMR in zebrafish larva. (A)** Optokinetic response: a rotating vertical grating creates a large coherent moving visual stimulus around the immobilized fish, that responds with following eye movements. **(B)** Optomotor response: the larvae swim to follow a moving grating below their tank. The direction of motion is indicated by arrows. Adapted from [Roeser and Baier, 2003].

both OKR and OMR can be reliably evoked in the laboratory at early larval stages, these behaviors have been largely used to study visuo-motor behaviors, notably in genetic screens, to identify mutations disrupting the development and function of neuronal visual circuits [Neuhauss et al., 1999, Huang and Neuhauss, 2008]. It should be noted that in the absence of visual cues, the zebrafish larvae also move the eyes: they make regular saccades spontaneously, between which the eyes either fixate or slowly decay to the central position.

The optokinetic response

The OKR is very robust and stereotyped. It is elicited by a visual coherent-moving environment around the fish. Its gain, defined as the ratio between stimulus and eye velocities, depends on the stimulus' angular velocity, spatial frequency and contrast, but not on its brightness [Rinner et al., 2005]. Qian *et al.* have studied the dependence of OKR gain and amplitude on several stimulation parameters. They found that the stimulus velocity did not impact the OKR amplitude, at least between 24 and 108 °/s. They also tested the influence of the spatial frequency of the stimulus when projected at a constant speed of 48 °/s and showed that the amplitude and gain of the OKR depended greatly on it, with a steep decline of both in the narrow range of 0.1-0.16 cycles/°. Another remarkable result from their study is that both eyes exhibited an asymmetric response to the stimulus, with greater response to temporal-to-nasal than to nasal-to-temporal rotation. This result was only reversed at spatial frequencies higher than 0.16 cycles/°. Overall, these results suggest that zebrafish larvae are more responsive in terms of OKR to objects with low spatial frequencies entering the larva's field of view from their caudal part, and to high-spatial frequencies of moving objects traversing the frontal field of view [Qian et al., 2005]. Moreover, it was independently demonstrated that spatial frequency tuning is similar across all points in the visual field [Dehmelt et al., 2019].

Using optogenetics, Kubo *et al.* showed that the pretectum is necessary and sufficient for the OKR [Kubo et al., 2014]. Along the same lines, Roeser and Baier used laser-ablation to show that the OKR did not depend on the intact optic tectum. The only effect of the ablation was a reduction of the frequency of saccades, but the velocity, gain and amplitude of the behavior was unaffected [Roeser and Baier, 2003]. Eye movements are controlled by an oculomotor region which is located in the caudal part of the hindbrain. Each of the neurons within this region is more or less tuned to eye position and/or velocity, with a gradient along the rostro-caudal axis: the rhombomeres 5/6 code mainly for eye position, and the rhombomeres 7/8 (more caudal) code along a velocity-to-position axis [Brysch et al., 2019]. This structure thus seems to store the velocity and position of the eyes and is in agreement with a feedforward mechanism of persistent activity generation, that explains why the larva performs saccades even in the dark. Ramirez and Aksay also recorded neurons in the hindbrain of zebrafish larva, and found different types of neuronal populations that responded around the saccades. Some neurons showed bursts only during saccades, others were active all along the fixation period, and a different population displayed a rise in activity several seconds before the saccade, going back to baseline after the saccade. They called the latter pre-saccadic rise neurons and were able to predict the timings of the saccades thanks to their activity alone [Ramirez and Aksay, 2020].

The OKR is evoked by a coherent-moving environment, and if the movement is long enough it can induce an illusory perception of movement in the opposite direction : the motion-after effect (MAE), also known as the waterfall illusion in humans. Zebrafish larvae perceive the MAE as well [Pérez-Schuster et al., 2016, Wu et al., 2020]. Ablating the optic tectum significantly weakened MAE and prevented behavioral habituation during the conditioning stimulus [Pérez-Schuster et al., 2016]. A second study showed that a pretectal subpopulation of neurons in the ventral lateral pretectum is also involved in the generation of the MAE after OKR [Wu et al., 2020].

1.3 Objectives of the thesis

In this introduction I have presented briefly what is already known on the mechanisms of visual perception. We have seen that many brain areas are involved and work in interaction to provide a coherent perception, in humans (retina, lateral geniculate nucleus, primary visual cortex, MT, MST areas) as well as in zebrafish (retina, optic tectum, pretectum). But the perception can change over time, either because of a change in the sensory stimulus, a change in the brain's internal state or in the case of an ambiguous

stimulus. In the latter, the brain is switching between percepts in the absence of any change in the environment. These perceptual alternations have been studied mostly in humans but information can only be accessed through external recordings like EEG or fMRI with low spatial resolution. A few studies in animals using electrophysiology gave more details on the precise regions, but were limited in the scope of regions that can be observed. Using the zebrafish larva, we can combine both advantages of looking at the whole brain with single-neuron resolution.

During my thesis, I focused on three main topics:

1. I investigated the neural representation of the square-wave vs. the missing fundamental stimulus (see section 1.1.1) in the tectum and the pretectum of zebrafish larva.

2. I modulated the power of the first Fourier component of the square-wave stimulus to generate an ambiguous stimulus for zebrafish larvae. I projected this moving ambiguous signal to the larva and studied its optokinetic behavioral response.

3. I recorded the activity of the whole brain of the larva to investigate the neural representation and mechanisms underlying the alternations in perceptive states.

I will detail the methods I used to conduct this project and the results I obtain on these three topics in the following chapters.

2

Methods and techniques

In this chapter, I will present the different methods and techniques I used for my study. I will first describe how we cross and take care of zebrafish, and what lines I used. Then, I will explain the set-up and data analysis I used for behavioral experiments. Finally, I will detail how was recorded the neuronal activity, with explanations on calcium imaging, on the different microscopes I used, and on data analysis.

2.1 Zebrafish lines and how to care for them

Zebrafish develop rapidly in eggs and hatch at approximately 2 days post-fertilization (dpf). They are then free-swimming larvae, and start to be autonomous at 5 dpf (visual behavior is functional and they can hunt for food). They undergo at approximately one month of age a metamorphosis, including fins development, ossification of skeleton and scale development, among other changes, and are then called juveniles. Afterwards, they reach sexual maturity at 3 months of age and can live up to 5 years.

For all experiments, zebrafish larvae from 6 to 9 dpf were used. All experiments were approved by the *comité d'éthique en expérimentation animale* n°005 (reference number APAFIS#27495-2020100614519712 v14).

2.1.1 Crossings and care of adults and larvae

In our zebrafish facility, adult fish are maintained in fish tanks whose water is running in a closed loop, with filters that keep the water clean and in a good chemical and physical state. They are fed with Artemia salina (crustaceans) or rotifers, and dry powder containing algae. The light/dark cycle is set on 14:10 hours with the lights on at 9:15 AM. Fish from 4 to 18 months can be crossbreed up to twice a week. Each mature female can produce between 50 to 200 eggs in one crossing so we can easily and quickly obtain a high number of larvae for the experiments.

For the crossings, two adult males and two adult females are placed at the end of the day in a fish tank, with a physical vertical separation between the two sexes to allow them to see and smell the others but not touch them. The next day, as soon as the lights go on, the four fish are put together above an horizontal grid. The eggs are produced and fall across the grid to the bottom of the tank where they are protected from the adults (that would otherwise eat them).

Embryos are then collected and placed in Petri dishes in a 28°C incubator, in an embryo medium (NaCl 5.0 mM, KCl 0.17 mM, CaCl2 0.33 mM, MgSO4 0.33 mM pH 7.2 in distilled water with 0.1% methylene blue as an antifungal) until they hatch. This medium is changed twice a day and the abnormal or unfertilized eggs are removed. After the hatching, the composition of the medium is the same except for the methylene blue. Once they have reached 5 dpf, the larvae are fed with paramecia twice a day.

2.1.2 Fish lines

The fish line I used is as follows: HuC:H2B-GCaMP6f (from [Dunn et al., 2016]) on a *nacre* (mitfa -/-) background.

We used *nacre* background zebrafish: mutants that lack melanophores (black pigmentation) except in the non-crest-derived retinal pigment epithelium (meaning they have a normal retina) [Lister et al., 1999]. Therefore, *nacre* larvae have a transparent skin enabling monitoring brain activity in an intact organism without the need to open the skin or use 1-phenyl 2-thiourea (PTU) to reduce pigmentation, as what was done before, but was highly inconvenient and teratogenic [Karlsson et al., 2001].

The animals were also expressing the calcium indicator GCaMP6f (Green fluorescent protein-CalModulin Protein sensor 6f, excitation peak 485nm, emission peak 510nm) in all neurons' nuclei thanks to the HuC promoter (targeting all neurons) and the H2B protein that was attached to the GCaMP6f (H2B being an histone that is directed to the nucleus) [Chen et al., 2013, Kanda et al., 1998]. The use of a genetically-encoded

fluorescent calcium indicator presents many advantages, notably the possibility to sample sub-populations of cells by the use of promoters, the stability of their expression over time, or the fact that optical imaging, contrary to electrophysiology, can capture the activity of thousands of neurons at the same time [Lin and Schnitzer, 2016]. Calcium is a second messenger for neurotransmitter reception and membrane depolarization. After a spike, there is an intracellular calcium concentration increase that lead to a higher fluorescence of the GCaMP, due to a conformational change of the protein when calcium is present. Many different calcium indicators exist but GCaMP is one of the most used in neuroscience, and GCaMP6 in particular has been shown to outperform the previous GCaMP in terms of signal-to-noise ratio notably [Chen et al., 2013]. The use of the H2B protein to target the sensor to the nucleus of the cells allows an even better signal-to-noise ratio because then the neurons can be separated from each other more easily in dense regions like the optic tectum, where the soma of the neurons are touching each other, and also separated from the neuropil [Shemesh et al., 2020]. The nucleus uses the calcium signals for the regulation of gene expression for example [Hardingham et al., 2001], but it was proven in hippocampal neurons that the nuclear envelope doesn't block calcium signals coming from the soma, and thus the intracellular wave of calcium increase can be detected in the soma as well as in the nucleus [Eder and Bading, 2007]. Nevertheless, the nuclear localisation of the fluorophore slows the kinetics of the fluorescence [Shemesh et al., 2020].

2.2 Behavioral experiments

To decipher what the larva was detecting during the experiments, we used the robust and well-known optokinetic response (OKR) that was already discussed in section 1.2.3, with custom-made stimulation and analysis.

2.2.1 Set-up for recording and analyzing the OKR

For recording the behavior, the larva was immobilized in a drop of 2% low-melting agarose in the middle of a chamber filled with embryonic medium (see section 2.1.1 for the composition) and surrounded by a screen (#216 White Diffusion, Rosco Cinegel). The larva doesn't have any scale and can breathe through its skin so we could leave it immobilized in agarose for a few hours without any impairments. The agarose around the eyes was carefully removed to allow the eyes to rotate freely. Visual stimuli were projected on the screen using a pico-projector (AAXA P4X). The stimulation field covered approximately

180°x60° (azimuth x height) of the larva's visual field. All stimuli were generated using Matlab (The MathWorks, Inc) and the Psychophysics Toolbox Version 3 [Brainard, 1997, Kleiner et al., 2007] extension. A geometrical deformation was imposed on the stimuli to take into account the curvature of the chamber, so that the larva was seeing evenly spaced bars. Red light (620 nm) was used in the projector, and a BLP01-561 Semrock long-pass filter was placed in front of it. This prevented interference of the visual stimulus with the emission of the GCaMP signal (emission peak 510nm). We chose to also use red light in the behavioral experiments even outside the microscope so that the conditions are conserved between experiments. It has been proven that the zebrafish react to red and/or green light for the OMR [Orger and Baier, 2005], that is driven by the same kind of stimuli than the OKR. Over the chamber, an infrared video camera (DMK 22BUC03, The Imaging Source) was recording the head of the larva, thanks to light from an infrared LED (820nm). To synchronize the video recordings with the visual stimuli we used an arduino board. A scheme of the set-up is shown in Figure 2.1.A.

Using either the Bonsai program [Lopes et al., 2015] or a custom-made program in

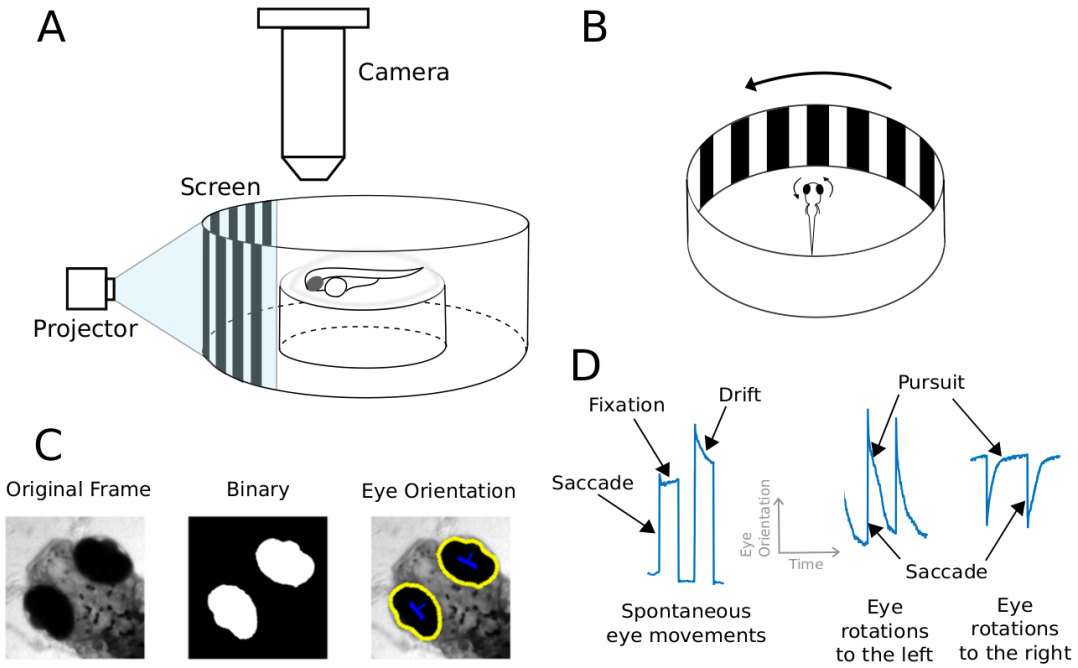

Figure 2.1: **Set-up for recording the OKR. (A)** Set-up for recording the eye movements of the larva that are induced by projected stimuli. The larva is immobilized in the middle of the chamber in a drop of 2% agarose, except around the eyes to allow their movement. **(B)** The larva responds with eye rotations following the movement of vertical gratings. **(C)** The eye detection algorithm: the original image is thresholded and converted into a binary image from which the eye orientation can be calculated. In blue: ellipsoid axis whose angle is calculated in each frame of the video. **(D)** Characterization of the three different eye movements that are caused by a static (spontaneous eye movements) or a moving vertical grating (eye rotations to the left or the right).

Matlab (The MathWorks, Inc.), we first converted the original image into a binary one: as the eyes are really darker than the rest, by thresholding the image it is easy to obtain only the eyes. We then calculated the orientation of each eye by measuring the orientation of the ellipsoid corresponding to each eye against an arbitrary x axis (see Figure 2.1.C). As this angle depended on the orientation of the larva, the average for each eye was then subtracted to obtain a zero baseline for all larvae.

The larva displays three types of stereotyped movements during the OKR. Either the bars are moving to the left or the right, leading to two types of induced movements, or they are not moving, leading to spontaneous eye movements. The induced eye movements are composed of pursuits in the same direction than the direction of movement, followed by a fast saccade in the opposite direction to reset the eyes; whereas the spontaneous eye movements are composed of saccades alternating in each direction, separated by fixations or small drifts (see Figure 2.1.D). During the analyses, I detected the saccades from the eye orientation traces thanks to a semi-automatic custom-built program written originally by Veronica Perez-Schuster and improved by myself. The orientation of each saccade was then calculated with the same methods as used by [Pérez-Schuster et al., 2016]. The behavior was sorted automatically into those three types: either spontaneous if the saccades were alternating in direction, or following to the right (respectively to the left) if the saccades were always from right to left (respectively from left to right). We thus obtained an alternation of type of behavior from the larvae corresponding to their detection of the movement in front of them.

2.2.2 Creating a missing-fundamental and an ambiguous stimulus

The usual stimulus for studying OKR is a vertical black and white square grating. For deciphering the role of the first Fourier component in the visual motion perception in the zebrafish larva, I also used a missing-fundamental stimulus, as presented in section 1.1.1. This stimulus is a square-wave with its fundamental frequency F1 (calculated by Fourier transform) subtracted (see Figure 1.2, page 6). When F1 is completely present (F1=100%), the perception of movement is in the same direction as the physical movement. In the contrary, as was already explained, when F1 is totally removed (F1=0%, missing fundamental signal) and the stimulus is presented in quarter-cycle jumps, the image is perceived as going in opposite direction compared to the physical motion of the edges and features of the stimulus. It is the case in humans [Chen et al., 2005] as well as in zebrafish [Orger et al., 2000]. For a graphical explanation of why this happens, see Figure 1.3 on page 7.

Some preliminary studies that were made in the laboratory with this set-up showed

that this effect was the strongest and less variable for a velocity of 180 °/s and each bar corresponding to 16° of visual angle, so that is the values I used for the experiments during my PhD.

Brown and He showed that adding back fractions of the fundamental frequency to a missing fundamental signal restored the perception of movement to the direction of physical movement in humans [Brown and He, 2000]. Aiming to create an ambiguous stimulus, we reasoned along the same idea: how much power of the fundamental frequency is needed back in the missing fundamental signal for the larva to reverse its perception, and more importantly is there an intermediate power where the signal would be ambiguous to the larva? We generated a moving grating with its fundamental frequency (F1) at a reduced power to answer this question, testing different power from 10% to 40% of F1. The different stimuli that we used are explained in Figure 2.2, with the example of F1=30% for the ambiguous one.

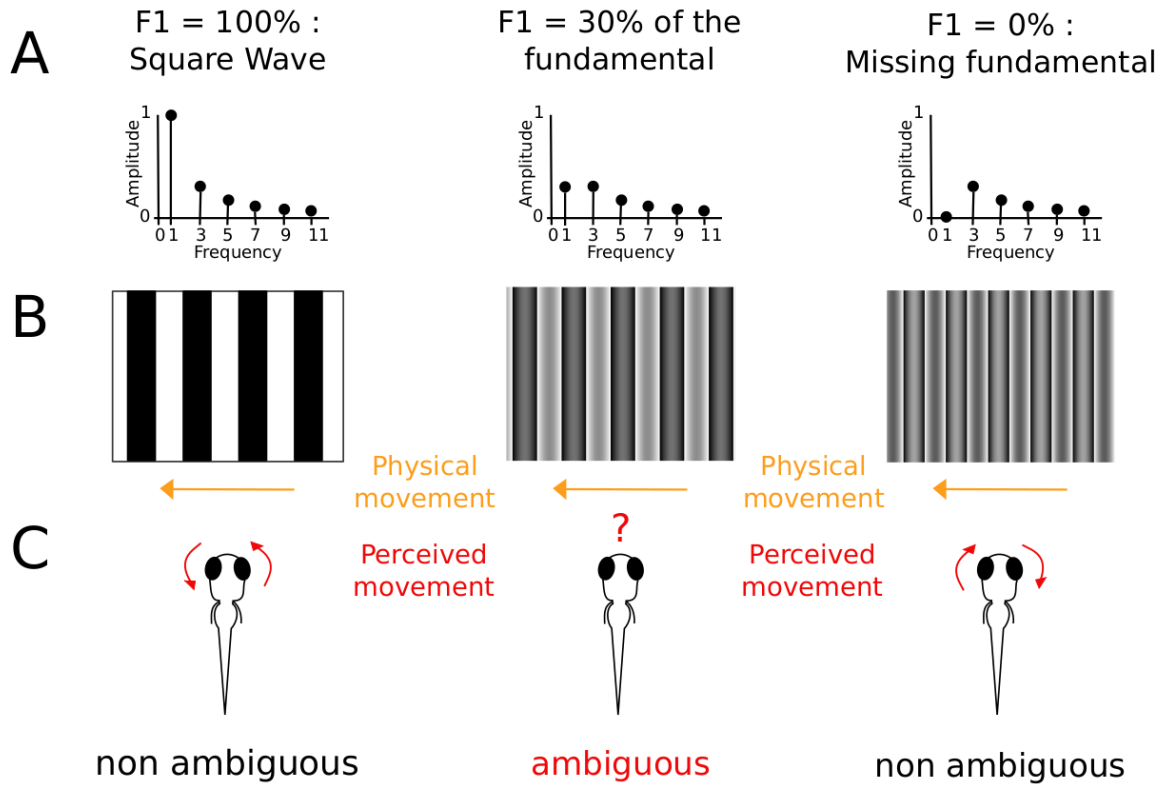

Figure 2.2: **Ambiguous and non-ambiguous stimuli. (A)** Harmonic content of the Fourier decomposition of each pattern. From left to right: F1=100%, F1=30% and F1=0%. **(B)** Visual appearance of the different gratings patterns. The yellow arrow indicates the direction of the physical movement of the stimulus. **(C)** The direction of the rotation of the larva's eyes (perceived movement, red arrows) when the gratings move to the left (physical movement). F1=100% and F1=0% are non ambiguous stimuli perceived as going in two opposite directions, while F1=30% is an ambiguous stimulus.

Larvae that did not coherently perceive the stimulation (F1=100% and F1=0% as going into opposite directions) or that did not display any spontaneous saccades were removed from subsequent analyses.

2.3 Neuronal activity recordings

Depending on the experiments, I used two different custom-built microscopes for recording the neuronal activity together with the behavior of the larva: a two-photon point-scanning microscope or a selective plane illumination microscope (SPIM).

2.3.1 Two-photon Ca^{2+} imaging

To study the neuronal activity and the behavior at the same time, we combined the behavioral set-up with a two-photon point scanning microscope, the only difference from the purely behavioral recordings being that the infrared camera is filming the fish from below to make room to the microscope objective from above (see Figure 2.3.A).

Two-photon calcium imaging in combination with transgenic zebrafish larvae express-

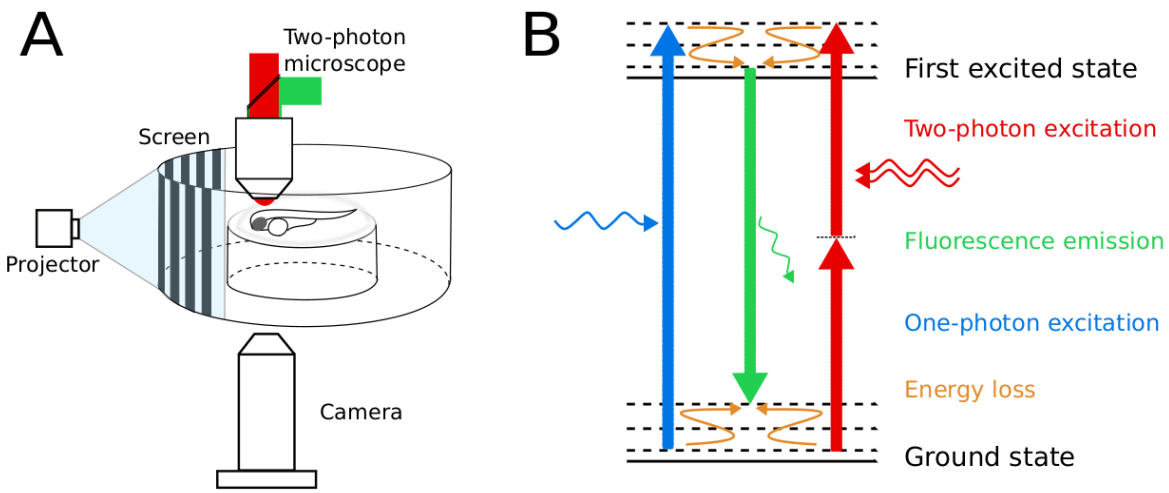

Figure 2.3: **Two-photon point-scanning calcium imaging set-up. (A)** Set-up for recording the neuronal activity together with the behavior. The laser is depicted in red and goes through a dichroic mirror down to the larva's brain, then the dichroic mirror reflects the upcoming green fluorescence to a sensor. **(B)** Jablonski diagram explaining the difference between the one- and two-photon excitation leading to the same fluorescence emission. Each photon from the two-photon excitation contains half the energy of the photon from the one-photon excitation.

ing H2B-GCaMP6f pan-neuronally makes it possible to study the dynamics of large neuronal networks, with single-cell resolution, while presenting the stimuli. The two-photon microscopy relies on a laser that produces pulses of light of extremely short duration (10^{-12} to 10^{-15} seconds) containing a very high density of photons. The set-up consisted of a modified version of the MOM (Movable Objective Microscope) system (Sutter Instruments) with a 25x NA 1.05 Olympus objective and a Mai-Tai DeepSee Ti:sapphire laser (Spectra-Physics) tuned at 920 nm, which is infrared, invisible to the fish and corresponds to half the absorption peak of the GCaMP's fluorophore GFP. When two photons of theoretically the half wavelength of the peak of the absorption curve excite the fluorophore within a time window of 10^{-15} seconds, the electrons of the fluorophore can reach the excitation state and release a photon upon relaxation (see Figure 2.3.B). The arrival of two photons in a sufficiently small time window only happens at the focal point, so the only fluorescence photons that are released come from the focal volume (confocality). The output power at the focal plane was less than 3 mW. Each measured light intensity becomes one pixel of the image and the focal point is scanned throughout the plane to form the entire image thanks to two mirrors whose orientation is altered by a galvanometer. The emission of the GCaMP signal passed through a FF705 dichroic filter, an AFF01-680 short-path filter (IR Blocker), and an FF01 520/70 band-pass filter (all from Semrock), and collected by a photomultiplier tube (H1070 GaAsP from Hamamatsu). The emission signal was pre-amplified with a SR-570 (Stanford Research Systems) and reconstituted and saved using *ScanImage 3.8* software [Pologruto et al., 2003] in Matlab (The MathWorks, Inc.). To synchronize the neuronal recordings with the visual stimuli we used an arduino board. We recorded from the optic tectum and the pretectum of 7-9 dpf larvae with a temporal resolution of ≈ 3.91 Hz (exactly 1000/256), with 256x256 pixels resolution.

This method leads to the precise localization of the excitation in the focal volume, thus optimizing the signal-to-noise ratio and limiting the phototoxicity of the laser to the living tissue, allowing longer recordings without damaging the tissue in and outside of the focal plane. An additional advantage is that the 920 nm wavelength can penetrate deeply in the tissue and does not stimulate the visual system of the larva, thus not interfering with the presented stimulus. With this method of point-scanning microscopy, we can have a very precise spatial resolution, however scanning each point is a relatively slow process, so it is at the expense of temporal resolution.

2.3.2 Selective plane illumination microscopy

Selective (or single) plane illumination microscopy (SPIM), also called Light-sheet fluorescence microscopy, doesn't use the point-scanning technique. Instead, it provides optical

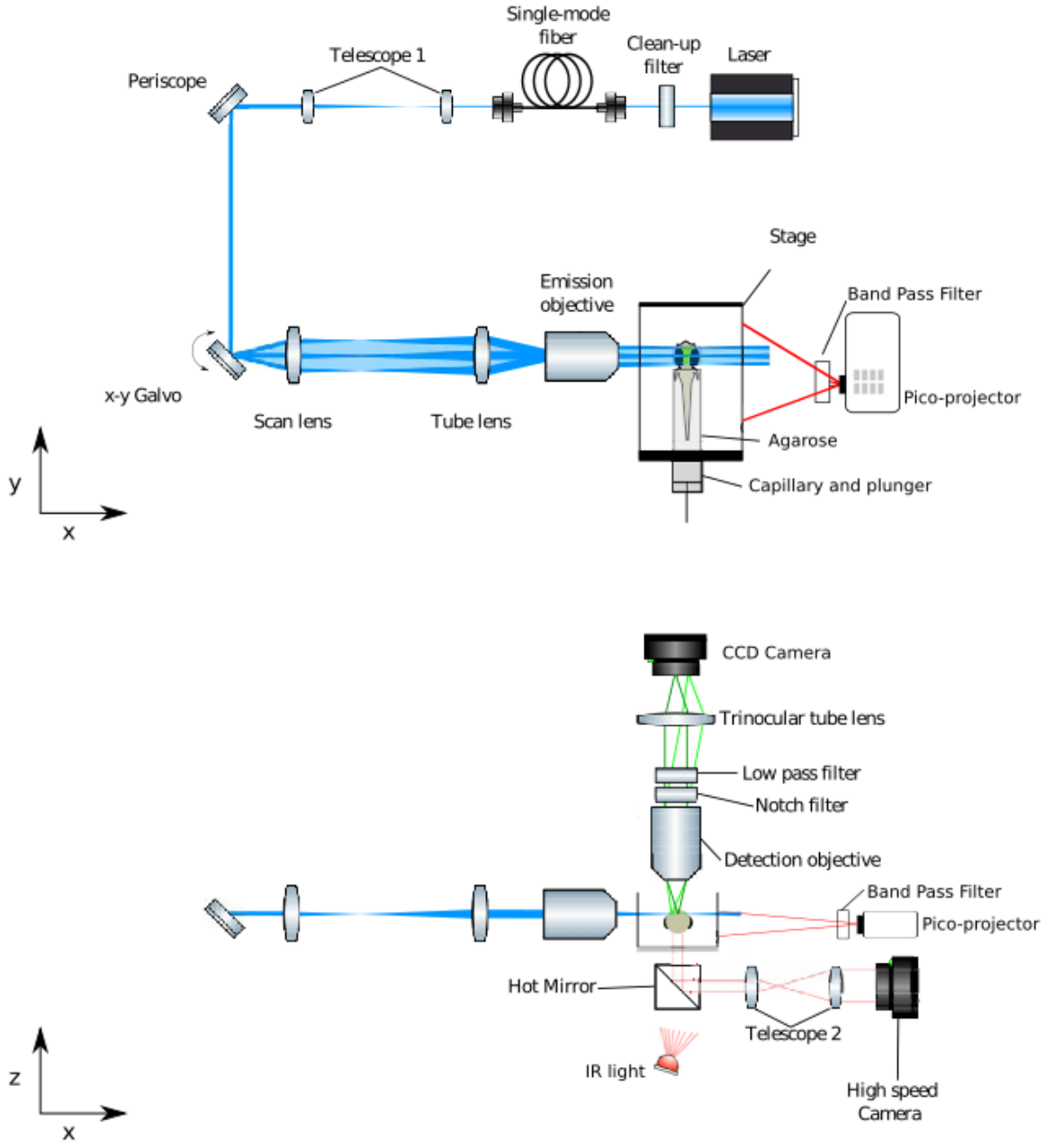

Figure 2.4: **SPIM set-up.** Up: top view. A light-sheet in the x-y plane allowed monitoring neuronal activity in a coronal section of the brain, while visual stimuli were projected to the right side of the stage. Down: side view. The eyes movements were recorded by an infrared camera situated below the stage. In blue, excitation path. In green, detection path. The control and data acquisition hardwares are not shown. Adapted from the thesis of Adrien Jouary [Jouary, 2015].

sectioning by exciting all the fluorophores in one plane at the same time, thanks to a scanning mirror that creates an horizontal sheet from a focused laser beam. Very fast frame rates can be achieved because all the pixels of one plane are recorded in parallel at high speed using a CMOS or CCD camera, the only limitations being the amount of light

one can supply and the maximum frame rate of the camera. A single plane of the larva's brain, containing usually thousands of neurons, can thus be recorded at very high frame rate (up to 100 Hz), or the brain can be scanned in depth to provide multiple planes, that allow to monitor very large number of neurons, up to virtually the entire brain of a zebrafish larva (which contains approximately 100,000 neurons) at lower frame rates [Panier et al., 2013, Ahrens et al., 2013].

This latter use of the SPIM is what I did during my PhD, to study the mechanisms underlying the perceptual switch at the whole-brain level. 40 planes were acquired with the Hamamatsu Orca Flash 4.0 sCMOS camera at a rate of 2 Hz per plane, spanning 200 µm and approximately 50,000 neurons ($\approx$ 50% of the whole brain). The larva was placed dorsal-side up in a tube of 2% agarose, with the agarose removed around the eyes to let them free to move. Visual stimulation was projected on a screen on the right side of the tank, while the laser was coming from the left side. In this set-up, I used a visible blue laser (488 nm) to probe the calcium sensor, which means that the larva was able to see the light but as this is a constant light and we calibrated each time the laser so that it didn't come into the eye of the larva it should not provide salient sensory cues. The quality of the blue laser beam was improved by adding a clean-up filter (BP 5 nm, 488nm) and a single-mode fiber. A scheme of the set-up can be observed in Figure 2.4.

The detection path consisted of a water-dipping objective (16x, 0.8 NA, Nikon) mounted on a piezo objective positioner. A band-pass filter (525-50, Semrock) and low-pass filter (FF01-680, Semrock) filtered the infrared and laser light in order to image the green GCaMP6f fluorescence signal.

With this first set-up, the brain part that is situated between the eyes of the fish (mostly habenula and telencephalon) was not accessible because the laser cannot go through the eyes. Thus we tried to overcome this downside by adding a second light-sheet illumination coming from the front of the animal. For the results explained in chapter 4, I used mostly the first version of our custom-built SPIM, but I discuss also results from the second version.

2.3.3 Calcium imaging data analysis

The extraction of significant events from the acquired calcium imaging data were performed using custom-made programs in Matlab (The MathWorks, Inc.) and Python, as well as a Matlab toolbox developed by Sebastian A. Romano in the lab [Romano et al., 2017]. Several steps are needed in order to obtain the fluorescence traces from every neuron across time :

- **Planes separation** (only necessary for the SPIM data). During the recording in

the light-sheet microscope, the 40 planes are recorded in parallel and for the next steps we then need to separate the planes to obtain each plane independently across time. It is done quite easily thanks to a sorting algorithm.

- **Image registration**. During the recording in the two-photon scanning microscope, a custom-made plugin for ScanImage allowed us to compensate online for any possible drift in the Z plane, by calculating every 100 frames the correlation of the plane being imaged with the first imaged plane and two other planes 2.2 µm dorsal and ventral to the initial plane. If the correlation was greater with another plane than the original one, the stage was moved up or down accordingly by 0.44 µm. If the videos displayed drifts in the ventro-dorsal direction despite this online curation, the experiment was discarded. For the SPIM data, the registered stacks are manually inspected after the recording to evaluate the drift in the ventro-dorsal direction, and experiments with such drifts were discarded. The series of images during a given experiment were saved as TIFF stacks. To compensate for possible slow drifts in the XY plane, we registered the stacks using the Image J plugin Template Matching, in combination with a custom-made algorithm (Matlab, The MathWorks, Inc) to further smooth the registration. This program allowed us to choose a reference plane in the middle of the recording and then calculated for each frame the position in which there is the maximum value of the cross-correlation with the reference frame.

- **Artifacts removal**. Movement artifacts were detected according to large deviations in the cross-correlation between successive frames. All frames with large deviations (z-score smaller than -3) were then manually inspected. Due to the agarose elasticity, the imaging plane almost invariantly returned to its original position, after observing movement artifacts. If this was not the case, the complete experiment was discarded. For the subsequent data analysis, we did not include frames showing moving artifacts.

- **Image segmentation**. Regions of interest (ROIs) corresponding to the imaged neurons were semi-automatically detected based on morphology according to a watershed algorithm [Romano et al., 2017]. Because the fluorescence of the H2B-GCaMP6f is located in the nuclei, the algorithm identified neurons by finding local fluorescence intensity peaks. This program produced putative ROIs layouts that were afterwards manually curated.

- **Fluorescence traces measurement**. For each neuron, the fluorescence time signal is extracted by evaluating the average intensity across the pixels in each ROI for each registered frame. The baseline fluorescence is calculated for each ROI as a smooth estimate over a 30s-long running window. Slow fluctuations unrelated to

the calcium transients are possible and are captured in this estimated baseline. The relative variation in fluorescence intensity $\frac{\Delta F}{F}$ is then calculated as

$$\frac{\Delta F}{F} = \frac{F(t) - baseline(t)}{baseline(t)}$$

A data sanity test afterwards discarded ROIs whose fluorescence signal was too low and/or presented artifactual fluorescence traces, usually corresponding to auto-fluorescence of the skin or laser artifacts. In order to infer the calcium related fluorescence events associated with neuronal activity, we calculated the statistical significance of single-neuron calcium dynamics in an adaptive and unsupervised manner. We considered that any event in the fluorescence time series data belongs to either a neuronal activity process, or to an underlying noisy baseline. In order to discriminate, with a desired degree of confidence, between these two sources, we built a data-driven model of the noise. Moreover, we took into account the biophysical constraints of the fluorescent calcium indicator (H2B-GCaMP6f fluorescence decay time constant 2.88s [Kawashima et al., 2016]). Then, we applied a Bayesian odds ratio estimation framework. This method labels as significant with at least 95% confidence the fluorescence data points whose dynamics meet two conditions: i) it cannot be explained by the underlying fluorescence noise; ii) they are compatible with the H2B-GCaMP6f time constant. We obtained significantly and non-significantly active portions of the ΔF/F traces. A more detailed explanation of the calculation significance can be found in [Romano et al., 2015]. Because of the size of the SPIM data ($\approx$350GB by fish by experiment), this method for calculating the significant events was too demanding, and the significant calcium transients in the SPIM data were calculated as the time points where $\frac{\Delta F}{F}$ is above 3 standard deviations of the baseline noise. Both $\frac{\Delta F}{F}$ and the significant calcium transients were used in the analyses.

The pipeline presented above is the one that was followed for each calcium imaging experiment. The details of analyses carried out specifically for each experiment are explained in the corresponding sections of the upcoming chapters.

3

Fourier motion processing in the optic tectum and pretectum of the zebrafish larva

Before creating an ambiguous stimulus to study the representation of switches in visual perception, it is interesting to decipher the differences in visual motion processing in the optic tectum and pretectum. Visual motion signals are composed of several features that the visual system needs to extract to detect movement. Fourier signals, or first-order signals, represent the luminance-defined features of the image, while the non-Fourier (second-order) signals correspond to other features such as edges, contrast, texture and so on. Studies using modified square-wave moving gratings in which the first-Fourier component was suppressed (missing-fundamental signal), showed that the perception of movement is dominated by the Fourier components of the signal (see Introduction section 1.1.1).

In zebrafish, when the missing-fundamental stimulus is presented to larvae, they constantly follow the direction of the Fourier energy rather than that of the other features [Orger et al., 2000]. Despite these advances on the behavioral analysis of Fourier motion signals, their representation in sensory brain areas of the zebrafish remains elusive.

To address this question, we used two-photon Ca^{2+} imaging of the pretectum and optic tectum of zebrafish larvae, in combination with visual stimuli in which we separated the Fourier energy from the rest of the features.

Using this approach, we found:

1. **The zebrafish larva mainly uses Fourier energy to detect visual motion**

   We monitored the zebrafish optokinetic response (see section 1.2.3) induced by square-wave and missing-fundamental moving stimuli. We observed that the zebrafish larva detects the missing-fundamental stimulus as moving in the opposite direction compared to the square-wave signal, even though its non-Fourier features (other features than the luminance) move in the same direction than the square-wave ones. Motion detection in zebrafish thus seems to follow the direction of the Fourier energy and not other stimulus' features (edges, contrast,...).

2. **The activity in the optic tectum represents several features of the presented stimuli**

   We found that the optic tectum responds to several features of the presented static and moving stimuli, including the contrast patterns, spatial frequency, the direction of a moving square-wave stimulus, etc. However, it did not represent the direction of the missing-fundamental moving stimuli in which the Fourier energy and second-order information is not coherent. It also did not show any topographic representation of these different features, apart from a lateralization of the representation of square-wave motion direction.

3. **The activity in the pretectum mainly represents the Fourier energy of the stimulus**

   In contrast to the optic tectum, the pretectum mainly responded to the motion of the Fourier energy of the stimulus regardless of the type of stimulus presented. It also shows a clear topographic representation of the Fourier energy direction in its caudal part.

In conclusion, we suggest that the optic tectum plays a role in the extraction of the different features of static (contrast patterns and spatial frequency) and moving stimuli (Fourier and second-order features), while the pretectum mainly responds to the Fourier energy of a moving visual stimulus to generate OKR and OMR.

In the following pages is enclosed the article, published in *Frontiers in Neural Circuits* [Duchemin et al., 2022], detailing the results summarized here.

frontiers in Neural Circuits

ORIGINAL RESEARCH
published: 07 January 2022
doi: 10.3389/fncir.2021.814128

Fourier Motion Processing in the Optic Tectum and Pretectum of the Zebrafish Larva

*Auriane Duchemin, Martin Privat and Germán Sumbre**

Institut de Biologie de l'ENS (IBENS), Département de Biologie, Ecole normale supérieure, CNRS, INSERM, Université PSL, Paris, France

In the presence of moving visual stimuli, the majority of animals follow the Fourier motion energy (luminance), independently of other stimulus features (edges, contrast, etc.). While the behavioral response to Fourier motion has been studied in the past, how Fourier motion is represented and processed by sensory brain areas remains elusive. Here, we investigated how visual moving stimuli with or without the first Fourier component (square-wave signal or missing fundamental signal) are represented in the main visual regions of the zebrafish brain. First, we monitored the larva's optokinetic response (OKR) induced by square-wave and missing fundamental signals. Then, we used two-photon microscopy and GCaMP6f zebrafish larvae to monitor neuronal circuit dynamics in the optic tectum and the pretectum. We observed that both the optic tectum and the pretectum circuits responded to the square-wave gratings. However, only the pretectum responded specifically to the direction of the missing-fundamental signal. In addition, a group of neurons in the pretectum responded to the direction of the behavioral output (OKR), independently of the type of stimulus presented. Our results suggest that the optic tectum responds to the different features of the stimulus (e.g., contrast, spatial frequency, direction, etc.), but does not respond to the direction of motion if the motion information is not coherent (e.g., the luminance and the edges and contrast in the missing-fundamental signal). On the other hand, the pretectum mainly responds to the motion of the stimulus based on the Fourier energy.

Keywords: zebrafish, Fourier motion, visual system, two-photon calcium imaging, neuronal circuit dynamics

OPEN ACCESS

Edited by:
Masahito Yamagata,
Harvard University, United States

Reviewed by:
Georg Zoidl,
York University, Canada
Yuko Sugita,
Osaka University, Japan

***Correspondence:**
Germán Sumbre
sumbre@bio.ens.psl.eu

Received: *15 November 2021*
Accepted: *13 December 2021*
Published: *07 January 2022*

Citation:
Duchemin A, Privat M and Sumbre G (2022) Fourier Motion Processing in the Optic Tectum and Pretectum of the Zebrafish Larva. Front. Neural Circuits 15:814128. doi: 10.3389/fncir.2021.814128

1. INTRODUCTION

Visual motion signals are composed of several features that the visual system needs to extract to detect movement. The specific features driving motion detection have been extensively studied. Fourier signals, or first-order signals, represent the luminance-defined features of the image, while the non-Fourier (second-order) signals correspond to other features such as edges, contrast, etc. Studies using modified square-wave moving gratings in which the first-Fourier component was suppressed (missing-fundamental signal), showed that the perception of movement is dominated by the Fourier components of the signal. Fourier transform of a pure square-wave results in its fundamental frequency and its odd harmonics (third, fifth, seventh, and so on), such that they have, respectively, amplitudes of one-third, one-fifth, one-seventh, etc. of the amplitude of the fundamental frequency. Using Fourier decomposition, it is possible to create a stimulus that has a Fourier motion energy moving in the opposite direction to that of the other features (edges,

contrast, textures, etc.) by removing the fundamental frequency of the square-wave. This stimulus is called the missing-fundamental stimulus (sometimes also depicted as fluted-square-wave) (Adelson and Bergen, 1985; Chen et al., 2005).

In humans, moving the missing-fundamental stimulus induces motion ambiguity. The initial ocular pursuit responses are always in the direction of the Fourier energy, even though other features move in the opposite direction (Chen et al., 2005; Sheliga et al., 2005). The effect is also present in monkeys (Miura et al., 2006) and in mice (Sugita et al., 2012). In zebrafish, the effect is not limited to the initial ocular pursuit responses: when the missing-fundamental stimulus is presented to larvae, they constantly follow the direction of the Fourier energy rather than that of the other features (Orger et al., 2000).

Despite these studies describing the psychophysical effects of Fourier motion and the missing-fundamental signals, their representation in sensory brain areas remains elusive.

Here, we use behavior, two-photon Ca2+ imaging of transgenic zebrafish larvae expressing the genetically encoded Ca2+ indicator GCaMP6f, to monitor the visual responses of the optic tectum and the pretectum to moving grids consisting of square-wave and missing-fundamental signals.

To assess the larva's detection of the direction of the moving stimuli, we used the optokinetic response (OKR). The OKR consists of slow eye rotations (pursuits) in the direction of the detected motion followed by rapid saccades in the opposite direction to reset the eyes position. It occurs in response to whole-field motion and serves to stabilize the external world on the retina of the fish (Huang and Neuhauss, 2008; Portugues and Engert, 2009).

In zebrafish, the optic tectum, homologous to the mammalian superior colliculus, mediates the detection of visual information, integrates multiple sensory modalities (Thompson et al., 2016) and generates goal-directed behaviors such as prey capture (Romano et al., 2015; Förster et al., 2020). The pretectum, homologous to the accessory optic system in mammals (Matsuda et al., 2021), is involved in optic flow processing and controls the optokinetic and optomotor responses (OKR and OMR). It has been shown that the pretectum is necessary and sufficient for the OKR (Kubo et al., 2014). The pretectum integrates monocular information to create binocular representation, that is essential for the optomotor response (Naumann et al., 2016). Wang et al. (2020) showed that the tectum responds mainly to small stimuli in the upper nasal visual field (corresponding to the location of prey during hunting), while the pretectum represents larger stimuli in the lower visual field (optic flow). However, it should be noted that the pretectum has at least two functional regions, one that is responsive to optic flow and another one, more rostral, that is involved in prey detection (Semmelhack et al., 2014). The latter region is retinotopic and innervated by the temporal retina, which creates a high-resolution representation of the anterior visual field (where the preys are located before being captured) (Robles et al., 2014).

Here, we found that the missing-fundamental signal and the square-wave signal, although capable of inducing a similar behavioral output, are processed differently by the larva's visual centers. The optic tectum did not show responses to the direction of the missing fundamental signal, although it did so to the direction of the square-wave signal. In contrast, the pretectum displayed activity specifically associated with the detected direction of motion (optic flow) independently of the type of stimulus presented, including the missing-fundamental signal. Our results suggest that the optic tectum cannot extract the direction of motion from the Fourier energy alone, in case the luminance and the other non-Fourier features of the signal display incoherent or ambiguous directional information. On the other hand, the Fourier energy seems to be sufficient for the pretectum to represent the general direction of optic flow.

2. MATERIALS AND METHODS

2.1. Ethics Statement

All experimental procedures were approved by the comité d'éthique en expérimentation animale n°005. Reference number APAFIS#27495-2020100614519712 v14.

2.2. Animals

All experiments were performed using zebrafish larvae from 7 to 9 days post-fertilization (dpf), expressing pan-neuronally the GCaMP6f indicator (HuC:H2B-GCaMP6f (from Dunn et al., 2016) on a *nacre* (mitfa -/-) background (Lister et al., 1999). The embryos were collected and raised at 28°C in 0.5x E3 embryo medium (E3 in mM: 5 NaCl, 0.17 KCl, 0.33 CaCl2, 0.33 MgCl2 pH 7.2). Larvae were kept under 14/10 h on/off light cycles and fed after 5 dpf with Paramecia.

2.3. Visual Stimulation

The larvae were placed in the center of a chamber surrounded by a screen. Visual stimuli were projected on the screen using a pico-projector (AAXA P4X). The stimulation field covered approximately 180°x60° (azimuth x height) of the larva's visual field. All stimuli were generated using Matlab (The MathWorks, Inc) and the Psychophysics Toolbox Version 3 (Brainard, 1997; Kleiner et al., 2007) extension. A geometrical deformation was imposed on the stimuli to take into account the curvature of the chamber, so not to affect the spatial frequency of the stimulus. To prevent interference of the visual stimulus with the emission of the GCaMP signal, we only used the red light LED of the projector (620 nm), and added to the projector a 561nm long-pass filter (BLP01-561 Semrock). The luminance of the black part of the screen (*Imin*) was 8 lux, and the luminance of the red part of the screen (*Imax*) was 800 lux. The contrast was calculated as 0.98 (Michelson contrast, commonly used for periodic functions: $\frac{(Imax-Imin)}{(Imax+Imin)} = \frac{792}{808} = 0.98$).

2.3.1. Generation of the Missing-Fundamental and the Square-Wave Visual Stimuli

The square-wave gratings moved with a velocity of 180°/s and each bar corresponded to 16° of visual angle. This stimulus is known to induce the optokinetic response (OKR). To generate the missing-fundamental stimulus, we subtracted the principal Fourier component F1 (fundamental) of the square-wave stimulus (F1 = 0%). When this stimulus is presented in quarter-cycle jumps, it induces in the larva OKR in the opposite

direction compared to the physical motion of the edges and features of the stimulus. This is because we create a movement by shifting the frames by quarter-wavelength steps (compared to the original square-wave). In this case, the third harmonic of the signal moves forwards by three-quarters of its own wavelength. In other words, it appears to move backwards by one-quarter of its wavelength. As the third harmonic is also the strongest Fourier component in the missing-fundamental stimulus, the latter appears to the larva as moving backwards as well, even though the rest of its features move forwards. A third stimulus that we projected to the larvae was a square-wave signal with the same velocity but with a spatial frequency of one-third of the first signal (approximately 5.3° of visual angle), that corresponds to the third harmonic of the first signal and to the highest power of harmonic in the missing-fundamental stimulus. This signal also induces OKR in the opposite direction compared to the first square-wave stimulus, but in contrast to the missing-fundamental signal, all its features go in the same direction.

The visual stimulation paradigm was composed of 4 min of a black screen to account for spontaneous activity baseline, followed by the 3 different stimuli (square-wave, missing-fundamental and 3rd harmonic signals, **Figure 1A**) were projected 20 times in each direction (left or right) in a random order. Each time the stimulus was projected for 8 s without movement (static) then it was moved either to the left or the right for 12 s, to avoid any interference of the potentially induced motion aftereffect by the previous moving stimulus (Pérez-Schuster et al., 2016).

To test whether the missing-fundamental signal depends on the orientation of the stimulus, we used the same missing-fundamental signal as before but moving in one of the 4 orthogonal directions (down, up, left or right). Each of these 4 directions of movements was presented to the larvae 10 times for 30 s, separated by 30 s of a black background and 30 s of a static missing-fundamental signal (horizontal or vertical according to the direction), and we presented also 10 times 30 s of a static square-wave stimulus.

2.4. Behavioral Assay

To monitor the visually induced eye rotations, we placed the larva in a drop of 2% low-melting point agarose in the center of a recording chamber. The agarose around the eyes was carefully removed to allow the eyes to rotate freely. The visual stimuli were projected on a screen (#216 White Diffusion, Rosco Cinegel) around the chamber using a pico-projecter (AAXA P4X). To record the eye movements, we illuminated the larva with a infrared LED (820 nm) and placed, above the chamber, an infrared video camera (DMK 22BUC03, The Imaging Source). To synchronize the video recordings with the visual stimuli we used an arduino board. Using the Bonsai program (Lopes et al., 2015), we first converted the original image into a binary one by thresholding the image. We then calculated the orientation of each eye by measuring the orientation of the ellipsoid corresponding to each eye against an arbitrary x axis. As this angle depended on the orientation of the larva, the average for each eye was then subtracted to obtain a zero baseline for all larvae. Using a semi-automatic custom-built program in Matlab (The MathWorks, Inc), we detected the saccades from the eye orientation traces and calculated the orientation of each saccade (Pérez-Schuster et al., 2016). The behavior was then sorted automatically into those three types: either spontaneous, pursuits to the right or pursuits to the left. If two consecutive saccades were alternating in their direction, the behavior was classified as spontaneous rotations. If two consecutive saccades were both going from the left to the right, the pursuits were from the right to the left thus the behavior was sorted as pursuits to the left. Inversely, if two consecutive saccades were from the right to the left, the behavior was classified as pursuits to the right.

2.5. Two-Photon Ca2+ Imaging

For the two-photon Ca2+ recordings we used the same approach as for the behavioral essays, however the eyes were not released from the agarose. The two-photon system consisted of a modified version of the MOM (Movable Objective Microscope) system (Sutter Instruments) with a 25x NA 1.05 Olympus objective and a Mai-Tai DeepSee Ti:sapphire laser (Spectra-Physics) tuned at 920 nm. The output power at the focal plane was less than 3 mW. The emission of the GCaMP signal passed through a FF705 dichroic filter, an AFF01-680 short-path filter (IR Blocker), and an FF01 520/70 band-pass filter (all from Semrock), and collected by a photomultiplier tube (H1070 GaAsP from Hamamatsu). The emission signal was pre-amplified with a SR-570 (Stanford Research Systems) and reconstituted and saved using *ScanImage 3.8* software (Pologruto et al., 2003) in Matlab (The MathWorks, Inc.). To synchronize the neuronal recordings with the visual stimuli we used an arduino board. We recorded from the optic tectum and the pretectum at an acquisition rate of 3.91 Hz, with 256x256 pixels resolution.

2.6. Data Analysis of Ca2+ Dynamics

2.6.1. Registration

During the recording, a custom-made plugin for ScanImage allowed us to compensate online for any possible drift in the Z plane, by calculating every 100 frames the correlation of the plane being imaged with the first imaged plane and two other planes 2.2 μm dorsal and ventral to the initial plane. If the correlation was greater with another plane than the original one, the stage was moved up or down accordingly by 0.44 μm. If the imaged sequences displayed drifts in the ventro-dorsal direction despite this online curation, the experiment was discarded. The series of images during a given experiment were saved as TIFF stacks (10,900 frames). To compensate for possible slow drifts in the XY plane, we registered the stacks using the Image J plugin Template Matching, in combination with a custom-made algorithm (Matlab, The MathWorks, Inc.) to further smooth the registration.

2.6.2. Movement Artifacts

Movement artifacts were detected according to large deviations in the cross-correlation between successive frames. All frames with large deviations (z-score smaller than -3) were then manually inspected. Due to the agarose elasticity, the imaging plane almost invariantly returned to its original position, after observing movement artifacts. If this was not the case, the

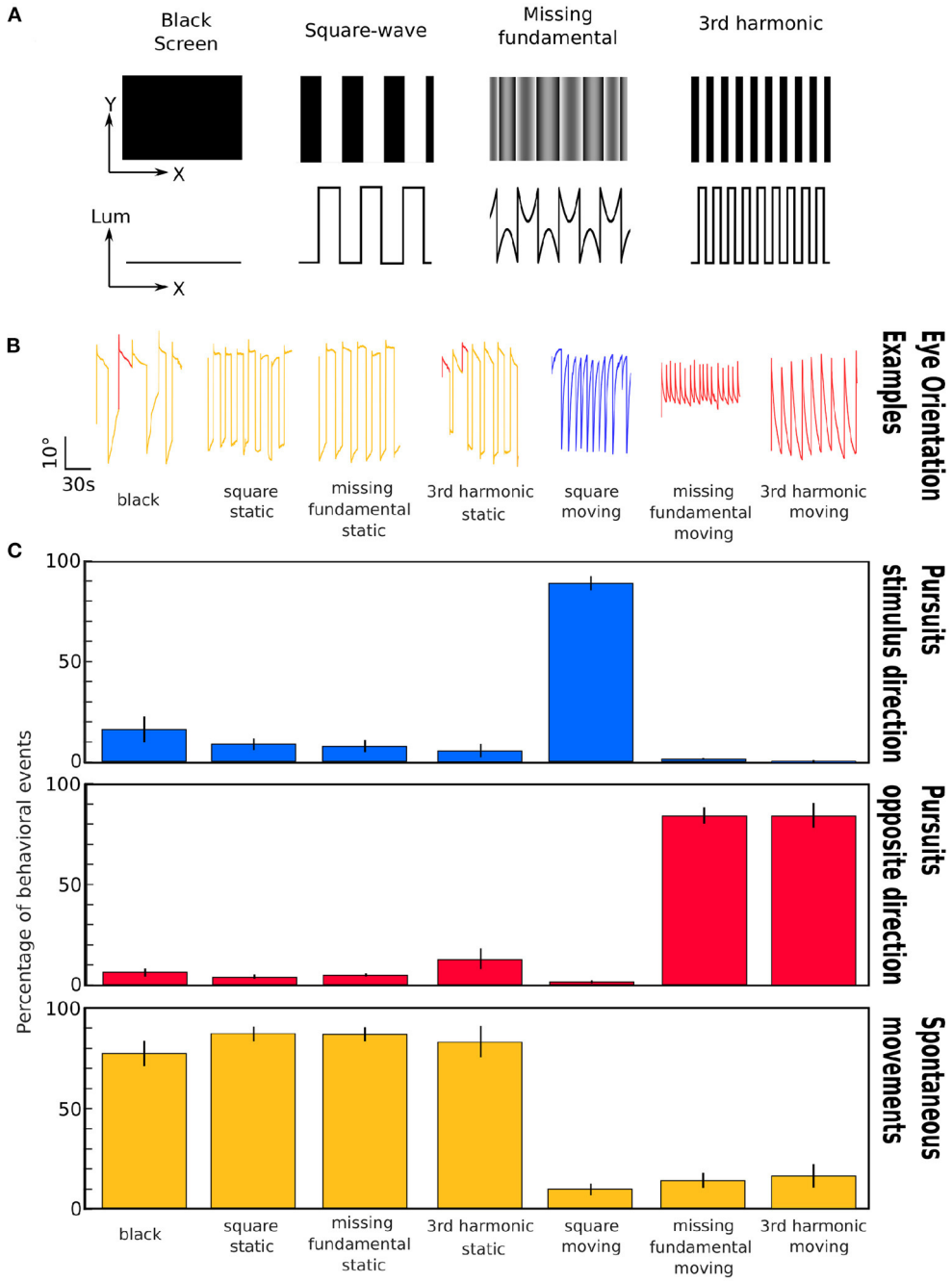

FIGURE 1 | Representation of the different stimuli and induced eye movements. **(A)** Images corresponding to the different stimuli projected to the larvae. First row: visual appearance of the stimuli; Second row: Plot of the luminance as a function of spatial position across the x axis. **(B)** Examples of the eye orientation traces induced by the different types of visual stimuli: black screen, static square-wave signal, static missing-fundamental signal, static 3rd harmonic signal, moving square-wave signal, moving missing-fundamental signal and moving 3rd harmonic signal. Yellow: spontaneous movements; blue: pursuits in the stimulus direction; red: pursuits in the opposite direction. **(C)** Percentage of behavioral events (pursuits in the direction of the stimulus' motion, pursuits in the opposite direction, spontaneous rotations) for the seven presented stimuli. The error bars represent the standard error of the mean. The behavioral experiment was performed on n = 6 larvae. Values as means±S.D.: Black: stimulus direction 16.3 ± 15.8%; opposite direction 6.3 ± 5.0%; spontaneous 77.4 ± 15.7%; p_anova = 2.10^{-7}. Static square-wave: stimulus direction 8.9 ± 6.9%; opposite direction 4.0 ± 2.7%; spontaneous 87.1 ± 8.7%; p_anova = 8.10^{-13}. Static missing-fundamental: stimulus direction 8.0 ± 7.5%; opposite direction 5.1 ± 1.7%; spontaneous 86.9 ± 8.3%; p_anova=8.10^{-13}. Static 3rd harmonic stimulus: stimulus direction 5.4 ± 7.9%; opposite direction 12.6 ± 12.4%; spontaneous 82.0 ± 19.0%; p_anova = 1.10^{-7}. Moving square-wave: stimulus direction 89.0 ± 8.7%; opposite direction 1.1 ± 1.8%; spontaneous 9.9 ± 7.3%; p_anova=5.10^{-13}. Moving missing-fundamental: stimulus direction 1.4 ± 1.8%; opposite direction 84.2 ± 9.9%; spontaneous 14.4 ± 9.2%; p_anova = 2.10^{-11}. Moving 3rd harmonic stimulus: stimulus direction 0.6 ± 1.5%; opposite direction 83.7 ± 15.0%; spontaneous 15.7 ± 14.3%; p_anova = 8.10^{-9}. See also **Supplementary Table 2** for more detailed statistical values.

complete experiment was discarded. For the subsequent data analysis, we did not include frames showing moving artifacts. In average, we detected 0.24% ± 0.08% of the total frames having moving artifacts.

2.6.3. Segmentation

Regions of interest (ROIs) corresponding to the imaged neurons were semi-automatically detected based on morphology according to a watershed algorithm (Romano et al., 2017). Because the fluorescence of the H2B-GCaMP6f is located in the nuclei, the algorithm identified neurons by finding local fluorescence intensity peaks. This program produced putative ROIs layouts that were afterwards manually curated. We then computed the changes in calcium associated to the activity of each imaged neuron by averaging the fluorescence of all pixels within the ROIs, across time.

2.6.4. Detection of Significant Calcium Events

The baseline of the time series of each neuron was computed as the 8th percentile in a 30 s-long running time window to obtain the slow fluctuations unrelated to the fast calcium transients associated with the neuronal activity (Romano et al., 2017). The relative change in fluorescence ($\Delta F/F$) corresponded to the difference between the fluorescence at each point in time and the baseline fluorescence. A data sanity test discarded ROIs with fluorescence signals too low and/or presenting artifactual fluorescence traces, i.e., sudden variation of the baseline fluorescence (as in unhealthy or dying neurons, or healthy neurons that drifted in and out of focus). In average, we discarded 3.6 ± 9.1% of the originally segmented neurons.

In order to infer the calcium related fluorescence events associated with neuronal activity, we calculated the statistical significance of single-neuron calcium dynamics in an adaptive and unsupervised manner (Romano et al., 2015, 2017; Pérez-Schuster et al., 2016). We considered that any event in the fluorescence time series data belongs to either a neuronal activity process or to an underlying noisy baseline. In order to discriminate, with a desired degree of confidence, between these two sources, we built a data-driven model of the noise (Romano et al., 2017). Moreover, we took into account the biophysical constraints of the fluorescent calcium indicator (H2B-GCaMP6f fluorescence time constant 2.88 s Kawashima et al., 2016). Then, we applied a Bayesian odds ratio estimation framework. This method labels as significant with at least 95% confidence the fluorescence data points whose dynamics meet two conditions: i) it cannot be explained by the underlying fluorescence noise; ii) they are compatible with the H2B-GCaMP6f time constant. We obtained significantly and non-significantly active portions of the $\Delta F/F$ traces. A more detailed explanation of the calculation significance can be found in Romano et al. (2015).

2.6.5. Determination of the Neurons Responsive to the Visual Stimuli

To find the neurons that were responsive to each type of presented visual stimulus, we measured the mean activity for each ROI:

$$mean\ activity\ during\ stimulus - mean\ activity\ during\ black$$

and from that the zscore:

$$zscore = \frac{mean\ activity - mean\ activity\ of\ all\ ROIs}{standard\ deviation\ of\ all\ ROI}$$

and discarded the ROIs that had a z-score inferior to –1. Then the ROIs were considered responsive if they showed at least 4 frames of significant activity (approximately 1 s) during the period of stimulation, in at least half of the repetitions of that stimulus.

2.6.6. Spatial Location of the Responsive Neurons

We recorded the neuronal activity from several larvae and we used custom-made algorithms in Matlab (The MathWorks, Inc.) to register all the neurons from the different larvae on the same reference brain. We chose a reference pretectal and tectal plane from a specific larva and calculated for each other larva the affine transformation that was necessary for aligning the individual plane to the reference one, with the help of anatomical landmarks. For the analysis, the neurons of interest from every larva could then be projected on the same reference brain.

2.7. Statistical Analysis and Reproducibility

To quantify and statistically compare the 3 types of behavior (spontaneous rotations, pursuits in the stimulus direction, pursuits in the opposite direction), we ran a One-Way ANOVA. When the p_anova value was less than 0.05, we ran a multiple comparison analysis between the different behaviors. We obtained a 95% confidence interval for each of the comparison and the associated *p*-values.

To assess the differences in the percentage of tectal vs. pretectal neurons that display the different response types, we used the non-parametric Wilcoxon rank sum test. To avoid false positive results that could happen due to the multiple number of response types, we corrected the *p*-values with the False Discovery Rate method from Benjamini and Hochberg (1995).

All values are reported as means ± SD throughout.

3. RESULTS

When confronted with moving visual stimuli, the majority of organisms follow the Fourier motion energy or luminance information, independently of other stimulus features such as edges or contrast. To investigate how Fourier components of moving visual stimuli are represented in the optic tectum and the pretectum (the main visual regions of the zebrafish brain), we presented to transgenic zebrafish larvae expressing pan-neuronally the genetically encoded calcium indicator GCaMP6f (Huc:H2B-GCaMP6f), vertical square-wave gratings and the corresponding missing-fundamental signal while monitoring neural circuits calcium dynamics by means of two-photon microscopy (see Materials and Methods).

To learn about the behavioral relevance of these two types of visual stimuli, we first monitored the eye movements along the horizontal plane (yaw) of the larva in the presence of square-waves or missing-fundamental stimuli. We classified the possible eye movements into three types: pursuits in the direction of the stimulation, pursuits in the opposite direction of the stimulus and spontaneous eye movements (see Materials and methods). The

stimulus paradigm consisted of projecting a black background for 5 min, then the static patterns of square-wave, missing-fundamental or 3rd harmonic stimuli for 5 min, and 5 min of moving square-wave, missing-fundamental or 3rd harmonic signals (**Figure 1A**). In parallel, we recorded the induced eye rotations of the larvae using a video camera (**Figure 1B** and **Supplementary Video 1**, see section 2).

During the black background presentation, the majority of the behaviors consisted of spontaneous eye rotations. Similar results were observed during the static square-wave, the static missing-fundamental or the static 3rd harmonic stimulus. During the moving square-wave stimulus, the majority of behaviors consisted of pursuits in the direction of the stimulus. During the presentation of the moving missing-fundamental stimulus the majority of eye rotations consisted of pursuits in the opposite direction of the stimulus. The same was observed for the moving 3rd harmonic stimulus (**Figure 1C** and **Supplementary Video 1**, **Supplementary Table 2**).

Therefore, motion detection in the zebrafish larva seems to follow the direction of the Fourier energy and not other stimulus' features (edges, contrast), as was previously observed using the optomotor response (Orger et al., 2000).

3.1. Visual Responses in the Optic Tectum and the Pretectum

To study the neuronal responses induced by the square-wave and the missing-fundamental stimuli, we performed two-photon calcium imaging of a dorsal optical plane of the optic tectum (n = 13 larvae), and of an optical plane of the pretectum (n = 7 larvae), while presenting to the larva the different types of visual stimuli. In addition to the square-wave signal and the missing-fundamental signal, we also projected to the larva a square-wave with the spatial frequency of the 3rd harmonic of the original square-wave (see **Figure 1A**). The latter served as a control since the larva detects its movement in the same direction as the missing-fundamental stimulus, but all of its features move in the same direction.

To classify the recorded neurons into groups according to their response patterns to the different features of the presented visual stimuli, we calculated for each neuron its z-score and the number of frames that it was significantly active during each of the presented stimuli (see Materials and Methods). The neurons were considered as responding to a given stimulus: 1) if they had a z-score >-1, 2) if they were active for at least 1s during the presentation of the stimulus, 3) if they were active for at least half of the repetitions of the stimulus. We then clustered the neurons according to their type of response. Most neurons were selectively responsive to a subset of the 6 different moving visual stimuli (**Figure 2**).

In the optic tectum, across all larvae, we found 3 neuronal groups (**Figures 2A,B**): 1) Neurons specifically responding to the square-wave stimulus to the right (18.6% of the responding neurons) and to the left (21.4%), with a small fraction of neurons responding to both directions (5.5%); 2) Neurons specifically responding to the missing-fundamental stimulus in both directions (15.0%), with just a small fraction responding to the right (4.3%) or to the left (3.6%); and 3) Neurons specifically responding to the 3rd harmonic stimulus to the right (6.7%) or to the left (3.8%). Other types of neurons represented less than 2% of the responding neurons. In the latter group, we found neurons responding unspecifically to all stimuli, neurons responding to the missing fundamental and the square-wave stimuli, and others responding to the square-wave signals independently of their spatial frequency. In total, the responding neurons to the different types of presented stimuli in the optic tectum represent 4.8 $\pm$ 0.4% of all recorded neurons.

We then reclassified the neurons according to their responses to the static and moving part of the presented stimuli (see Materials and Methods). We found that neurons responding to the square-wave and 3rd harmonic stimuli, responded specifically to the moving part of the stimulus. In contrast, most of the neurons responding to the missing-fundamental stimulus in both directions responded to the static part of the stimulus (61.6%), or to both the static and moving parts (36.0%) (**Supplementary Figures 3A,C**). Only a very small percentage responded specifically to the moving part (2.4%). We thus suggest that for the missing-fundamental stimulus, the tectal neurons mainly responded to the specific contrast pattern of the stimulus rather than to its motion (the local contrast in the missing-fundamental signal is different from that of the square-wave and the 3rd harmonic stimuli). This response does not represent a motion illusion induced by the static missing-fundamental signal since this stimulus induced spontaneous eye rotations rather than pursuit movements (**Figure 1C**). Overall, directional neurons in the optic tectum respond to moving visual stimuli when the Fourier energy and other movement feature are coherent. This directional response also depends on the spatial frequency of the stimulus.

In the pretectum, we found 5 neuronal groups (**Figures 2C,D**): 1) Neurons specifically responding to the square-wave stimulus to the right (11.7% of the responding neurons), to the left (8.8%), or to both directions (13.4%); 2) Neurons specifically responding to the missing-fundamental stimulus in both directions (13.3%), to the right (3.7%) or to the left (5.3%); 3) Neurons specifically responding to the 3rd harmonic stimulus to the right (4.2%) or to the left (4.8%); 4) Neurons responding to the square-wave to the left, the missing-fundamental to the right and the 3rd harmonic stimuli to the right (5.4%, corresponding to the larva's behavioral output: pursuits eye movements to the left), or just to the missing-fundamental and 3rd harmonic stimuli to the right (2.9%, corresponding to the behavioral output induced by the 3rd harmonic frequency going to the left); and 5) Neurons responding to the square-wave to the right, the missing-fundamental to the left and the 3rd harmonic stimuli to the left (5.4%, behavioral output to the right), or just to the missing-fundamental and 3rd harmonic stimuli to the left (3.7%, corresponding to the behavioral output induced by the 3rd harmonic frequency going to the right). Other types of neurons represented less than 2% of the total number of responding neurons. Overall, the responding neurons to the different types of presented stimuli in the pretectum represent 10.1 $\pm$ 1.3% of all recorded neurons. The groups 4) and 5) are populations of

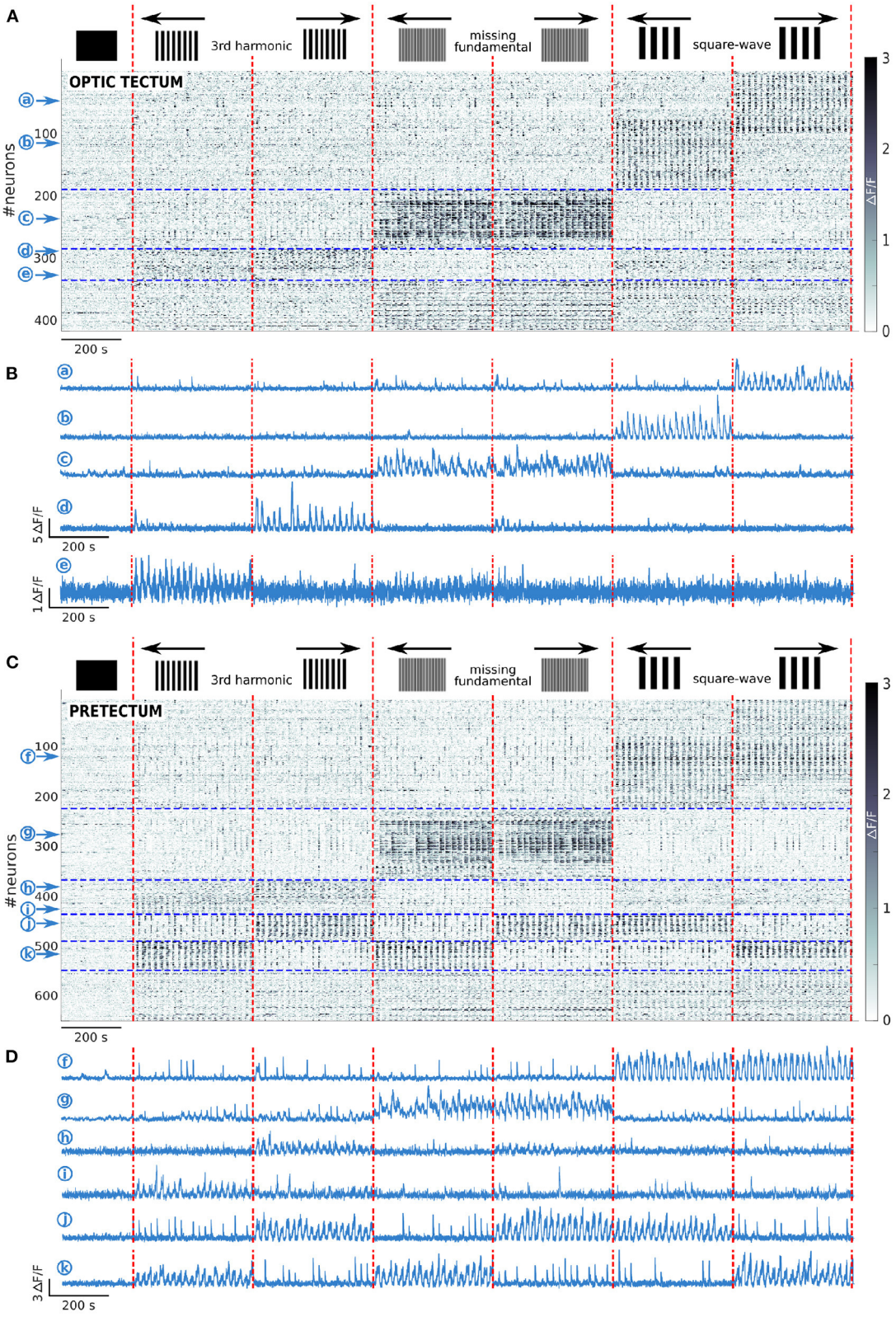

FIGURE 2 | Tectal and pretectal neuronal representation of the visual stimuli. **(A)** Raster of activity of the neurons responding to at least one of the presented stimuli in the optic tectum (n = 13 larvae). The imaged frames are sorted on the x axis so that stimuli of the same type are grouped together (separated by vertical red dashed

(Continued)

FIGURE 2 | lines). The neurons are sorted on the y axis according to the type of response they display (separated by horizontal blue dashed lines). Note that the frequency in the Ca2+ signal observed during the presentation of the stimulus is due to the alternation between static and moving stimuli. **(B)** Examples of the neuronal responses of 5 neurons of the optic tectum induced by the square-wave stimulus to the right (a), or the left (b), the missing-fundamental stimulus in both directions (c), the 3rd harmonic stimulus to the right (d), or the left (e). **(C)** Same as **(A)** but for the pretectum (n = 7 larvae). **(D)** Examples of the stimulus-induced activity of 6 neurons in the pretectum that responded to the square-wave stimulus in both directions (f), to the missing-fundamental stimulus in both directions (g), to the 3rd harmonic stimulus to the right (h), or to the left (i), according to the behavioral output to the left (j, 3rd harmonic and missing-fundamental stimuli to the right and square-wave stimulus to the left), according to the behavioral output to the right (k, 3rd harmonic and missing-fundamental stimuli to the left and square-wave stimulus to the right).

neurons that we did not observe in the optic tectum and that represent the Fourier motion direction independently of the other motion features of the stimulus (second order features), and also independently of the spatial frequency of the signal, corresponding to the behavioral output (following the direction of motion).

In the pretectum, we found that the neuronal population responding to the missing-fundamental stimulus in both directions was mostly responding to both the static and the moving part of the stimulus (67.0%), with less neurons responding only to the static part (24.1%) or only to the moving part (8.9%) (**Supplementary Figures 3B,C**).

The 6 different visual moving stimuli that we presented to the larvae could induce 2^6 different types of neuronal responses. To quantify the differences in the neuronal response types in both the optic tectum and the pretectum, we selected the response types for which we found at least 0.1% of the total recorded neurons in the pretectum or the optic tectum. This criteria revealed 17 different types of responses from the 64 possible ones (**Figure 3A**).

We found that the pretectum responded with a significantly larger portion of neurons than the optic tectum for 4 different classes of stimulus combinations. 1) Non-direction selective responses to the square-wave signal (neuron (a) in **Figure 3B**). 2) Non-direction selective response to the missing-fundamental stimulus (neuron (b) in **Figure 3B**), or direction selective responses to the left. The fact that we did not find a significant difference for the responses to the missing-fundamental stimulus going to the right might be due to the recordings of a non-uniform neuronal population across the entire circuit. 3) Neurons that responded to the Fourier motion energy in one or the other directions, regardless of the type of stimulus presented. For example, neuron (c) that responded to movement to the left or neuron (e) that responded to movement to the right (**Figure 3B**). 4) Neurons that responded specifically to the Fourier motion of the missing-fundamental and 3rd harmonic stimuli to the right (neuron (d) in **Figure 3B**), or to the left (neuron (f) in **Figure 3B**). These neurons are probably specific to a precise band of spatial frequencies including the 3rd harmonic frequency but not the frequency of the fundamental of the square-wave signal. We also found a significant difference for a small portion of neurons in the response to the missing-fundamental signal moving to the left and the square-wave stimulus moving to the right.

For the response to both directions, the neurons that respond are by definition not direction-selective. For these types of responses (square-wave, missing-fundamental or 3rd harmonic stimuli in both directions) the neurons are not responding to Fourier energy but to other components that we can only guess (edges, contrast, or motion in no specific direction). We argue that the pretectum detect Fourier energy through the direction-selective neurons (responses to either one or the other direction): the amount of response to the missing-fundamental signal to the left, missing-fundamental signal to the right, 3rd harmonic signal to the left or 3rd harmonic signal to the right are equivalent. Moreover, the responses to all signals that display the same Fourier motion direction (square-wave to the left, missing-fundamental to the right and 3rd harmonic to the right for the Fourier motion to the left; and square-wave to the right, missing-fundamental to the left and 3rd harmonic to the left for the Fourier motion to the right) are significantly larger in the pretectum than in the tectum.

Overall, we found that the pretectum show more non-direction selective responses to the square-wave and missing-fundamental stimuli than the optic tectum, and better responds to the Fourier energy motion of moving visual stimuli than the optic tectum, including the missing-fundamental signal.

3.2. Spatial Organization of the Visual Responses

To assess the topographic distribution of the responsive neurons to the different types of visual stimuli, we registered the position of all neurons of each larva to a single reference plane (see Materials and Methods) (**Figure 4**). In the optic tectum, the responses to the square-wave (**Figure 4A**) and the missing-fundamental signals (**Figure 4B**) were not spatially organized. The responsive neurons were sparsely distributed with the same fraction of neurons in both hemispheres (49.7% right vs. 50.3% left hemisphere for the square-wave signal, 47.9% right vs. 52.1% left hemisphere for the missing-fundamental signal). However, we observed a light lateralization of the responses to the direction of the square-wave moving stimulus (66.7% right vs. 33.3% left hemisphere for responses to the right, and 26.7% right vs. 73.3% left for responses to the left) (**Figure 4A**). In the pretectum, the responses to the square-wave signal were also sparsely distributed (49.5% right vs. 50.5% left hemisphere), with more neurons in the caudal (66.8%) than the rostral part (33.2%). We also observed a lateralization of the responses to the direction of the square-wave moving stimuli (65.8% right vs. 34.2% left hemisphere for responses to the right, and 26.3% right vs. 73.7% left for responses to the left) (**Figure 4C**). In contrast, the responses to the missing-fundamental signal were principally found in the rostral part of the pretectum (68.7%) rather than in the caudal part (31.3%), without showing a lateralization of the responses to

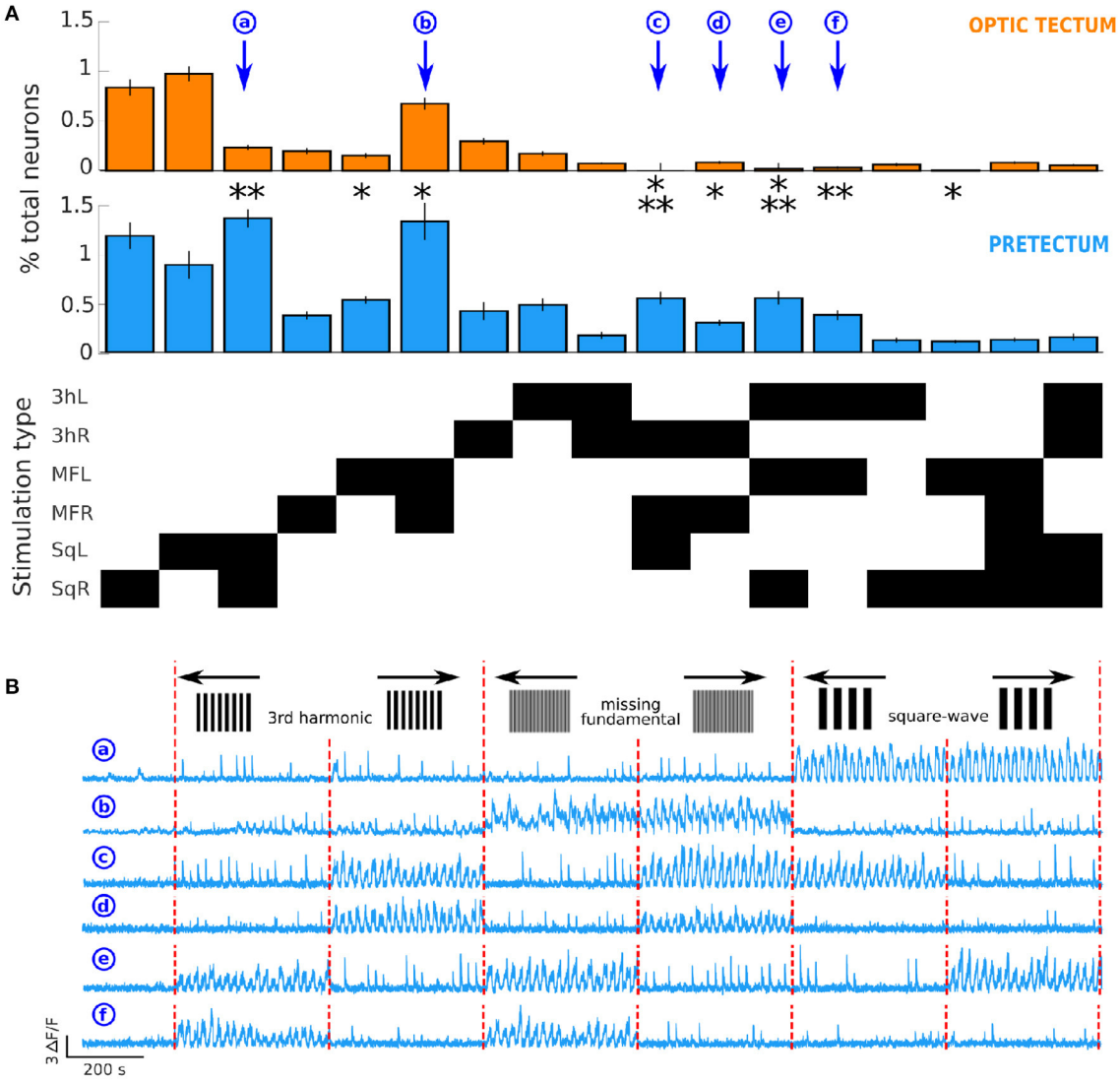

FIGURE 3 | Differences in neuronal response types in the optic tectum and the pretectum. **(A)** Top: proportion of neurons responsive to the different types of presented stimuli in the optic tectum ($n = 13$) and Middle: in the pretectum ($n = 7$). Bottom: The response types that involved ≥ 0.1% of the total recorded neurons in the optic tectum or the pretectum. The stimulation types are represented on the y axis, the black rectangles indicate the type of stimulation represented in top and middle panels. 3hL: 3rd harmonic signal to the left; 3hR: 3rd harmonic signal to the right; MFL: missing-fundamental signal to the left; MFR: missing-fundamental signal to the right; SqL: square-wave signal to the left; SqR: square-wave signal to the right. Wilcoxon rank sum test corrected with the false discovery rate: $^{*}p \leq 0.05$, $^{**}p \leq 0.01$, $^{***}p \leq 0.001$. Values as means±S.D.: Response to SqL and SqR (a): pretectum 1.34 ± 0.18% of all recorded pretectal neurons, optic tectum 0.24 ± 0.05% of all recorded tectal neurons, $p = 0.002$. Response to MFL: pretectum 0.52 ± 0.08%, optic tectum 0.16 ± 0.05%, $p = 0.014$. Response to MFL and MFR (b): pretectum 1.31 ± 0.99%, optic tectum 0.68 ± 0.43%, $p = 0.046$. Response to 3hR, MFR and SqL (c): pretectum 0.54 ± 0.13%, optic tectum 0 neurons, $p = 5.10^{-4}$. Response to 3hR and MFR (d): pretectum 0.30 ± 0.06%, optic tectum 0.08 ± 0.03%, p = 0.018. Response to 3hL, MFL and SqR (e): pretectum 0.54 ± 0.13%, optic tectum 0.02 ± 0.02%, $p = 7.10^{-4}$. Response to 3hL and MFL (f): pretectum 0.37 ± 0.10%, optic tectum 0.03 ± 0.02%, $p = 0.006$. Response to MFL and SqR: pretectum 0.11 ± 0.09%, optic tectum 0.01 ± 0.03%, $p = 0.014$. **(B)** Examples of the activity of 6 neurons of the pretectum that respond, respectively to the square-wave signal moving in both directions (a), to the missing-fundamental signal moving in both directions (b), according to the behavioral output to the left (c, 3rd harmonic and missing-fundamental signals to the right and square-wave signal to the left), to the 3rd harmonic and the missing-fundamental signals to the right (d), according to the behavioral output to the right (e, 3rd harmonic and missing-fundamental signals to the left and square-wave signal to the right), or to the 3rd harmonic and the missing-fundamental signals to the left (f). Vertical red dashed lines separate the different types of presented stimuli.

the direction of motion (45.8% right vs. 54.2% left hemisphere for responses to the right, and 50.0% right vs. 50.0% left for responses to the left) (**Figure 4D**). When we looked at the spatial organization of neurons responding according to the behavioral output (i.e., the type of eye rotation induced by the stimulus), we observed a clear topographic structure. Neurons responsive to visual stimuli that induced pursuit eye movements to the left were localized in the caudal part of the left hemisphere (85.7%

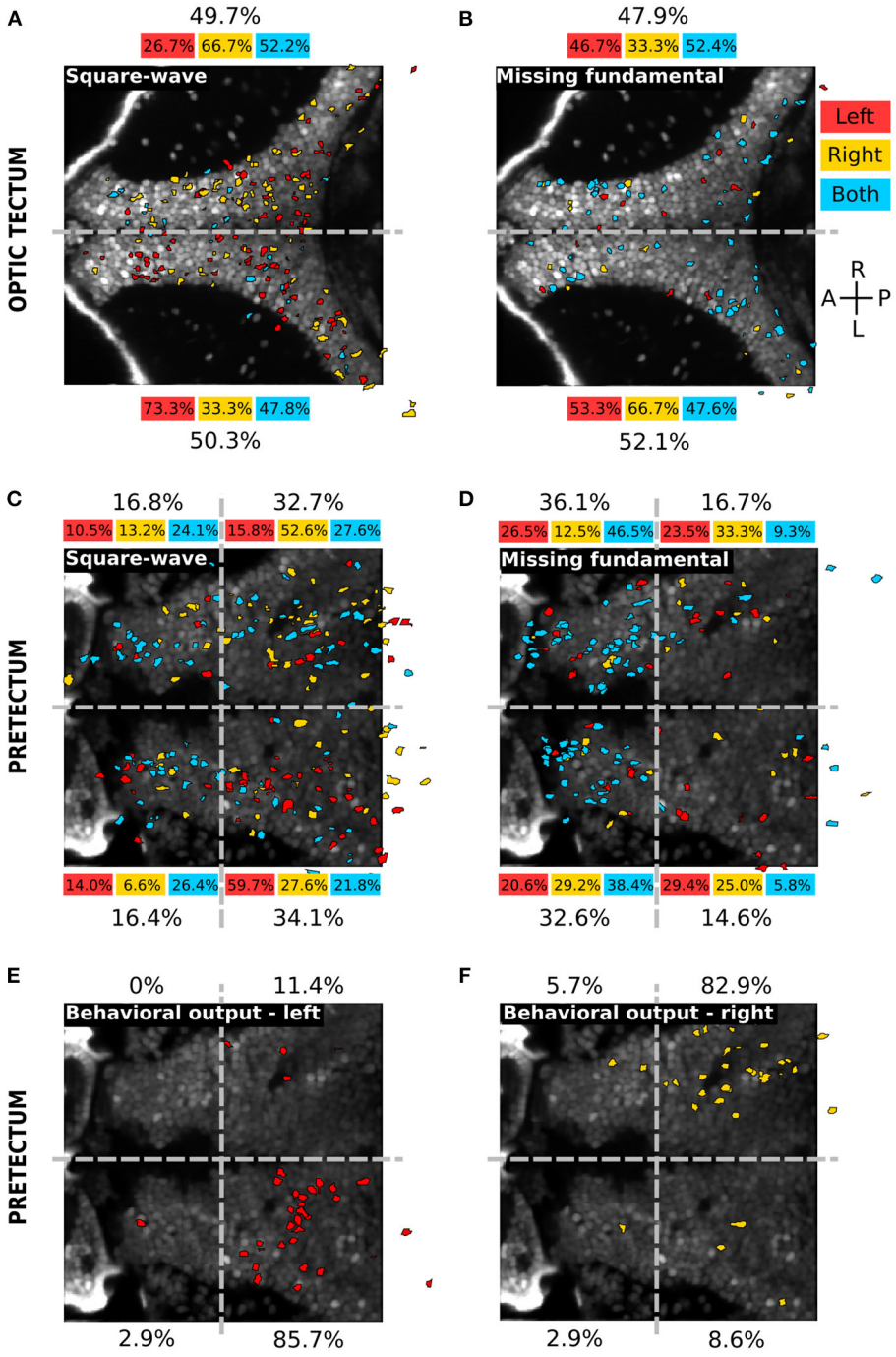

FIGURE 4 | Spatial distribution of the different neuronal response types in the optic tectum and the pretectum. **(A)** Spatial distribution of the neurons responding to the square-wave signal to the left (red), to the right (yellow) or to both directions (cyan), in the optic tectum ($n = 13$). The percentages on top and bottom indicate the proportion of responsive neurons in the right and left hemispheres, for the responses to the left (red), to the right (yellow), to both directions (cyan) or in global for the square-wave stimulus (black). Gray dashed line: midline. **(B)** Same as **(A)** for the missing-fundamental signal. Note that the responses to both left and right directions of the missing-fundamental signal (cyan) are mostly induced by the static missing-fundamental stimulus (**Supplementary Figure 3A**). **(C)** Spatial distribution of the neurons responding to the square-wave signal to the left (red), to the right (yellow) or to both directions (cyan) in the pretectum ($n = 7$). The percentages next to each quadrant indicate the proportion of responsive neurons in each region, for the responses to the left (red), to the right (yellow), to both directions (cyan) or in global for the square-wave stimulus (black). Gray dashed horizontal line: midline. Gray dashed vertical line: separates between the anterior and posterior part of the pretectum. **(D)** Same as **(C)** for the missing-fundamental signal. Note that the responses to both left and right directions of the missing-fundamental signal (cyan) are mostly induced by the static missing-fundamental stimulus (**Supplementary Figure 3B**). **(E)** Same as **(C)** according to the behavioral output to the left (response to 3rd harmonic and missing-fundamental signals to the right and square-wave signal to the left). **(F)** Same as **(C)** according to the behavioral output to the right (response to 3rd harmonic and missing-fundamental signals to the left and square-wave signal to the right).

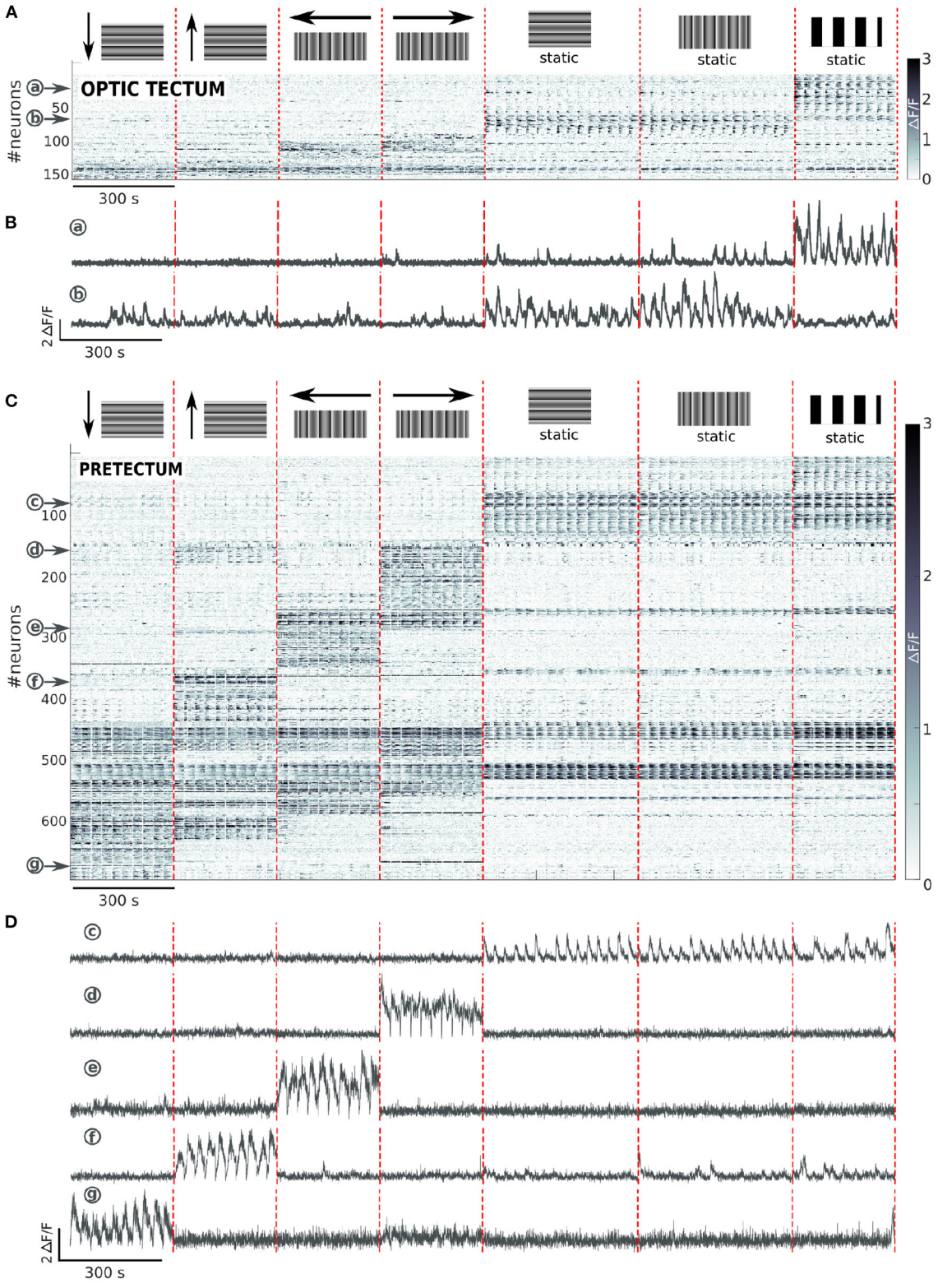

FIGURE 5 | Tectal and pretectal neuronal representation of different directions of the missing-fundamental stimulus. **(A)** Raster of activity of the neurons responding to at least one of the 4 directions of the missing-fundamental signal, or to the static missing-fundamental or square-wave, in the optic tectum ($n = 6$ larvae). The imaged frames are sorted on the x axis so that stimuli of the same type are grouped together (separated by vertical red dashed lines). The neurons are sorted on the y axis

(Continued)

FIGURE 5 | according to the type of response they display (separated by horizontal blue dashed lines). **(B)** Examples of the activity of 2 neurons in the optic tectum that respond, respectively to the static square-wave signal (a), or to the static horizontal and vertical missing-fundamental (b). **(C)** Same as **(A)** for the pretectum (n = 6). **(D)** Examples of the activity of 5 neurons in the pretectum that respond, respectively to the static vertical and horizontal missing-fundamental signal and the static square-wave signal (c), or to the missing-fundamental signal going to the right (d), to the left (e), up (f) or down (g).

of neurons, **Figure 4E**). Neurons responsive to visual stimuli inducing eye movements to the right were found in the caudal part of the right hemisphere (82.9% of neurons, **Figure 4F**). Therefore, the neuronal representation of the direction of the square-wave signal is spatially organized for the pretectum and the optic tectum. In contrast, the representation for the static missing-fundamental stimulus and the behavioral output were spatially organized in the pretectum but not in the optic tectum.

3.3. Visual Orientation Responses to the Missing Fundamental Stimulus

To investigate whether the observed neuronal responses to the missing-fundamental signal are dependent on the orientation of the stimulus, we presented to the larvae the missing-fundamental stimulus moving in 4 orthogonal directions: down, up (horizontal grating), left and right (vertical grating). We recorded from n = 6 larvae in the optic tectum and n=6 larvae in the pretectum. In the optic tectum, 4.5 ± 2.8% of the total recorded neurons were responsive to at least one of the directions or the static stimuli. We observed 2 types of neuronal responses (**Figure 5A**). 1) Neurons specifically responding to the static stimulus, either square-wave (34.4%, neuron a in **Figure 5B**) or horizontal (4.5%), vertical (4.5%) or both horizontal and vertical (7.0%, neuron b in **Figure 5B**) missing-fundamental signal. The latter neurons seemed to be responsive to the change of contrast and not the orientation. A few neurons also responded to any type of static stimuli (3.8%). 2) Neurons specifically responding to the different directions of orthogonal motion of the missing-fundamental stimulus: down (3.2%), up (2.5%), left (7.0%) or right (7.0%). Some neurons responded to both left and right directions (6.4%, orientation-selective neurons) but none were found to specifically respond both to up and down motion.

In the pretectum 10.9 ± 2.6% of the total recorded neurons were responsive to at least one of the directions or the static stimuli. We observed 3 types of neuronal responses (**Figure 5C**). 1) Neurons specifically responding to the static stimulus, either square-wave (8.8%) or horizontal (1.0%), vertical (4.3%) or both horizontal and vertical (1.5%) missing-fundamental signal. Neurons also responded to all static stimuli (5.5%, neuron c in **Figure 5D**). 2) Neurons specifically responding to the different directions of orthogonal motion of the missing-fundamental stimulus: right (10.1%, neuron d in **Figure 5D**), left (9.3%, neuron e in **Figure 5D**), up (9.9%, neuron f in **Figure 5D**) or down (9.8%, neuron g in **Figure 5D**). Some neurons were also orientation-specific, responding either to up and down (6.0%) or left and right (3.6%) motion. Other neurons were responding to visual motion regardless of its direction or orientation (3.0%). 3) Neurons responding not specifically to all types of stimuli (static and moving) (4.8%). The pretectal neurons responding to the 4 directions of the missing-fundamental moving stimulus were principally distributed in the caudal region (86.5% caudal vs. 13.6% rostral for the down direction; 86.6% caudal vs. 13.3% rostral for the up direction; 76.8% caudal vs. 23.2% rostral for the left direction; 78.7% caudal vs. 21.2% rostral for the right direction) (**Figure 6**). The horizontal directions moving stimuli induced responses specific to the ipsilateral hemisphere (67.9% of the responses in the left hemisphere during motion to the left, and 77% of the responses in the right hemisphere during motion to the right), but the responses to vertical directions did not show this lateralization (52.6% of the responses in the right vs. 47.5% in the left hemisphere for down motion, and 41.6% in the right vs. 58.3% in the left hemisphere for up motion). It is possible that the vertical directions are represented in the dorso-ventral axis and therefore impossible to observe when recording from a single optical plane, or alternatively according to the cell identity in the caudal region (different neurons in the caudal area respond to the up or down stimuli).

Overall, the pretectum represents in a topographic manner the 4 orthogonal directions of the missing-fundamental signal, but the optic tectum does not.

4. DISCUSSION

Several studies have demonstrated that the missing-fundamental stimulus induces motion perception in the direction of the Fourier energy in humans (Chen et al., 2005; Sheliga et al., 2005) and monkeys (Miura et al., 2006), and correlate with the behavioral output of the OKR in mice (Sugita et al., 2012) and the optomotor response (OMR) in zebrafish (Orger et al., 2000). Here, we showed that in zebrafish larvae, the presentation of a missing-fundamental moving visual stimulus induces OKR in the opposite direction of that induced by square-wave moving stimuli. The missing-fundamental stimulus has all motion features in the direction of the square-wave signal except for the Fourier energy which moves in the opposite direction. Thus, we suggests that OKR in zebrafish larvae principally follows the Fourier energy of the moving visual stimulus. We then investigated the neuronal representation of these two moving visual patterns (square wave vs. missing fundamental), in the two main visual centers of the larva: the optic tectum and the pretectum. We found that the activity in the pretectum mainly represents the eyes behavioral output regardless of the type of stimulus presented (square-wave, missing-fundamental or 3rd harmonic). Therefore, the pretectum represents the Fourier energy of the moving visual stimulus (in the missing-fundamental stimulus, the Fourier energy is the only feature that correlates with the direction

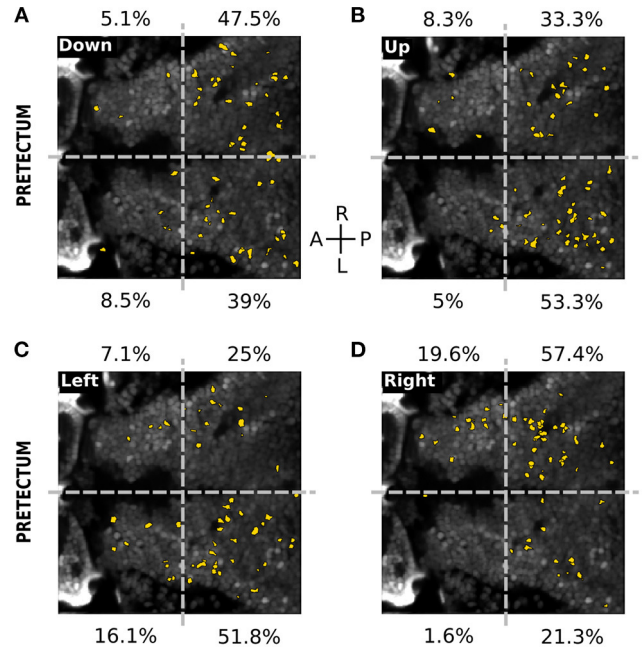

FIGURE 6 | Spatial distribution of neurons responding to the directions of the missing-fundamental signal in the pretectum. **(A)** Spatial distribution of the neurons (yellow) responding to the horizontal missing-fundamental signal moving downwards in the pretectum. The percentages next to each quadrant indicate the proportion of responsive neurons in each region. Gray dashed horizontal line: midline. Gray dashed vertical line: separates between the anterior and posterior part of the pretectum. **(B)** Same as **(A)** for the horizontal missing-fundamental signal moving upwards. **(C)** Same as **(A)** for the vertical missing-fundamental signal moving leftwards. **(D)** Same as **(A)** for the vertical missing-fundamental signal rightwards.

of the induced eye pursuits). In contrast, the optic tectum responds to the missing-fundamental stimulus, but rather to its contrast pattern than to its motion direction (the tectum responds to the static missing-fundamental stimulus but not to its movement). Our results are coherent with the fact that the pretectum has been shown to be necessary and sufficient for the OKR (Kubo et al., 2014) and that ablation of the optic tectum only minimally affects the kinematics of OKR (Roeser and Baier, 2003). Moreover, the pretectum is one of the main regions involved in the detection of optic flow (Matsuda et al., 2021), responding to large-field motion stimuli (Kubo et al., 2014).

In the optic tectum, the spatial structure of the visual responses to the different types of visual stimuli showed no topographic organization. This is in line with the finding that direction-selective neurons in the optic tectum are not topographically organized (Romano et al., 2015). In contrast, the pretectum showed responses to the direction of motion in the caudal part of the pretectum more than the rostral part (**Figures 4**, **6**). In line with our results, a rostrally located region of the pretectum has been shown to be involved in prey capture (Semmelhack et al., 2014), thus implying that the optic-flow responsive part of the pretectum is located in its caudal part.

In this study, we found that the rostral part of the pretectum is responsive mainly to the static missing-fundamental stimulus (**Figure 4**), suggesting that this part is reacting to the contrast pattern rather than the Fourier energy of the stimulus. The caudal region of the pretectum responded differently according to the direction of motion: each caudal hemisphere responded to Fourier energy toward one direction (left caudal: motion to the left—right eye moves in the temporal to nasal direction, and right caudal: motion to the right—left eye moves in the temporal to nasal direction). These observations are in agreement with the results obtained by Chen et al. (2016) showing that eye pursuits were longer in the temporal-to-nasal direction than the nasal-to-temporal direction, and Wang et al. (2019) that showed that pretectum's cells respond more to temporal-to-nasal than nasal-to-temporal monocular moving stimuli, together with the fact that the retina in zebrafish projects almost exclusively to the contralateral hemisphere of the brain (Burrill and Easter, 1994).

Finally, the optic tectum responded specifically to the static square-wave and missing-fundamental stimuli. In contrast, in the pretectum, the neurons responding to the static square-wave stimuli also responded to the static missing-fundamental.

Overall, we suggest that the optic tectum represents multiple features of visual motion (the Fourier motion but also the contrast, texture, edges, etc.). In case that Fourier energy does not coherently move in the direction of other features, the optic tectum cannot represent the direction of motion. In contrast, the pretectum's activity, mainly in its caudal part, represents the optic flow principally based on the Fourier energy information. A previous study showed that zebrafish larvae follow, using the OMR, second-order motion in the absence of Fourier content (Orger et al., 2000), thus it is possible that when confronted to only second-order motion, the optic tectum rather than the pretectum controls OKR and OMR. In conclusion, we suggest that the optic tectum plays a role in the extraction of the different features of static (contrast patterns and spatial frequency) and moving stimuli (Fourier and second-order features), while the pretectum mainly responds to the Fourier energy of a moving visual stimulus to generate OKR and OMR.

DATA AVAILABILITY STATEMENT

The toolbox used for the analysis of calcium dynamics is detailed in Romano et al. (2017) and is available in Github at this address https://github.com/zebrain-lab/Toolbox-Romano-et-al. The datasets as well as data analysis programs generated specifically for this study are available on request to the corresponding author.

ETHICS STATEMENT

The animal study was reviewed and approved by Comité d'éthique en expérimentation animale n°005. Reference number APAFIS#27495-2020100614519712 v14.

AUTHOR CONTRIBUTIONS

AD designed the experiment, recorded and analyzed data, and wrote the manuscript. MP wrote analysis programs and discussed data analysis. GS designed the experiment, advised data analysis, and wrote the manuscript. All authors contributed to the article and approved the submitted version.

FUNDING

This research was supported by the Labex Memolife, and the ENS Paris-Saclay Ph.D. fellowships to AD, the Fondation pour la Recherche Medicale and the ENS Lyon Ph.D. fellowship to MP, and the ERC CoG 726280 to GS. The funders had no role in the study design, data collection and analysis, decision to publish, or preparation of the manuscript.

ACKNOWLEDGMENTS

We would like to thank Veronica Perez-Schuster, Mario Dipoppa, Boris Gutkin and Anirudh Kulkarni for the preliminary ideas and protocols, and Virginie Candat and Firas Bouallague for the care of the fish and larvae. We want to thank also all members of the Sumbre lab for interesting discussions and ideas.

SUPPLEMENTARY MATERIAL

The Supplementary Material for this article can be found online at: https://www.frontiersin.org/articles/10.3389/fncir.2021.814128/full#supplementary-material

REFERENCES

Adelson, E. H., and Bergen, J. R. (1985). Spatiotemporal energy models for the perception of motion. *J. Opt. Soc. Am. A* 2, 284. doi: 10.1364/JOSAA.2.000284

Benjamini, Y., and Hochberg, Y. (1995). Controlling the false discovery rate: a practical and powerful approach to multiple testing. *J. R. Stat. Soc.* 57, 289–300. doi: 10.1111/j.2517-6161.1995.tb02031.x

Brainard, D. H. (1997). The psychophysics toolbox. *Spat. Vis.* 10, 433–436. doi: 10.1163/156856897X00357

Burrill, J. D., and Easter, S. S. (1994). Development of the retinofugal projections in the embryonic and larval zebrafish (*Brachydanio rerio*). *J. Compar. Neurol.* 346, 583–600. doi: 10.1002/cne.903460410

Chen, C.-C., Bockisch, C. J., Straumann, D., and Huang, M. Y.-Y. (2016). Saccadic and postsaccadic disconjugacy in zebrafish larvae suggests independent eye movement control. *Front. Syst. Neurosci.* 10:80. doi: 10.3389/fnsys.2016.00080

Chen, K. J., Sheliga, B. M., Fitzgibbon, E. J., and Miles, F. A. (2005). Initial ocular following in humans depends critically on the fourier components of the motion stimulus. *Ann. N. Y. Acad. Sci.* 1039, 260–271. doi: 10.1196/annals.1325.025

Dunn, T. W., Mu, Y., Narayan, S., Randlett, O., Naumann, E. A., Yang, C. T., et al. (2016). Brain-wide mapping of neural activity controlling zebrafish exploratory locomotion. *Elife* 5, 1–29. doi: 10.7554/eLife.12741

Förster, D., Helmbrecht, T. O., Mearns, D. S., Jordan, L., Mokayes, N., and Baier, H. (2020). Retinotectal circuitry of larval zebrafish is adapted to detection and pursuit of prey. *Elife* 9, 1–26. doi: 10.7554/eLife.58596

Huang, Y.-Y., and Neuhauss, S. C. F. (2008). The optokinetic response in zebrafish and its applications. *Front. Biosci.* 13:1899–1916. doi: 10.2741/2810

Kawashima, T., Zwart, M. F., Yang, C.-T., Mensh, B. D., and Ahrens, M. B. (2016). The Serotonergic system tracks the outcomes of actions to mediate short-term motor learning. *Cell* 167, 933.e20–946.e20. doi: 10.1016/j.cell.2016.09.055

Kleiner, M., Brainard, D., Pelli, D., Ingling, A., Murray, R., and Broussard, C. (2007). What's new in psychtoolbox-3. *Perception* 36:1–16. doi: 10.1177/03010066070360S101

Kubo, F., Hablitzel, B., Dal Maschio, M., Driever, W., Baier, H., and Arrenberg, A. B. (2014). Functional architecture of an optic flow-responsive area that drives horizontal eye movements in zebrafish. *Neuron* 81, 1344–1359. doi: 10.1016/j.neuron.2014.02.043

Lister, J. A., Robertson, C. P., Lepage, T., Johnson, S. L., and Raible, D. W. (1999). Nacre encodes a zebrafish microphthalmia-related protein that regulates neural-crest-derived pigment cell fate. *Development* 126, 3757–3767. doi: 10.1242/dev.126.17.3757

Lopes, G., Bonacchi, N., Frazao, J., Neto, J. P., Atallah, B. V., Soares, S., et al. (2015). Bonsai: an event-based framework for processing and controlling data streams. *Front. Neuroinf.* 9:7. doi: 10.3389/fninf.2015.00007

Matsuda, K., Kubo, F., and Bene, F. D. (2021). Circuit organization underlying optic flow processing in zebrafish. *Front. Neural Circ.* 15:709048. doi: 10.3389/fncir.2021.709048

Miura, K., Matsuura, K., Taki, M., Tabata, H., Inaba, N., Kawano, K., et al. (2006). The visual motion detectors underlying ocular following responses in monkeys. *Vision Res.* 46, 869–878. doi: 10.1016/j.visres.2005.10.021

Naumann, E. A., Fitzgerald, J. E., Dunn, T. W., Rihel, J., Sompolinsky, H., and Engert, F. (2016). From whole-brain data to functional circuit models: the zebrafish optomotor response. *Cell.* 167, 947.e20–960.e20. doi: 10.1016/j.cell.2016.10.019

Orger, M. B., Smear, M. C., Anstis, S. M., and Baier, H. (2000). Perception of Fourier and non-Fourier motion by larval zebrafish. *Nat. Neurosci.* 3, 1128–1133. doi: 10.1038/80649

Pérez-Schuster, V., Kulkarni, A., Nouvian, M., Romano, S. A., Lygdas, K., Jouary, A., et al. (2016). Sustained rhythmic brain activity underlies visual motion perception in zebrafish. *Cell Rep.* 17, 1098–1112. doi: 10.1016/j.celrep.2016.09.065

Pologruto, T. A., Sabatini, B. L., and Svoboda, K. (2003). ScanImage: flexible software for operating laser scanning microscopes. *Biomed. Eng. Online* 2, 13. doi: 10.1186/1475-925X-2-13

Portugues, R., and Engert, F. (2009). The neural basis of visual behaviors in the larval zebrafish. *Curr. Opin. Neurobiol.* 19, 644–647. doi: 10.1016/j.conb.2009.10.007

Robles, E., Laurell, E., and Baier, H. (2014). The retinal projectome reveals brain-area-specific visual representations generated by ganglion cell diversity. *Cur. Biol.* 24, 2085–2096. doi: 10.1016/j.cub.2014.07.080

Roeser, T., and Baier, H. (2003). Visuomotor behaviors in larval zebrafish after GFP-guided laser ablation of the optic tectum. *J. Neurosci.* 23, 3726–3734. doi: 10.1523/JNEUROSCI.23-09-03726.2003

Romano, S. A., Pérez-Schuster, V., Jouary, A., Boulanger-Weill, J., Candeo, A., Pietri, T., et al. (2017). An integrated calcium imaging processing toolbox for the analysis of neuronal population dynamics. *PLoS Comput. Biol.* 13:e1005526. doi: 10.1371/journal.pcbi.1005526

Romano, S. A., Pietri, T., Pérez-Schuster, V., Jouary, A., Haudrechy, M., and Sumbre, G. (2015). Spontaneous neuronal network dynamics reveal circuit's functional adaptations for behavior. *Neuron* 85, 1070–1085. doi: 10.1016/j.neuron.2015.01.027

Semmelhack, J. L., Donovan, J. C., Thiele, T. R., Kuehn, E., Laurell, E., and Baier, H. (2014). A dedicated visual pathway for prey detection in larval zebrafish. *Elife* 3:1–19. doi: 10.7554/eLife.04878

Sheliga, B. M., Chen, K. J., FitzGibbon, E. J., and Miles, F. A. (2005). Initial ocular following in humans: a response to first-order motion energy. *Vision Res*. 45, 3307–3321. doi: 10.1016/j.visres.2005.03.011

Sugita, Y., Miura, K., and Kawano, K. (2012). Principal Fourier component of motion stimulus dominates the initial optokinetic response in mice. *Neurosci. Res*. 73, 133–141. doi: 10.1016/j.neures.2012.03.007

Thompson, A. W., Vanwalleghem, G. C., Heap, L. A., and Scott, E. K. (2016). Functional profiles of visual-, auditory-, and water flow-responsive neurons in the zebrafish tectum. *Curr. Biol*. 26, 743–754. doi: 10.1016/j.cub.2016.01.041

Wang, K., Hinz, J., Haikala, V., Reiff, D. F., and Arrenberg, A. B. (2019). Selective processing of all rotational and translational optic flow directions in the zebrafish pretectum and tectum. *BMC Biol*. 17:29. doi: 10.1186/s12915-019-0648-2

Wang, K., Hinz, J., Zhang, Y., Thiele, T. R., and Arrenberg, A. B. (2020). Parallel channels for motion feature extraction in the pretectum and tectum of larval zebrafish. *Cell Rep*. 30, 442.e6–453.e6. doi: 10.1016/j.celrep.2019.12.031

Conflict of Interest: The authors declare that the research was conducted in the absence of any commercial or financial relationships that could be construed as a potential conflict of interest.

Supplementary Material

1 SUPPLEMENTARY DATA

2 SUPPLEMENTARY TABLES AND FIGURES

2.1 Figures

Figure S1. (Video related to Figure 1) Behavioral eye output during the presentation of the static square-wave (left), the moving square-wave (middle) and the moving missing-fundamental (right) stimuli. The stimulus motion is rightwards. **(Top)** Visual appearance of the stimuli. **(Bottom)** Video of a 7dpf larva showing eye rotations induced by the visual stimuli. The larva performs spontaneous rotations during the static square-wave stimulus, pursuits to the right during the square-wave stimulus moving rightwards, and pursuits leftwards during the missing-fundamental stimulus moving to the right. The video is speeded up 2x with respect to the original recording.

Stimulus	black	square static	missing fundamental static	3rd harmonic static	square moving	missing fundamental moving	3rd harmonic moving
p_anova	2.10^{-7}	8.10^{-13}	8.10^{-13}	1.10^{-7}	5.10^{-13}	2.10^{-11}	8.10^{-9}
F value	51.23	299.28	301.34	55.86	320.67	190.99	82.11
95%CI opposite vs samedir	-29.8 : 9.7	-14.8 : 5.0	-12.7 : 7.0	-13.6 : 28.0	-97.8 : -77.9	71.0 : 94.6	65.2 : 101.1
p_value	0.41	0.42	0.73	0.65	1.10^{-9}	1.10^{-9}	1.10^{-8}
95%CI samedir vs spontaneous	-80.8 : -41.3	-88.0 : -68.3	-88.8 : -68.3	-97.4 : -55.8	69.1 : 89.0	-24.8 : -1.1	-33.0 : 2.9
p_value	2.10^{-6}	1.10^{-9}	1.10^{-9}	3.10^{-7}	1.10^{-9}	0.03	0.11
95%CI opposite vs spontaneous	-90.8 : -51.4	-93.0 : -73.2	-91.7 : -72.0	-90.3 : -48.7	-18.7 : 1.1	58.0 : 81.7	50.1 : 86.0
p_value	3.10^{-7}	1.10^{-9}	1.10^{-9}	9.10^{-7}	0.09	2.10^{-9}	2.10^{-7}

Figure S2. (Table related to Figure 1) Statistical values for the ANOVA tests used to compare the different eye behaviors (pursuits in the same direction than the stimulus, pursuits in the opposite direction,spontaneous rotations) induced by each of the presented stimuli. Row from top to bottom: Stimulus type; p_value of the ANOVA test; F value of the ANOVA test; 95% confidence interval for the comparison between the pursuits in the stimulus direction and the opposite direction, and the p_value associated; 95% confidence interval for the comparison between the pursuits in the stimulus direction and the spontaneous rotations, and the p_value associated; 95% confidence interval for the comparison between the pursuits in the opposite direction and the spontaneous rotations, and the p_value associated. Significant p_values (inferior to 0.05) are displayed in dark orange.

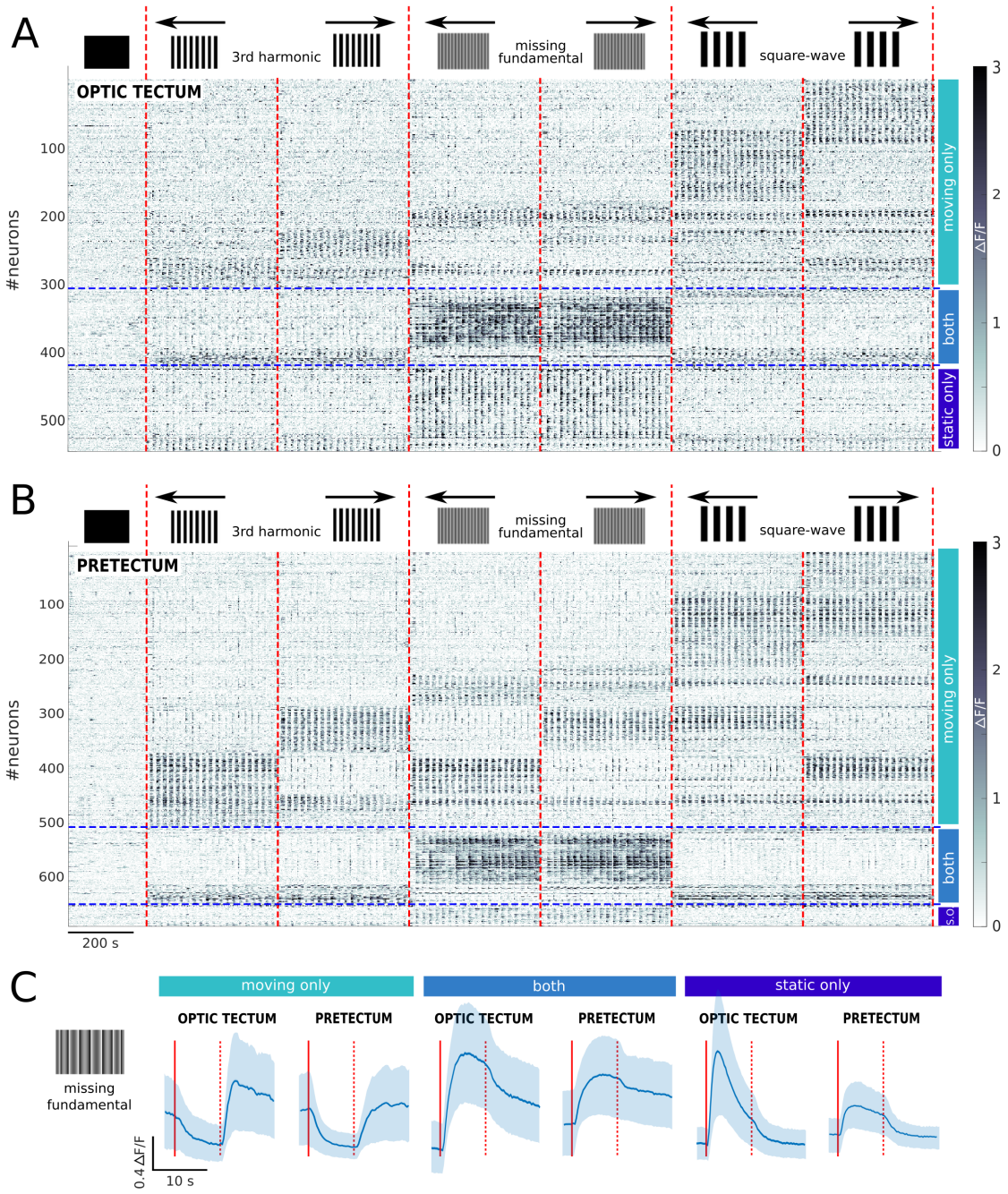

Figure S3. **(related to Figure 2)** Tectal and pretectal neuronal activity induced by the presentation of the different types of visual stimuli. **(A)** Raster of activity of the neurons responding to at least one of the presented stimuli in the optic tectum (n=13 larvae). The imaged frames are sorted on the x axis so that stimuli of the same type are grouped together (separated by vertical red dashed lines). The neurons are sorted on the y axis according to the type of response they display. The neurons are also separated in three categories (separated by horizontal blue dashed lines): 1) show activity only during the moving stimulus (cyan), 2) show activity only during the static part of the stimulus (purple), or 3) show activity during the static and the moving part (blue). Note that the frequency in the Ca2+ signal observed during the presentation of the stimulus is due to the alternation between static and moving stimuli. **(B)** Same as **A** but for the pretectum (n=7 larvae). S.O. in the purple box stands for static only. **(C)** Average of the activity of tectal and pretectal neurons responding only to the moving part of the missing-fundamental stimulus, to the moving and static part or only to the static part. Vertical red solid line: onset of the static stimulus. Vertical red dashed line: onset of stimulus motion. Light blue: standard deviation.

4

Behavioral and neuronal responses to an ambiguous visual stimulus

The psychophysics of visual bistability has been studied mostly in humans and monkeys (see Introduction section 1.1.2). For my PhD project, I have studied visual bistability in the zebrafish larva, which in contrast to other animals, allows monitoring whole-brain activity with single-neuron resolution in an intact behaving vertebrate.

4.1 Do zebrafish show visual bistability?

To study the neuronal basis of visual bistability in the zebrafish larva, I first created a visual stimulus based on a moving grid that induces an optokinetic response (OKR, see Methods sections 1.2.3 and 2.2.1). Suppressing the first Fourier component of this stimulus induces a change in the visual motion direction detection in humans and monkeys (see Introduction section 1.1.1), as well as in zebrafish [Orger et al., 2000] (see Chapter 3). I adapted this stimulus to create an ambiguous stimulus for zebrafish larvae.

4.1.1 Zebrafish behavior in response to an ambiguous moving grating

When projecting a vertical rotating square-wave grating to a zebrafish larva, it follows the motion with its eyes, in the same direction as the direction of motion of the stimulus. This visuomotor behavior is known as OKR (see Introduction section 1.2.3 and Methods section 2.2.1). However, when removing the fundamental frequency (F1) of the signal (missing-fundamental stimulus (F1=0%)), the zebrafish larva generated pursuits in the opposite direction of motion (see Introduction section 1.1.1 and Methods section 2.2.2). Aiming to create an ambiguous stimulus, I tested the behavior of larvae when presenting stimuli with different fractions of the fundamental frequency (see Figure 2.2), expecting that I will find a specific value in which larvae would alternatively generate pursuits to the left or to the right.

For this purpose, I monitored the eye rotations of the larva along the horizontal plane (yaw) while projecting either square-wave stimulus, missing-fundamental stimulus, or stimulus with intermediate percentages of the fundamental F1 power (10, 20, 30 or 40% of F1, see Figure 4.1A with the example of F1=30%). I then classified the eye movements into three types: pursuits in the direction of the stimulation, pursuits in the opposite direction and spontaneous eye movements (see Methods section 2.2.1 and Figure 4.1B). The stimulus paradigm consisted of projecting the static square-wave signal for 5 minutes, then the moving patterns of square-wave and missing-fundamental stimuli for 5 minutes (in random order in each trial), then a black background for 10 minutes and finally, 45 minutes of the moving stimulus with different values of the Fourier component (F1=10%, 20%, 30% or 40% depending on the trial). The black background was used to avoid the potential motion aftereffect (MAE), that could interfere with the eye rotations induced by the presented stimuli [Pérez-Schuster et al., 2016].

During the static square-wave presentation, the majority of the behaviors consisted of spontaneous eye rotations (stimulus direction: 5.6 ± 6.3% ; opposite direction: 4.1 ± 4.8% ; spontaneous: 90.4 ± 7.8% ; p_anova=2.10^{-102}). Similar results were observed during the black background (stimulus direction: 8.4 ± 8.4% ; opposite direction: 14.8 ± 13.2% ; spontaneous: 76.8 ± 14.3% ; p_anova=7.10^{-56}). During the moving square-wave stimulus (F1=100%), the majority of behaviors consisted of pursuits in the direction of the stimulus (stimulus direction: 84.0 ± 15.0% ; opposite direction: 0.8 ± 1.5% ; spontaneous: 15.1 ± 14.3% ; p_anova=9.10^{-65}). During the presentation of the moving missing-fundamental (F1=10%) the majority of eye rotations consisted of pursuits in the opposite direction of the stimulus (stimulus direction: 0.5 ± 1.2% ; opposite direction: 83.2 ± 11.9% ; spontaneous: 16.3 ± 11.6% ; p_anova=3.10^{-75}). For F1=10%, we saw either pursuits in the opposite direction of the stimulus or spontaneous rotations (stimulus

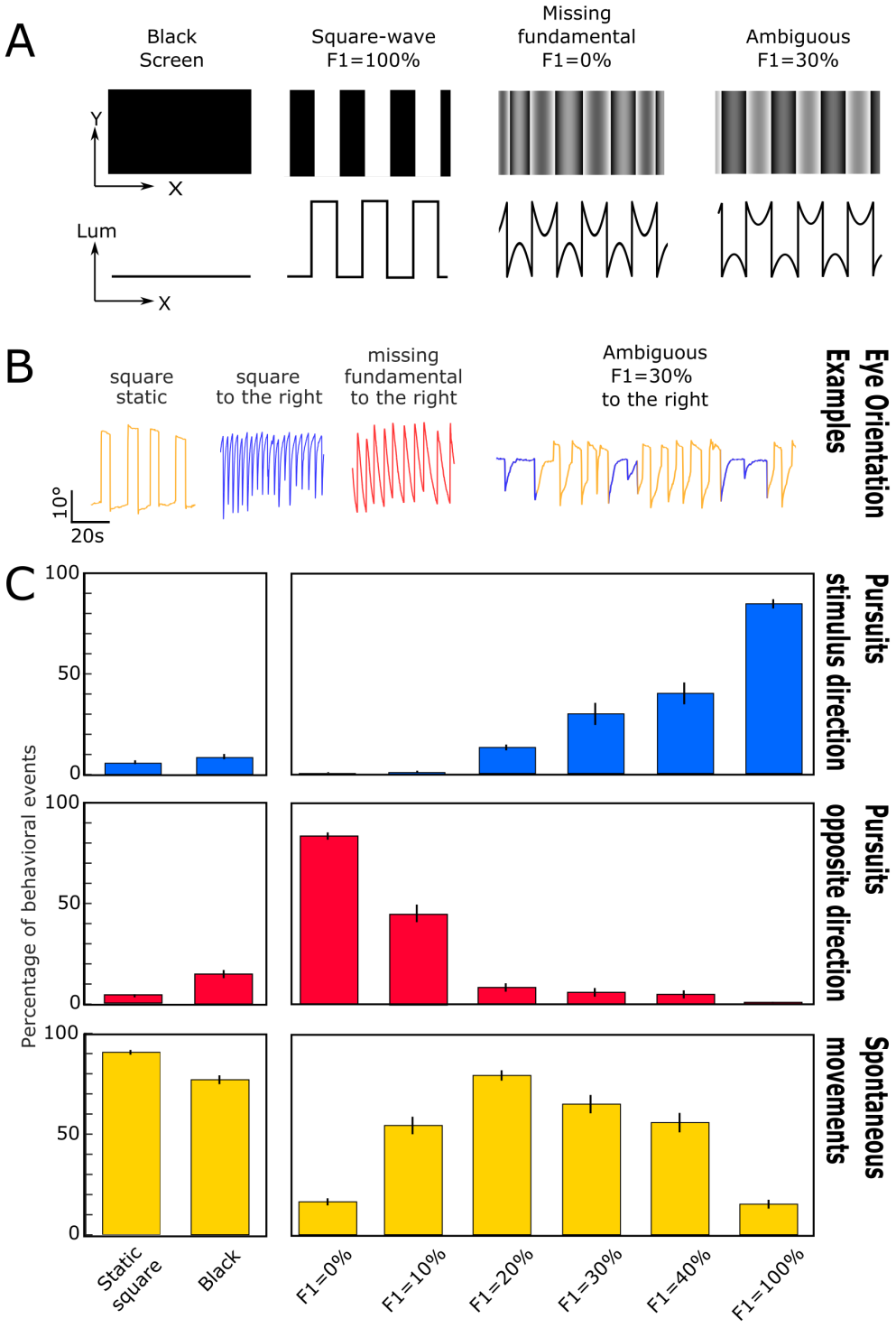

Figure 4.1: **Stimuli and behavior for testing the ambiguous gratings.** **(A)** Images corresponding to the different stimuli projected to the larvae, with the example of F1=30% for the ambiguous stimulus. First row: visual appearance of the stimuli ; Second row: Plot of the luminance as a function of spatial position across the x axis. **(B)** Examples of the eye orientation traces induced by the different types of visual stimuli: static square-wave, moving square-wave, moving missing-fundamental and moving ambiguous stimuli. All stimuli move to the right here. Yellow: spontaneous movements ; blue: pursuits in the stimulus direction ; red: pursuits in the opposite direction. **(legend continues on next page)**

direction: 0.9 ± 1.4% ; opposite direction: 44.9 ± 13.8% ; spontaneous: 54.1 ± 13.7% ; p_anova=2.10^{-102}). For F1=20%, we observed mostly spontaneous rotations (stimulus direction: 12.9 ± 4.6% ; opposite direction: 8.2 ± 6.6% ; spontaneous: 78.9 ± 8.1% ; p_anova=3.10^{-20}). For F1=30%, we saw mostly spontaneous rotations but also some pursuits in the stimulus direction (stimulus direction: 29.5 ± 19.7% ; opposite direction: 5.8 ± 7.8% ; spontaneous: 64.7 ± 16.4% ; p_anova=7.10^{-11}). For F1=40%, we found either pursuits in the same direction than the stimulus or spontaneous rotations (stimulus direction: 39.7 ± 17.1% ; opposite direction: 4.8 ± 6.3% ; spontaneous: 55.5 ± 15.2% ; p_anova=3.10^{-8}) (Figure 4.1C).

Therefore for an increasing percentage of F1 there is an increase of the pursuits in the stimulus direction and a decrease of the pursuits in the opposite direction. Spontaneous rotations increase for Fourier component (F1) of intermediate values, reaching a maximum at F1=20%.

To claim that the generated visual stimulus induces in zebrafish larvae a bistable visuomotor behavior, it is necessary that the larvae display alternation of pursuits states in the stimulus direction and in the opposite direction (periods in which the larva performs pursuits to the right and periods in which the pursuits are generated in the opposite direction). I did not observe alternations in the direction of the pursuits. Instead, as the number of pursuits in the direction of the energy of the first Fourier component decreases, the number of spontaneous saccades rather the number of pursuits in the opposite direction increases. The larvae never displayed an alternation between pursuits in opposite directions, but an alternation between periods of "perception" (pursuits behavioral output) and periods of "no perception" (spontaneous eye rotations), as it can be observed for F1=40% (alternation between spontaneous rotations and pursuits in the stimulus direction) and F1=10% (alternation between spontaneous rotations and pursuits in the opposite direction compared to the stimulus). I thus decided to study the neural dynamics of the alternations in "perception" (switches) using the ambiguous gratings of F1=10%.

Figure 4.1 (continued): **(C)** Percentage of behavioral events (pursuits in the direction of the stimulus' motion, pursuits in the opposite direction, spontaneous rotations) for the presented stimuli. The behavioral experiment was performed on n=10 larvae for F1=10%, n=10 larvae for F1=20%, n=13 larvae for F1=30% and n=10 larvae for F1=40%. The results for the static square-wave, the black background, F1=0% (moving missing-fundamental signal) and F1=100% (moving square-wave signal) are on all previous larvae (n=43). The error bars represent the standard error of the mean.

About high drifts during the spontaneous phase

Looking at the eye orientation traces in Figure 4.1B for the ambiguous stimulus, I observed that the drifts between saccades during the spontaneous phase were usually higher that the ones observed during the static square-wave stimulus presentation. Thus I wondered if the behavior would be better separated in five types of movements (pursuits in the direction of the stimulus' motion, pursuits in the opposite direction, spontaneous rotations, high drifts in the direction of the stimulus' motion, high drifts in the opposite direction) instead of only three (pursuits in the direction of the stimulus' motion, pursuits in the opposite direction, spontaneous rotations). To this aim, I added to the sorting algorithm presented in section Materials 2.2.1 the two other types of motion: high drifts in the right direction if the saccades were alternating in direction and the drift before a saccade going from left to right was higher than this saccade; and high drifts in the left direction if the saccades were alternating in direction and the drift before a saccade going from right to left was higher than this saccade. The same results than the ones in Figure 4.1 but with this new sorting algorithm are displayed in Figure 4.2.

There are nearly no high drifts in either direction for the static square-wave, the moving square-wave (F1=100%) and the missing-fundamental (F1=0%) stimuli. However for the black screen and the different ambiguous signals (F1=10%, 20%, 30% or 40%), between 20 and 30% of the behavioral events are high drifts in one or the other direction. It was already shown that during a black screen presentation, the eyes tended to drift centripetally after each saccade, and that the larvae showed a lot more stable eye fixation when the surrounding environment was structured and static [Chen et al., 2014]. But because the moving ambiguous stimuli were not static, it was impossible here to differentiate the drifts that would be produced because the larvae were detecting some motion to one direction from the drifts that would be corresponding to a centripetal spontaneous drift. Thus, when the larvae were displaying high drifts, I considered that the stimuli were not strong enough to initiate proper OKR rotations and I sorted them back into the spontaneous movements (with the algorithm described in section Materials 2.2.1).

4.1.2 Zebrafish behavior in response to ambiguous dots motion

To test whether the behavior observed in response to the ambiguous grating was not due only to the type of stimulus used, we tested also the behavior of the larva when exposed to dots moving in two opposite directions. This work was made with Jade Seguin, a L3 student in the lab. Each dot represented 0.1° of the visual field of the larva and it moved coherently and constantly to one direction with a speed of 3°/s, or in a direction that changed randomly between each frame (jitter).

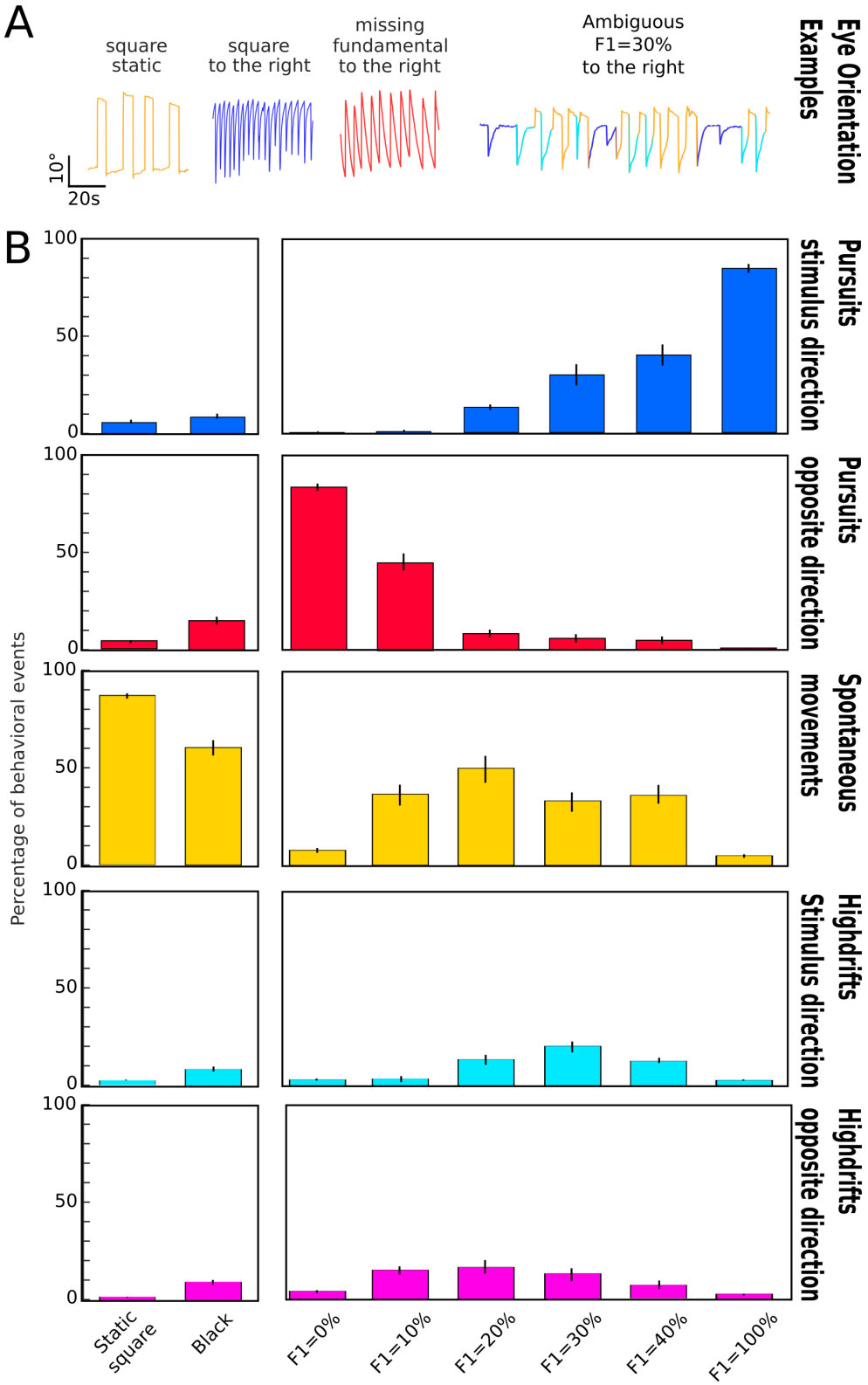

Figure 4.2: **Behavior for testing the ambiguous gratings taking the high drifts into account. (A)** Examples of the eye orientation traces induced by the different types of visual stimuli: static square-wave, moving square-wave, moving missing-fundamental and moving ambiguous stimuli. All stimuli move to the right here. Yellow: spontaneous movements ; blue: pursuits in the stimulus direction ; red: pursuits in the opposite direction ; cyan: high drifts in the stimulus direction. **(legend continues on next page)**

We then designed a visual stimulation paradigm as follows: 2 minutes of static dots, then 2 minutes of randomly moving dots, then every 2 minutes 10% of the randomly moving dots started to move to the right, until all dots were moving to the right (100% coherence, Figure 4.3A).

During the presentation of the static dots, the majority of eye movements were spontaneous rotations (stimulus direction: 8.9 ± 8.7% ; opposite direction: 10.5 ± 10.5% ; spontaneous: 80.5 ± 16.2% ; p_anova=3.10^{-8}). We observed a similar behavior for the randomly moving dots (0% to the right) (stimulus direction: 10.6 ± 10.4% ; opposite direction: 7.3 ± 7.4% ; spontaneous: 82.0 ± 10.7% ; p_anova=8.10^{-10}). Then for every larger percentage of dots moving to the right that we tested, the majority of rotations were pursuits in the direction of the dots motion: for 10% of dots to the right (stimulus direction: 71.8 ± 24.1% ; opposite direction: 0 ± 0% ; spontaneous: 28.2 ± 24.1% ; p_anova=5.10^{-5}), 20% of dots moving to the right (stimulus direction: 76.2 ± 15.5% ; opposite direction: 1.0 ± 1.5% ; spontaneous: 22.8 ± 16.0% ; p_anova=1.10^{-7}), 30% of dots moving to the right (stimulus direction: 89.8 ± 13.6% ; opposite direction: 0 ± 0% ; spontaneous: 10.2 ± 13.6% ; p_anova=7.10^{-10}), 40% of dots moving to the right (stimulus direction: 85.0 ± 15.4% ; opposite direction: 0 ± 0% ; spontaneous: 15.0 ± 15.4% ; p_anova=1.10^{-8}), 50% of dots moving to the right (stimulus direction: 88.3 ± 11.6% ; opposite direction: 1.7 ± 4.1% ; spontaneous: 10.0 ± 8.8% ; p_anova=3.10^{-11}), 60% of dots moving to the right (stimulus direction: 94.0 ± 14.6% ; opposite direction: 1.2 ± 2.9% ; spontaneous: 4.8 ± 11.7% ; p_anova=2.10^{-10}), 70% of dots moving to the right (stimulus direction: 89.4 ± 13.2% ; opposite direction: 0 ± 0% ; spontaneous: 10.6 ± 13.2% ; p_anova=5.10^{-10}), 80% of dots moving to the right (stimulus direction: 86.0 ± 12.9% ; opposite direction: 0 ± 0% ; spontaneous: 14.0 ± 12.9% ; p_anova=8.10^{-10}), 90% of dots moving to the right (stimulus direction: 90.8 ± 11.1% ; opposite direction: 0 ± 0% ; spontaneous: 9.2 ± 11.1% ; p_anova=3.10^{-11}), or all dots moving to the right (100%) (stimulus direction: 89.5 ± 7.8% ; opposite direction: 0.4 ± 1.0% ; spontaneous: 10.1 ± 7.0% ; p_anova=1.10^{-13}) (Figure 4.3B).

These results show that zebrafish larvae generated pursuits in the direction of the moving dots similar to a moving grid. We found that only 10% coherence (10% of the

Figure 4.2 (continued): **(B)** Percentage of behavioral events (pursuits in the direction of the stimulus' motion, pursuits in the opposite direction, spontaneous rotations, high drifts in the direction of the stimulus' motion, high drifts in the opposite direction) for the presented stimuli. The behavioral experiment was performed on n=10 larvae for F1=10%, n=10 larvae for F1=20%, n=13 larvae for F1=30% and n=10 larvae for F1=40%. The results for the static square-wave, the black background, F1=0% (moving missing-fundamental signal) and F1=100% (moving square-wave signal) are on all previous larvae (n=43). The error bars represent the standard error of the mean.

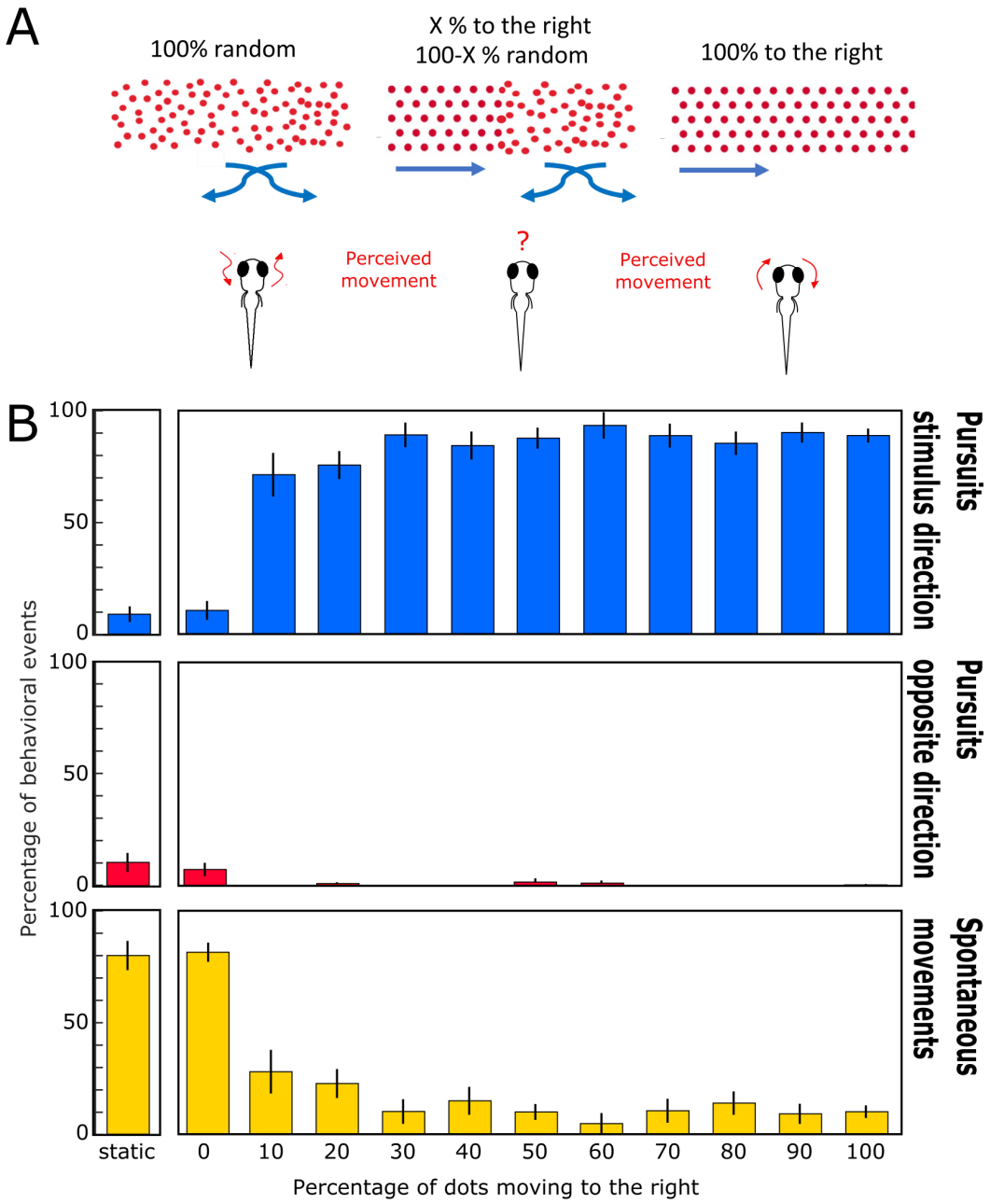

Figure 4.3: **Stimuli and behavior for testing the fish response to dots motion against noise. (A)** The different stimuli that were projected to the fish. Either the dots were moving randomly with no motion that the larva could follow (left panel), or the dots were moving coherently to the right and the larva could follow the motion (right panel), or it was a mixture of the two, with only a fraction of dots moving to the right and the rest randomly (middle panel). **(B)** Percentage of behavioral events (pursuits in the direction of the stimulus' motion, pursuits in the opposite direction, spontaneous rotations) for the presented stimuli: static dots, randomly moving dots (0% to the right), randomly moving dots except for 10%, 20%, 30%, 40%, 50%, 60%, 70%, 80%, 90% to the right, or 100% of dots moving to the right. The behavioral experiment was performed on n=6 larvae. The error bars represent the standard error of the mean.

dots moving in one direction while the resting 90% moved in random directions) was sufficient to induce OKR.

To study visual ambiguity using the moving dots, we created an ambiguous paradigm based on dots simultaneously moving in two opposite directions. The stimulus paradigm consisted of presenting to the larvae the static dots for 1 minute, then all dots moving to the left for 1 minute and to the right for 1 minute (these stimuli were presented in random order depending on the trial), then 50% of the dots moving to the left and 50% to the right for 10 minutes, 60% of dots moving to the left and 40% to the right for 10 minutes and 70% of dots moving to the left and 30% to the right for 10 minutes. These different stimuli were separated by the presentation of static dots for 2 minutes to prevent interference with the potential motion after-effect (MAE) that could be induced by the movement of the dots during the previous presentation [Pérez-Schuster et al., 2016] (Figure 4.4A).

During the presentation of the static dots, the majority of the eye movements consisted of spontaneous rotations (to the right: 21.1 ± 20.7% ; to the left: 21.2 ± 24.2% ; spontaneous: 57.7 ± 18.2% ; p_anova=1.10^{-3}). When all dots moved to the right (0% to the left), the majority of eye rotations consisted of pursuits to the right (to the right: 83.1 ± 9.0% ; to the left: 2.9 ± 4.5% ; spontaneous: 14.0 ± 7.4% ; p_anova=4.10^{-18}). During the presentation of dots moving 50% to the left and 50% to the right, we observed mostly spontaneous rotations (to the right: 17.6 ± 22.2% ; to the left: 9.7 ± 9.5% ; spontaneous: 72.7 ± 19.9% ; p_anova=2.10^{-7}). For dots moving 60% to the left and 40% to the right, the behavior was either spontaneous rotations or pursuits to the left (to the right: 2.7 ± 1.9% ; to the left: 42.5 ± 19.3% ; spontaneous: 54.8 ± 19.1% ; p_anova=7.10^{-7}). During the presentation of dots moving 70% to the left and 30% to the right, the majority of eye rotations consisted of pursuits to the left (to the right: 0.9 ± 1.2% ; to the left: 84.1 ± 9.5% ; spontaneous: 15.0 ± 8.7% ; p_anova=5.10^{-18}). Similar results were observed for dots 100% moving to the left (to the right: 11.4 ± 27.2% ; to the left: 69.8 ± 27.1% ; spontaneous: 18.9 ± 8.1% ; p_anova=2.10^{-5}) (Figure 4.4B).

These results show that when the visual motion information is ambiguous (50% of the dots in each direction), the vast majority of eye rotations are spontaneous, as what was observed in the ambiguous gratings experiments using F1=20% (section 4.1.1). Given that only 10% of the dots moving in one direction is enough to induce eye pursuits in the direction of the moving stimulus, the spontaneous eye rotations observed when 50% of the dots were moving in one direction and the other 50% towards the opposite one are due to the ambiguity of the stimulation and not due to the small number of dots moving in the same direction. The larva's behavior induced by the different percentages of dots' moving coherence resembles the one induced by the different powers of the first Fourier component of a moving grid.

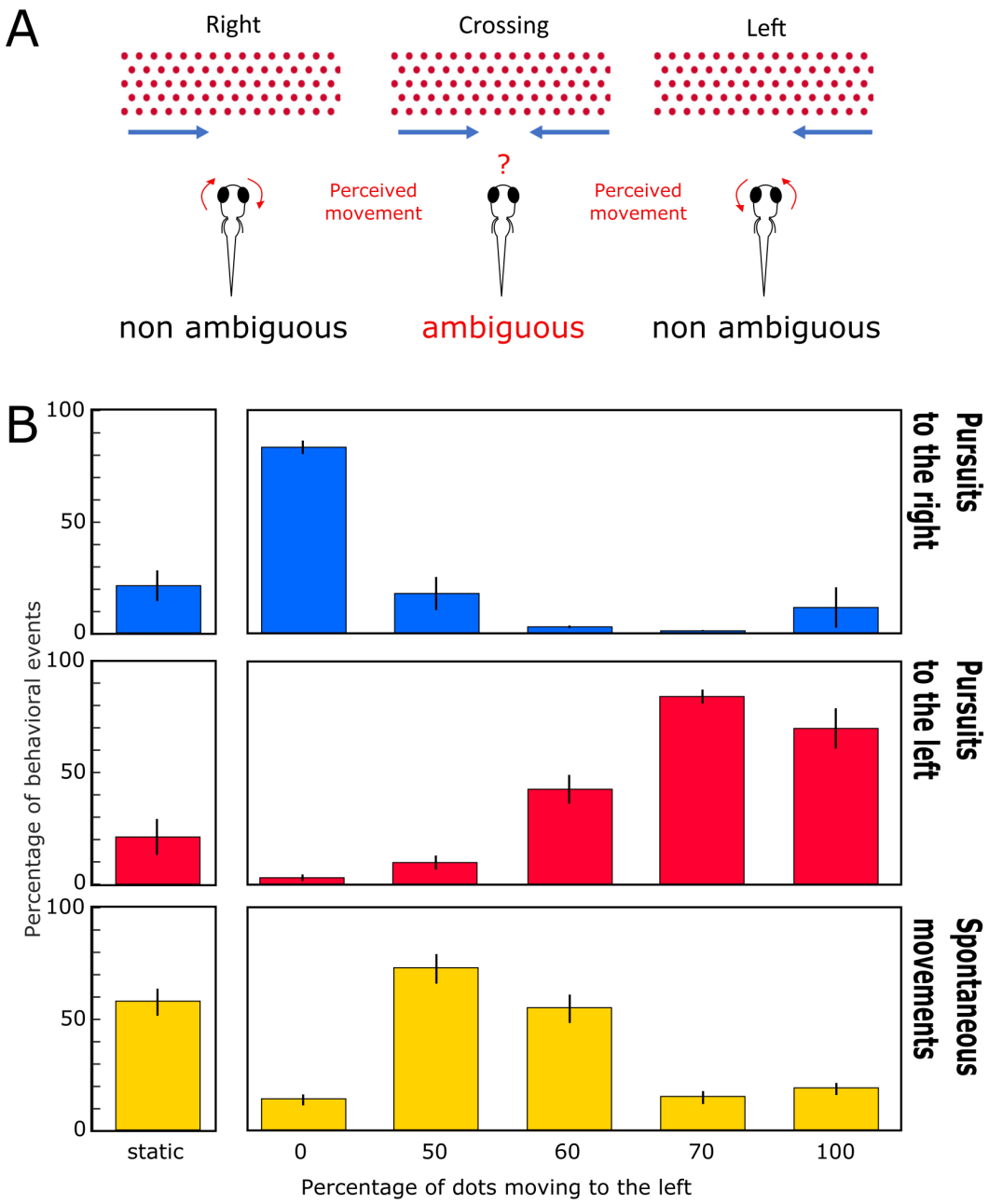

Figure 4.4: **Stimuli and behavior for testing the fish response to dots ambiguous motion. (A)** The different stimuli that were projected to the fish. Either the dots were moving to the left (left panel), or the dots were moving to the right (right panel), or the dots were crossing to the left and to the right with a certain percentage (middle panel). **(B)** Percentage of behavioral events (pursuits to the right, pursuits to the left, spontaneous rotations) for the presented stimuli: static dots, dots moving to the right (0% to the left), dots moving 50%, 60% or 70% to the left with the rest of the dots moving to the right, or 100% of dots moving to the left. The behavioral experiment was performed on n=9 larvae. The error bars represent the standard error of the mean.

These results indicate that the eye behavior induced by the moving grid in which the power of the first Fourier component was modulated is not a result of the particular contrast pattern of the grid but rather represents the mechanism underlying visual motion processing of the zebrafish brain.

Overall, we suggest that in contrast to humans and monkeys, the zebrafish larvae does not ”perceive” ambiguous visual moving stimuli. This could be the consequence of a different visual motion processing brain mechanism, where the zebrafish larvae may sum up the opposite percepts, thus cancelling them, while in humans and monkeys, the brain detects both ambiguities but is capable of perceiving only one at a given time. The alternation in perception in humans and monkeys could also be based on a winner-takes-all mechanism, but at the level of perception rather than at the level of detection.

I thus decided to study the neural basis of the alternations between periods of visual motion ”perception” and ”non-perception”. Note that I define ”perception” in zebrafish as the central computational process necessary to detect a visual stimulus leading to a goal directed motor behavior.

4.2 Neuronal basis of alternation of behavioral states

Using the grid visual stimuli (F1=10%) which induces sporadic alternations between perceptive states (periods in which the larva generates visually induced behavioral outputs and periods in which it does not), I studied the neural dynamics associated with the alternation from a perceptive state to a non-perceptive state and vice versa, across the whole brain of the larva. For this purpose, I used selective plane illumination microscopy (SPIM, see Methods section 2.3.2) to image calcium dynamics across the entire brain of the larva while presenting the ambiguous moving grid. The results presented here will focus on only one larva and are still preliminary. In the conclusions, I will discuss the results also in the light of results obtained from additional larvae.

4.2.1 Eye behavior in the SPIM

The microscope imposes certain constraints on the recording chamber (rectangular instead of cylindrical for letting the laser go through with no angle (see Methods section 2.3.2 and Figure 2.4). The stimulus was thus presented only on the right side of the larva. Before doing further experiments, I tested the behavior of the larvae outside of the microscope when the ambiguous grating was projected on one side of the chamber. For n=7 larvae and the ambiguous stimulus F1=10%, the rotations were as follows: in

the direction of the stimulus 4.7 ± 4.7%, in the opposite direction 20.8 ± 17.7%, spontaneous rotations 74.5 ± 15.7% (p_anova=6.10^{-8}). The pursuits in the opposite direction compared to the stimulus were shorter than in the cylindric chamber (see Results section 4.1.1). However, I still observed alternations of the behavior between two states: one where the larva displays spontaneous rotations and the other one where the larva displays pursuits in the opposite direction to that of the moving stimulus.

The perceptual switch from spontaneous rotations to following pursuits was defined as the time of the first saccade in the same direction as its previous saccade (after an alternation of the directions of the saccades during the spontaneous rotations). Inversely, the perceptual switch from following pursuits to spontaneous saccades was defined as the time of the first saccade in the opposite direction compared to the previous one (during the pursuits the saccades are always in the same direction). In the behavioral experiment in the rectangular chamber, with the stimulation projected on one side, we found in 20 minutes 19.6 ± 10.5 alternations in the perceptive state.

In the microscope, the larva from which I show the results below displayed pursuits in the same direction as the stimulus for 1.5%, pursuits in the opposite direction for 31.3% and spontaneous rotations for 67.2% of the behavioral rotations. There were 12 alternations of behavioral states during the 40 minutes of the ambiguous stimulus presentation (Figure 4.5).

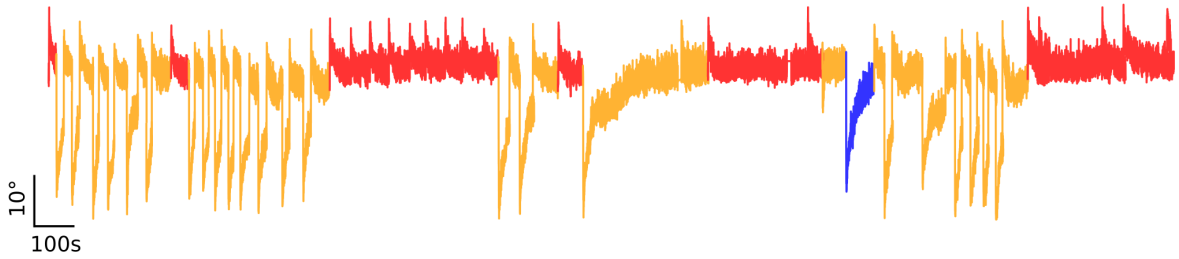

Figure 4.5: **Eye orientation of one larva in the SPIM microscope.** Eye Orientation across time for one larva during the presentation of the ambiguous stimulus F1=10% in the SPIM microscope. Blue: pursuits in the same direction than the stimulus ; Red: pursuits in the opposite direction ; Yellow: spontaneous rotations.

4.2.2 Methods for the analysis of neuronal circuit dynamics

In the SPIM microscope, I recorded from 40 planes in the brain of the zebrafish larva, starting on top of the optic tectum and going down with steps of 5 µm, registering 200 µm of depth. Each brain volume was recorded at 2.1 Hz, while presenting the ambiguous grating F1=10% (see Results section 4.1.1) on the side of the larva for 40 minutes. The

calcium imaging data analysis steps necessary to obtain the fluorescence traces of each neuron from the video of the fluorescence are detailed in the Methods section 2.3.3.

Determining neuronal assemblies

The relative variation in fluorescence intensity $\frac{\Delta F}{F}$ calculated corresponds to the activity for each neuron across time. To find groups of neurons associated with the alternations of the perceptive states, I first reduced the dimensionality of the data by finding neurons with covariations in their activity (functional units of multiple neurons that show significantly correlated activity during the experiment (synchronous calcium events)). Neurons whose activities covariated were regrouped as a single neuronal assembly [Romano et al., 2015].

The extraction of the assemblies was performed using a Matlab (The MathWorks, Inc.) toolbox developed by Sebastian A. Romano in the lab [Romano et al., 2017]. I ran principal component analysis (PCA) on the complete time series of neuronal activities to represent them in a space of reduced dimensionality. I used the z-score neuronal time series in order to normalize variance and avoid the biasing towards the most active neurons. For N neurons and T discrete time points, only the principal components (PCs) with eigenvalues bigger than λ_{max} were kept, λ_{max} being a theoretical lower bound to the eigenvalues of informative PCs, given by the Tracy-Widom corrected Marcenko-Pastur distribution [Peyrache et al., 2010]:

$$\lambda_{max} = (1 + \sqrt{N/T})^2 + N^{-2/3}$$

These significant PCs could be used to isolate assemblies (clusters of correlated neurons), but this would lead to non-overlapping assemblies because of the orthogonality condition of PCA. In my data, a neuron could theoretically belong to multiple assemblies, being correlated with different neurons across time. Thus the PCA orthogonality condition was relaxed by means of non-orthogonal factor rotation *promax* [Hendrickson and White, 1964], that tended to sparsely concentrate the PC loadings along non-orthogonal rotated PCs. After z-scoring loadings on rotated PCs, a neuron was included in a particular assembly defined by a rotated PC if its z-scored loading on that rotated PC exceeded the value of 4. After these steps, I checked that the clusters were not redundant by merging clusters if the dot product of their unitary rotated PCs exceeded 0.6 (meaning that the rotated PCs were extensively overlapping). Then, the clusters were compared to null models and only significantly correlated and synchronous clusters were kept ($p \leq 0.05$). The null model was made by permuting the indexing of the entire neuronal population. These permutations created a set of shuffled surrogate assemblies for each experiment by using the original dataset clustering (i.e. the original non-permuted neuronal assemblies) but sampling neurons according to the permuted indexes. A dataset of null models

containing 1000 permutation rounds was generated. This procedure randomized only the assemblies topographies, while keeping intact every other feature of a given dataset (e.g. the particular overlaps between assemblies, the number of neurons per assembly, the topographical position and the activation time series of each neuron). Once I obtained the assemblies from the data, there was still a final step of pruning: to limit the noise in further analysis, I kept for each assembly only the 75% of neurons that are the most correlated, then removed assemblies that have all their neurons in the same plane (artifact assemblies), as well as assemblies that are composed of less than 50 cells.

From the 63051 neurons registered in the example larva, we obtained 623 assemblies regrouping 61885 neurons (98% of the total recorded neurons).

Registration to a reference brain

To determine the regions of the brain that each assembly represents, I registered the data to a reference brain: the Elavl3-H2BRFP larva from the Z brain atlas of the Engert lab [Randlett et al., 2015], using a Matlab script written by Martin Privat in the lab that used landmarks-based affine transformation. On the Z Brain Atlas website, the mask database is available, that details the pixels that fall inside each brain region. Thus, I wrote a code in Matlab that could determine from this information and the affine transformation of our data the number of cells enclosed in each brain regions for each of the previously defined assemblies.

4.2.3 Neural circuit dynamics associated with the alternation of perceptive states

For each assembly, I calculated the mean activity around the alternations of the perceptive states (eye pursuits vs. spontaneous eye rotations): the change of regime from pursuits to spontaneous rotations (from now on called ”switch to spontaneous”) and from spontaneous rotations to pursuits (from now on called ”switch to pursuits”). This mean activity was computed from 5 seconds before to 5 seconds after the switch.

When observing the total mean activity, the assemblies were generally more active after the switch than before, and this was more pronounced for the switch to spontaneous than the switch to pursuits. The global activity for the switch to spontaneous displayed a transient inhibition at the time of switch followed by a rebound increase in activity. For the switch to pursuits it was possible to observe a mild decrease in activity followed by rapid increase at the time of the switch (Figure 4.6). However, this mean activity is not representative of the entire assemblies population. Note that some assemblies were already standing out, with a lot more activity after the switch than before, or a little

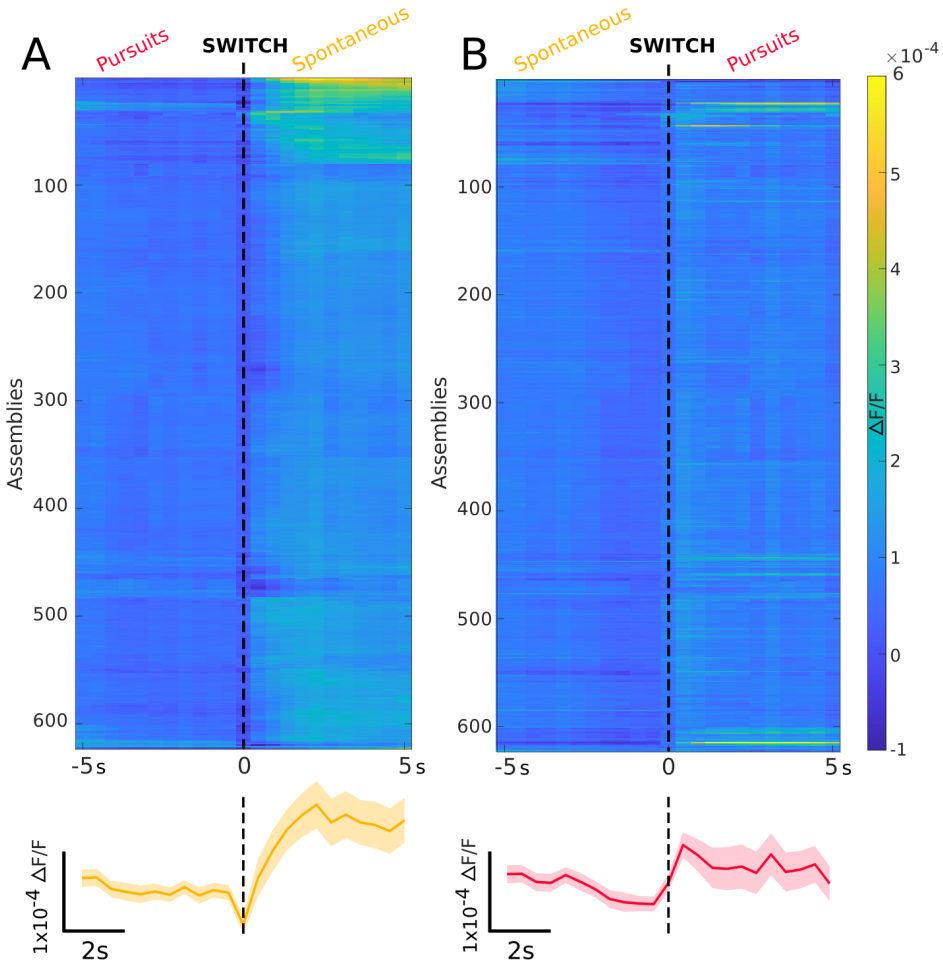

Figure 4.6: **Mean activity of the assemblies around the perceptual switches. (A)** Raster of the mean activity of each assembly from the example larva from 5s before to 5s after the switch to spontaneous. The assemblies (y axis) are arranged following an optimal leaf ordering. The vertical black dashed line represents the time of switch. Below is the mean ± S.D. of the activities taking all assemblies together. **(B)** Same as (A) for the switch to pursuits. The assemblies (y axis) are arranged in the same order than in (A).

more activity before the switch than after, or an inhibition at the time of switch. Some assemblies examples are shown in Figure 4.7.

When analysing the topography of certain assemblies that change their average activity in association with the alternation in the perceptive state, I found that some of the assemblies are relatively compact (the neurons belonging to the assembly are found close to each other) while others were sparse across different brain regions. Assemblies in the pallium and subpallium (forebrain) decrease their mean activity just before the switch to eye pursuits and an increase of activity after the switch to spontaneous, implying a change of state of these assemblies with the change in eye behavior (Figure 4.7A). Another example of an assembly situated in the pallium displayed ramping increase in activity that gradually decreased right after the switch, and an increase after the switch

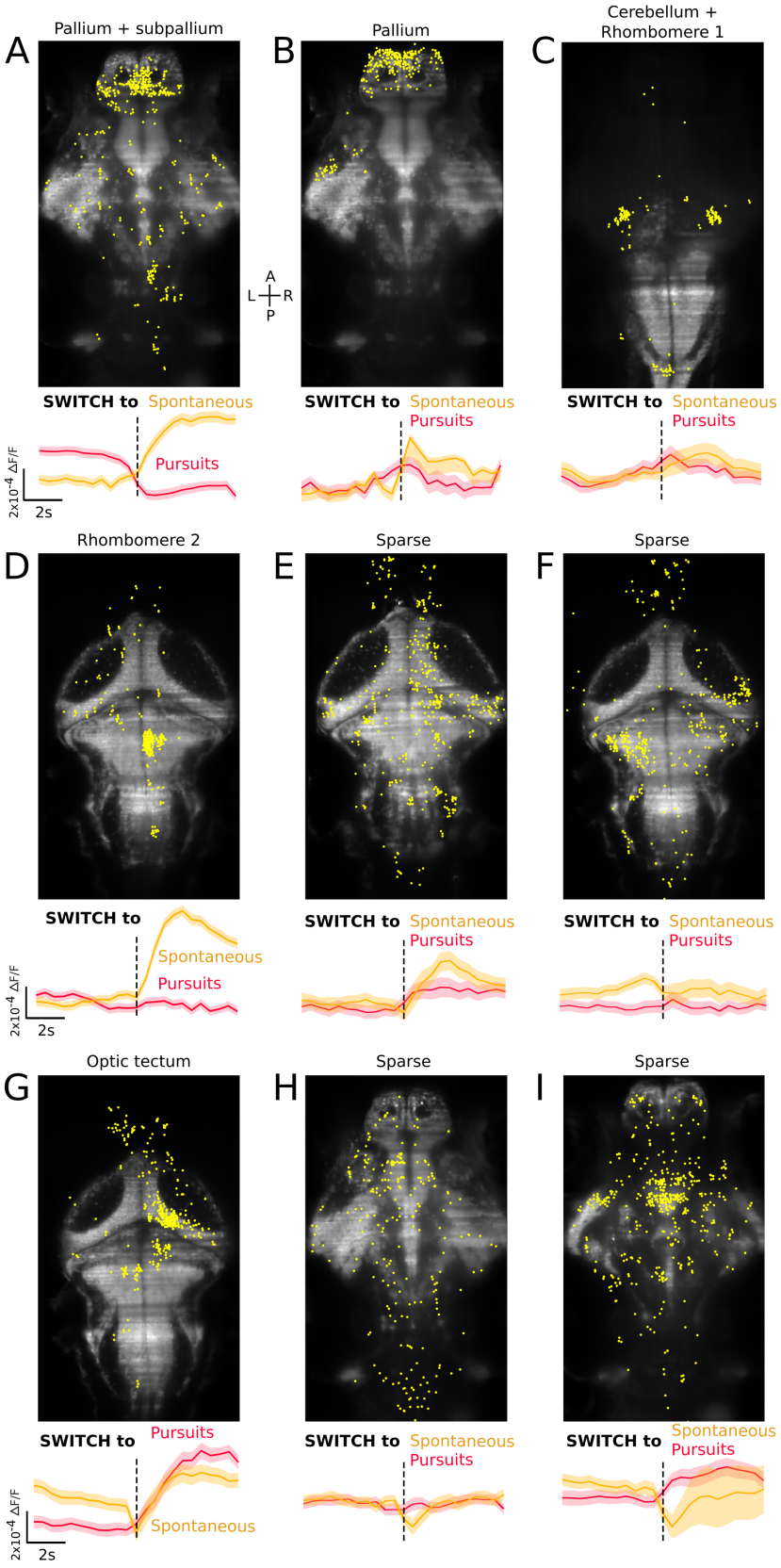

Figure 4.7: **Examples of different assemblies active around the switch. (A-I)** Location in the brain of 9 example assemblies (yellow dots), with the indication on top of the main region(s) where the neurons are found. **(legend continues on next page)**

to spontaneous eye movements (Figure 4.7B). A small bilateral area in the cerebellum (VGlut2-enriched area) showed a rise of activity just before both switches (Figure 4.7C). There was also an increase in activity after the switch to spontaneous in regions of the hindbrain (ex. Rhombomere 2), while the activity did not change around the switch to pursuits (Figure 4.7D). For some assemblies located in the optic tectum, I observed a decrease in activity at the time of switch to spontaneous, followed by an increase after the switch, and the same increase of activity after the switch to pursuits but without the previous decrease (Figure 4.7G). Finally, several assemblies had a sparse topography, with no clear nodes, and they showed different types of activities around the switch. One increased its activity for both types of switches (Figure 4.7E), another one displayed an increase in activity just before the switch to spontaneous (Figure 4.7F), while another one showed a decrease of activity during the switch to spontaneous (Figure 4.7H), or yet another one was increasing its activity after the switch to pursuits and decreasing its activity during the switch to spontaneous (Figure 4.7I).

While observing the activity of the assemblies, taking as an example the ones in Figure 4.7, I observed that the onset of the deviation from the activity baseline (measured only qualitatively) was different across the assemblies. For the switch to pursuits, the order of the assemblies was C, B, A, I, E, G, ranging from 1.5s before to 500ms after the switch (Figure 4.8). These assemblies were active around the switch, except the assembly A that displayed a decrease in the activity. The assemblies D, F and H did not show a change of activity around the switch to pursuits. For the switch to spontaneous eye movements, the order of the assemblies according to the onset of deviation from the activity baseline was F, B, G, H, I, D, A, E, C, ranging from 2.5s before to 500ms after the switch (Figure 4.9). These assemblies showed an increase of mean activity except for the assemblies G, H, and I which decreased their mean activity during the switch followed by a rebound in activity.

Overall, I observed several neuronal assemblies associated with the alternations in the visuomotor behaviors (changes in perceptive state). Interestingly, most of them were active after the switch and not before, and only a few of them showed a transient decrease or increase in their mean activity before the switch. This suggest that the latter assemblies could play a role in the transition between a perceptive to a non-perceptive state of the zebrafish larva.

Figure 4.7 (continued): The background plane is the plane in which the most neurons of this assembly are found. Below is the mean ± S.D. activity of the assembly around the switch to pursuits (red) and to spontaneous (yellow). The vertical black dashed line represents the time of switch.

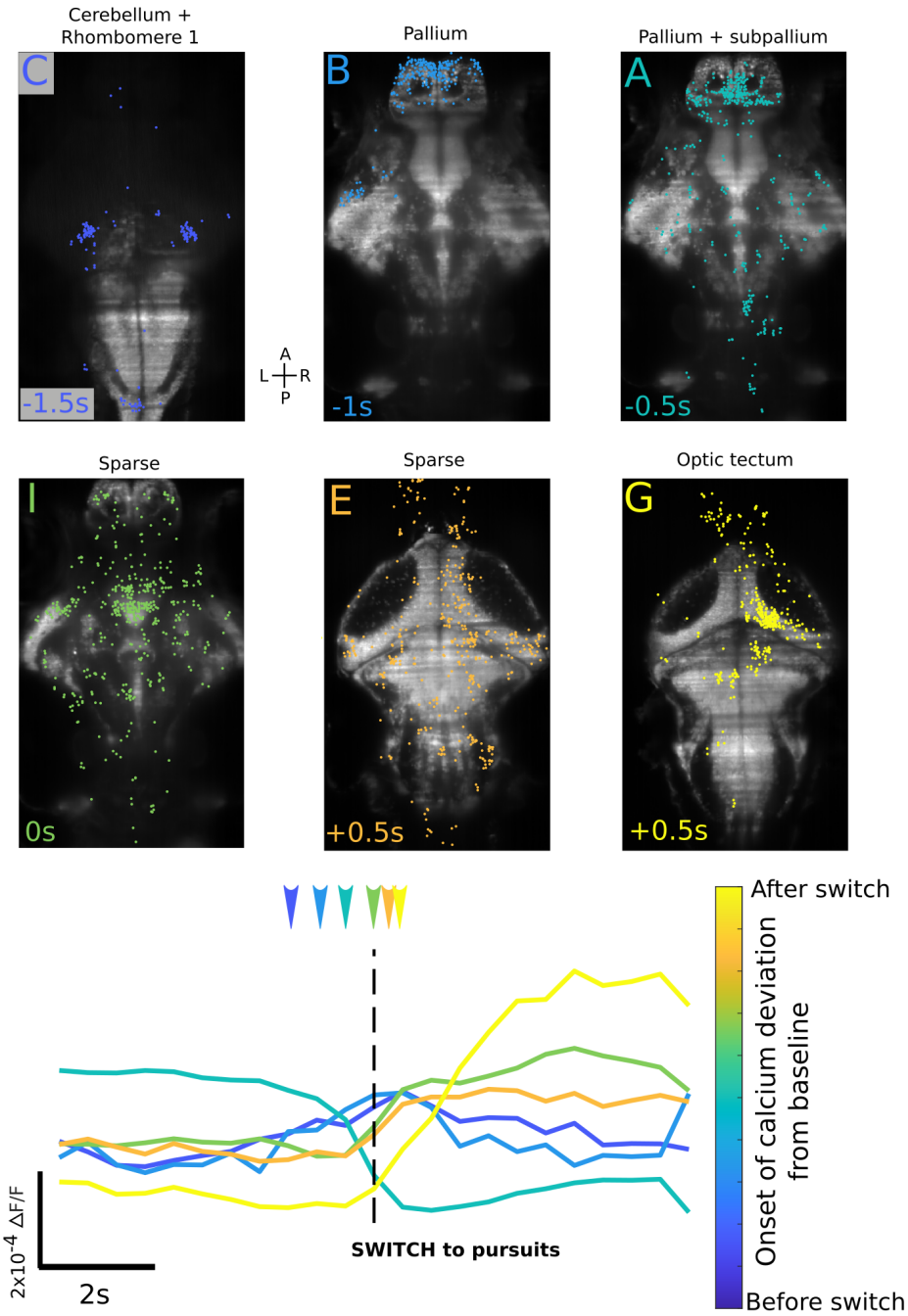

Figure 4.8: **Activation of the assemblies associated with the switch to eye pursuits.** Order of activation (or inhibition) of the assemblies around the switch to pursuits. Top: location and regions of each assembly, as well as timing of the onset of calcium deviation on the bottom left corner. The letters correspond to the assemblies in Figure 4.7. The background plane is the plane in which the majority of the neurons of this assembly are found. Bottom: mean activity of each assembly around the switch to pursuits, color-coded depending on the assembly. Arrows correspond to the timing of the onset of calcium deviation for each assembly.

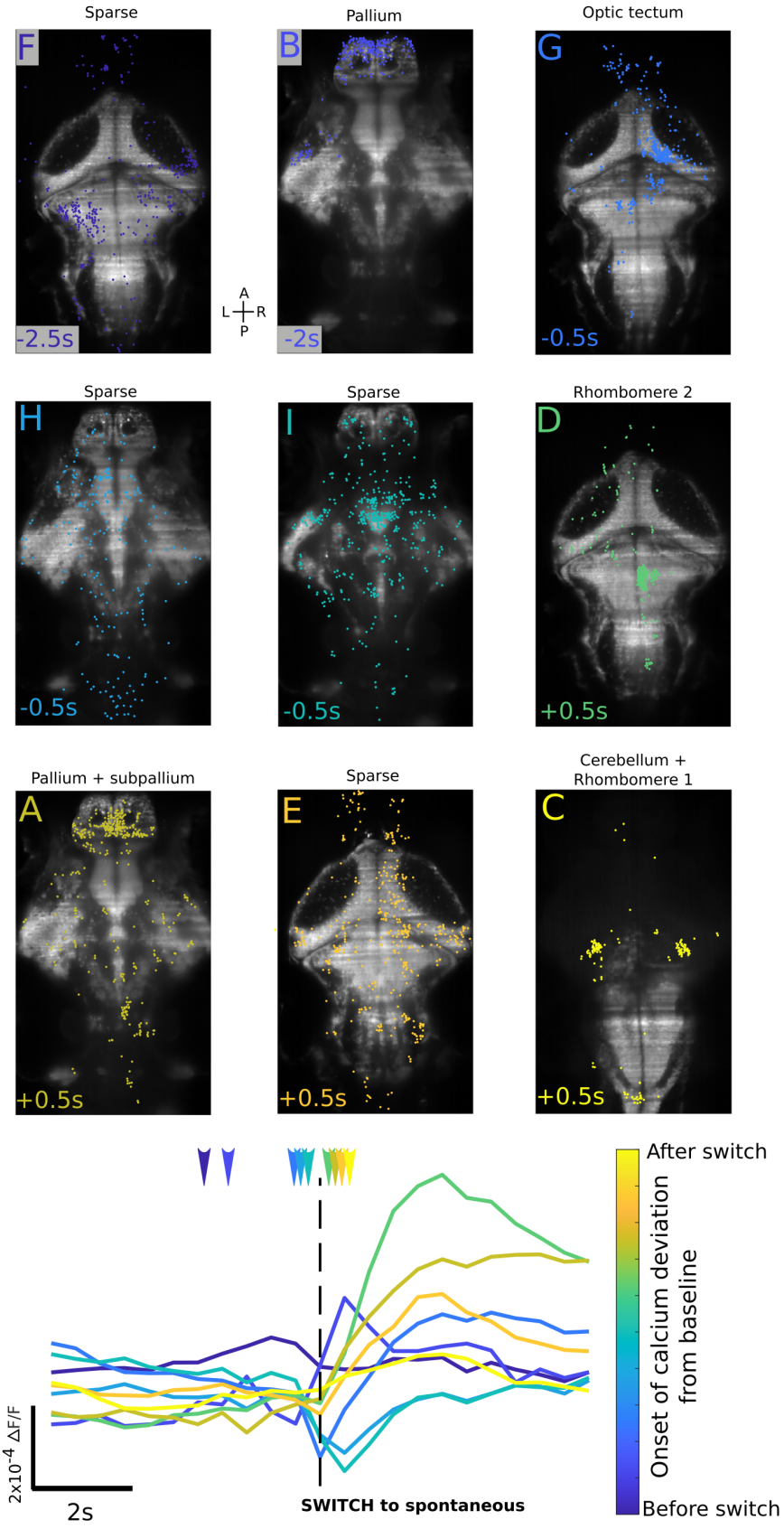

Figure 4.9: **Activation of the assemblies associated with the switch to spontaneous rotations.** Order of activation (or inhibition) of the assemblies around the switch to spontaneous. **(legend continues on next page)**

4.2.4 A Bayesian decoder for predicting the onset of the alternation in the perceptive states

Implementation of a Bayesian Decoder

During the presentation of the ambiguous stimulus, the spontaneous and pursuits behavioral states spontaneously alternate (Figure 4.10A). To find the assemblies capable of predicting the alternations in the behavioral states I created a Bayesian decoder that used the behavioral states as predictors.

During the experiment, I simultaneously recorded behavior and neuronal activity. For each frame of the experiment, the neuronal activity was associated with the corresponding behavioral state (either spontaneous rotations, eye pursuits, 5 seconds before the switch to spontaneous, or 5 seconds before the switch to pursuits). For each neuron that I tested, its activity during each behavioral "trial" was averaged. For decoding, I used part of the neural activity data as the training data for the decoder, and the second part as the "test" dataset so the decoder could find neural activity predictive of the switch in the behavioral state. More precisely, the decoder used Bayes' theorem :

$$P(B|A) = \frac{P(A|B) * P(B)}{P(A)}$$

with

- A: the activity of neurons of interest
- B: the behavioral state
- $P(B|A)$: the posterior probability, i.e. the probability that the behavioral state was B given that we know the activity of neurons A
- $P(A|B)$: the likelihood, i.e. the probability of observing the activity A given the behavioral state B
- $P(B)$: the prior probability, here 25% because there were 4 different behavioral states

Figure 4.9 (continued): Top: location and regions of each assembly, as well as timing of the onset of calcium deviation on the bottom left corner. The letters correspond to the assemblies in Figure 4.7. The background plane is the plane in which the majority of the neurons of this assembly are found. Bottom: mean activity of each assembly around the switch to spontaneous, color-coded depending on the assembly. Arrows correspond to the timing of the onset of calcium deviation for each assembly.

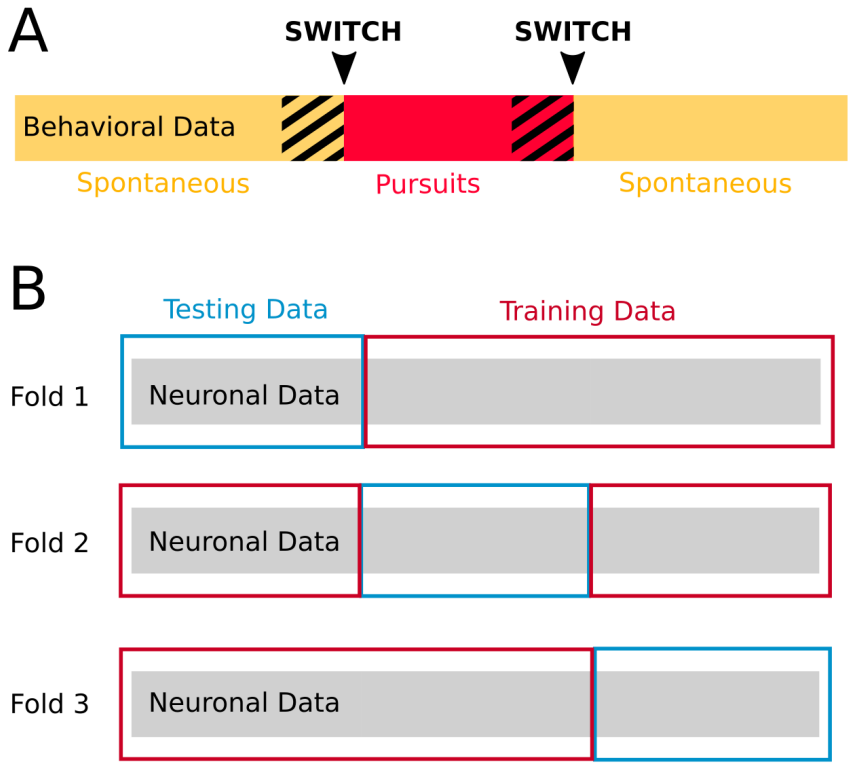

Figure 4.10: **Schematic explanation of the Bayesian decoder. (A)** Schematic representation of a part of the behavioral data. The spontaneous state, pursuits state, 5s before the switch to spontaneous, and 5s before switch to pursuits are the different predictors for the decoder. Yellow: spontaneous state ; Red: pursuits state ; Dashed black square: 5s before the switch ; Black arrow: switch. **(B)** Schematic representation of the way the decoder works, with 3 folds in which the testing and training part of the data are changing. Grey: neuronal data ; Blue box: one-third of the data that is the testing data ; Red box: two-third of the data that is the training data.

- $P(A)$: the evidence or marginal probability

The decoder finds the behavioral state that gave the maximum posterior probability given the observed activity of neurons. For this, the decoder uses information about the Gaussian fitting parameters (mean and standard deviation) of the distribution of the neuronal activity in each behavioral state from the training data, and calculates for the testing data the likelihood $P(A|B)$ that the observed activity of one neuron was obtained from each behavioral state. $P(B)$, in our case, is a constant for each experiment. As for $P(A)$, I could exclude it from the decoder because for each activity A it was constant. The importance is not the absolute value of the posterior probability $P(B|A)$, but the relative value for each behavioral state. To avoid potential numerical instability due to calculation using small percentages, I changed the calculation from the product of probabilities to the sum of log probabilities. Then the calculation made by the decoder

was :

$$log(P(B|A)) = log(P(B)) + \sum log(P(A|B))$$

Calculating the natural logarithm of probabilities (that are by definition inferior to 1) creates negative numbers, with the smaller probabilities being further from zero. Therefore the activity of the neurons were classified as the behavioral state for which $log(P(B|A))$ was maximum (closer to zero).

The classification of the decoder was then compared with the real observed behavior. I calculated its accuracy as the percentage of trials where the decoder gave the correct classification on the total number of trials. All of this was made in 3 different folds, by taking a different third of the data as the testing data in each fold (Figure 4.10B), and the accuracy of the decoder was averaged from the 3 folds.

Accuracy of the decoder for each assembly

I ran the decoder independently for each of the 623 assemblies of the example larva, obtaining an accuracy value for each of them. I ordered them according to this accuracy of the decoder and ran again the decoder taking the neurons from the first 10, 20, 30, etc. assemblies up to all assemblies together (representing 98% of all recorded neurons).

The majority of the assemblies had an accuracy value around 60% (Figure 4.11A), and 13 of them had an accuracy value above 80%. When taking the best 10 assemblies together

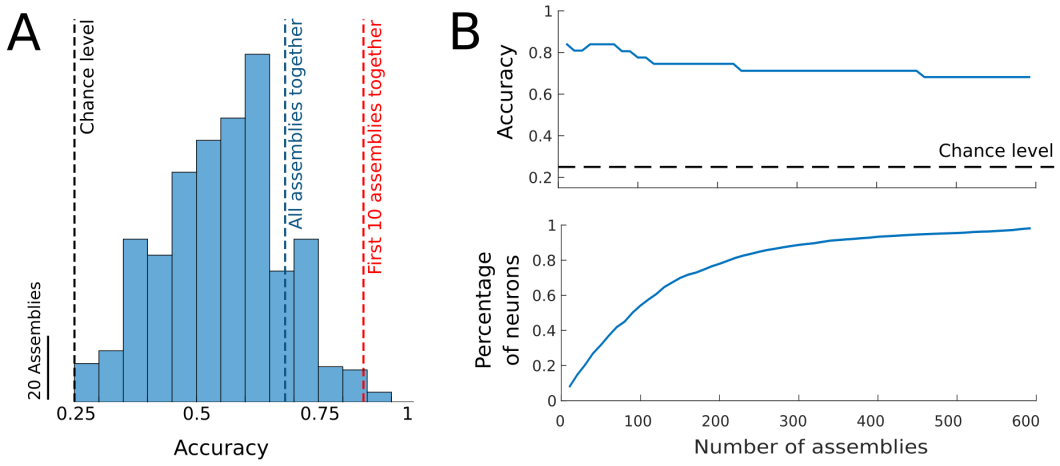

Figure 4.11: **Summary of the accuracy of the decoder for the assemblies. (A)** Histogram of the accuracy of each assembly. Black dashed line: chance level ; Blue dashed line: accuracy for every assemblies together ; Red dashed line: accuracy for the best 10 assemblies together. **(B)** Top: Evolution of the accuracy of the decoder when adding assemblies 10 by 10. Black dashed line: chance level. Bottom: Evolution of the percentage of neurons taken into account when adding assemblies 10 by 10.

the accuracy was 84.2%, whereas all assemblies together had an accuracy of 67.7%. All assemblies together thus showed a better decoding than many individual assemblies, but also worse than other combinations. The number of assemblies that had an individual decoding accuracy better than the accuracy for all assemblies were the first 100 assemblies (assembly 100 accuracy: 67.9% ; assembly 101 accuracy: 67.6%). Adding every assembly together just seem to add noise on the ones that are really able to decode. I observed that also by plotting the accuracy of the decoder by adding to it assemblies 10 by 10 (Figure 4.11B): up to 70 assemblies together the accuracy of the decoder was still 84.2% but then adding more and more just made the accuracy lower. 70 assemblies represented 42% of the recorded neurons, and it thus seemed that the rest of the assemblies are just adding noise to the decoding. Even the first 10 assemblies already showed an accuracy of 84.2%, and represented only 7.7% of the neurons. Even more interesting, the best 3 assemblies, displaying each an accuracy of 87.1%, corresponded to 0.5%, 1% and 1.5% only of all recorded neurons. A few neurons contained enough information for the decoder to reliably identify which behavioral state, including 5 seconds before the alternation, the activity of the neurons corresponded to. This suggest that the alternations in behavioral states are underlay by a handful of assemblies rather than a single one.

The example assemblies from Figure 4.7, which were found by looking at the change of activity around both switches, had various decoding accuracies and did not all decode well the alternations (A: 70.9% ; B: 60.9% ; C: 38.8% ; D: 64.2% ; E: 61.2% ; F: 28.8% ; G: 58.2% ; H: 51.5% ; I: 67.9%).

When analysing the topography of the decoding assemblies, I found that most of them were sparse (neurons are disperse around a large volume). However, when looking in which brain regions the assemblies are located, I found for the 10-best decoding assemblies were located mainly in the rhombomeres 1,2,6 and 7, the tectum, the cerebellum and in particular the cerebellar VGlut2-enriched area, the tegmentum, and the torus semicircularis.

I then looked at the activity around the switch of the 100 assemblies that best decoded the behavioral states and I clustered them according to their similarity using the k-means algorithm. The number of clusters was defined using the silhouette algorithm. For the switch to eye pursuits the maximum mean of the silhouette value corresponded to k=6 (silhouette mean: 0.52) and for the switch to spontaneous it was for k=9 (silhouette mean: 0.49) (Figures 4.12 and 4.13).

For the switch to pursuits, I observed only one assembly that was active before the switch (cluster 1 in Figure 4.12) and that was inhibited after the switch. The other clusters either did not show any activity (cluster 2), showed a transient increase in activity at the time of switch (cluster 3) or a sustained increase (clusters 4, 5 and 6). The difference

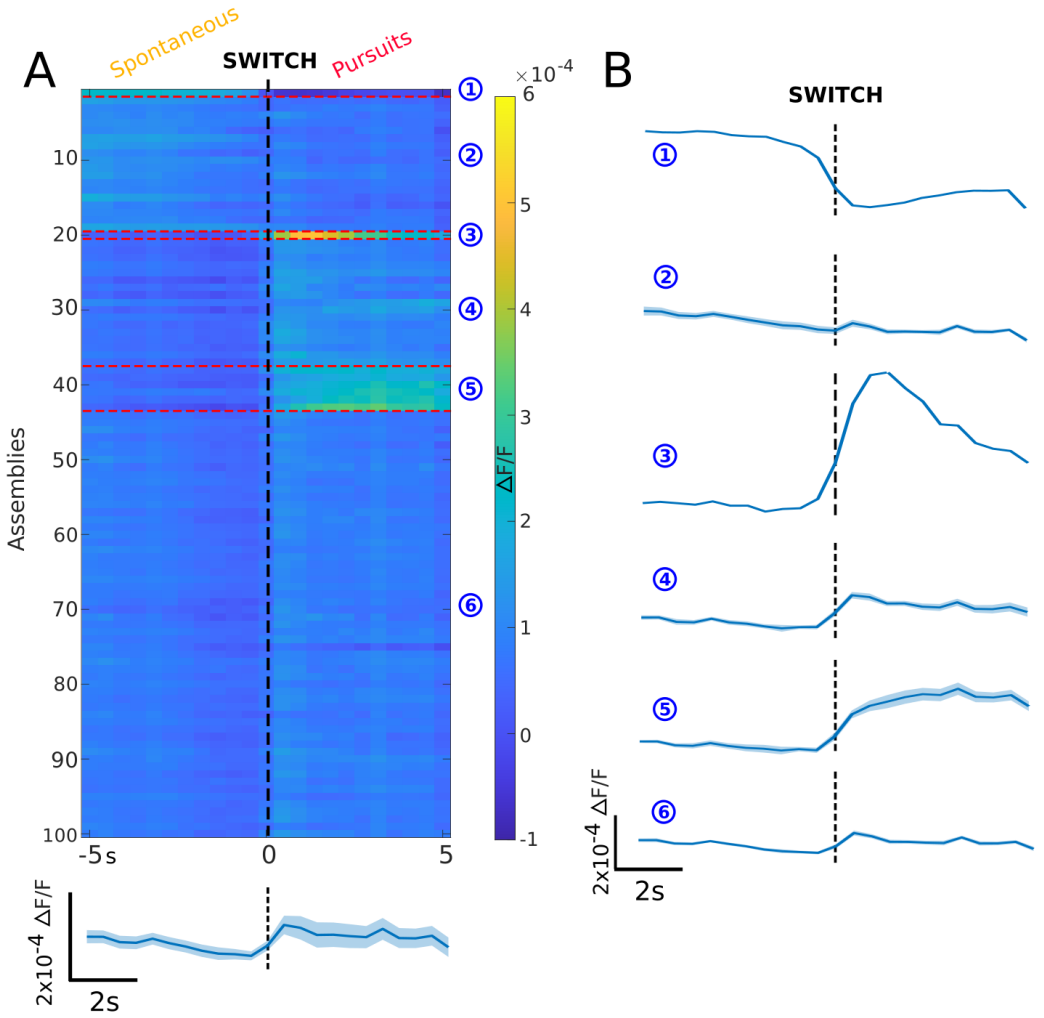

Figure 4.12: **Temporal dynamics of the 100 best predictive assemblies around the switch to pursuits. (A)** Raster of the mean activity of each of the 100 best assemblies in the decoder from the example larva from 5s before to 5s after the switch to pursuits. The assemblies (y axis) are arranged by clusters of similar activity, separated by horizontal red dashed lines. The vertical black dashed line represents the time of switch. Below is the mean ± S.D. of the activities taking all 100 assemblies together. **(B)** Mean activity ± S.D. of each of the 6 clusters from (A). The vertical black dashed line represents the time of switch.

between the clusters 4, 5 and 6 seemed to be on the amount of relative increase of activity. For the switch to spontaneous, there was also only one assembly active before the switch (cluster 1 in Figure 4.13) which displayed a transient decrease in activity around the switch. The other clusters had an increase of activity after the switch, either transient (cluster 3) or sustained (all the rest of the clusters). The amount of relative increase in activity was the main difference between these latter clusters.

For the decoder, I used the spontaneous rotations, the eye pursuits, and 5 seconds before the switch to both. The decoder did not take into account specifically the 5 seconds after the switches. Yet the majority of the assemblies capable of decoding display activity

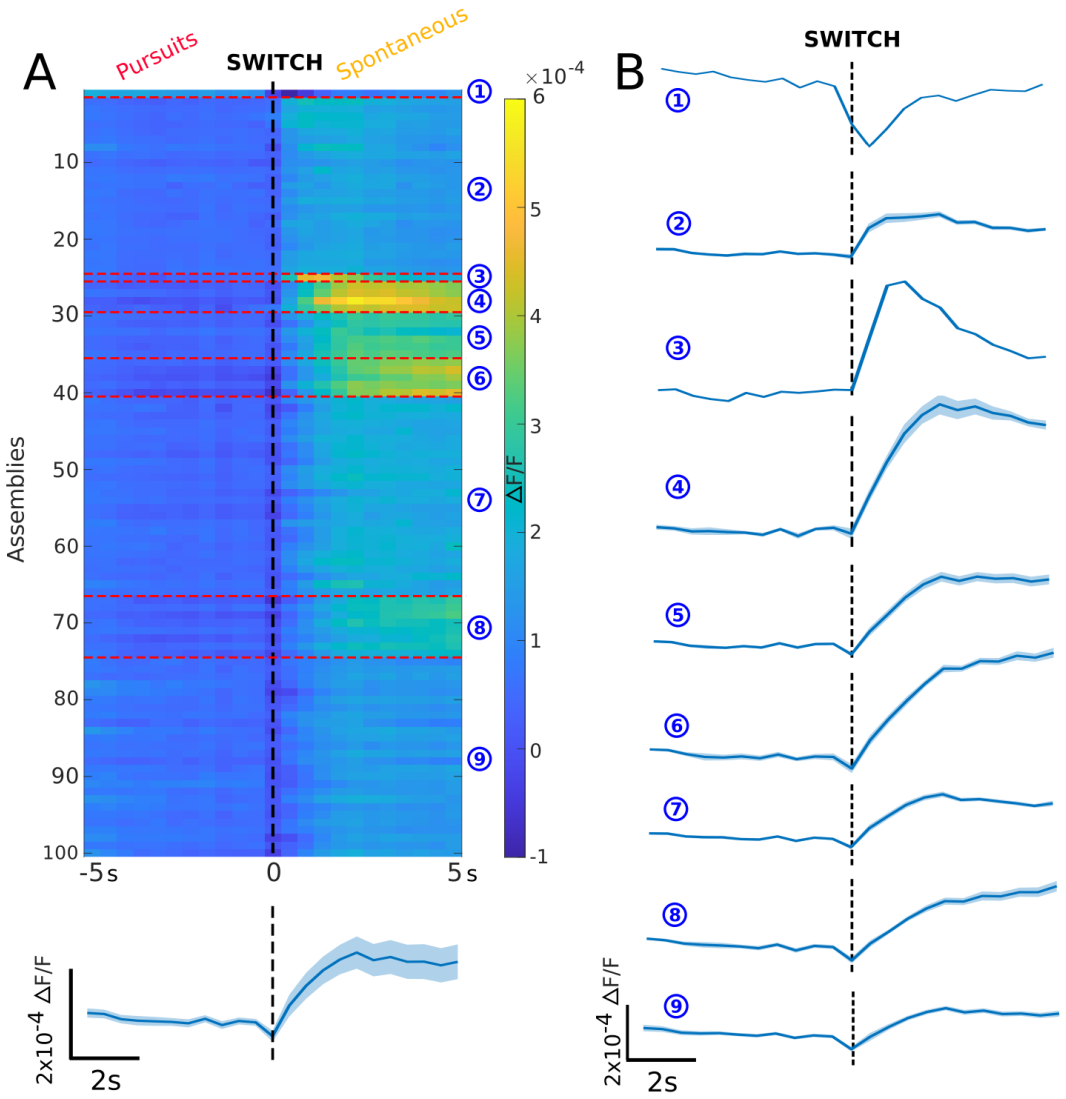

Figure 4.13: **Temporal dynamics of the 100 best predictive assemblies around the switch to spontaneous. (A)** Raster of the mean activity of each of the 100 best assemblies in the decoder from the example larva from 5s before to 5s after the switch to spontaneous. The assemblies (y axis) are arranged by clusters of similar activity, separated by horizontal red dashed lines. The vertical black dashed line represents the time of switch. Below is the mean ± S.D. of the activities taking all 100 assemblies together. **(B)** Mean activity ± S.D. of each of the 9 clusters from (A). The vertical black dashed line represents the time of switch.

mainly after the switch. The mean activity of the assembly thus may not be the main information that the decoder relies on.

To understand what parameter of the assemblies activity best decode the alternations in behavioral states, I plotted the confusion matrices of the decoding, that gave information on where the decoding was making mistakes.

The main error made by the decoder was the misclassification of other behavioral states as spontaneous rotations, for the 3 best decoding assemblies as well as for all

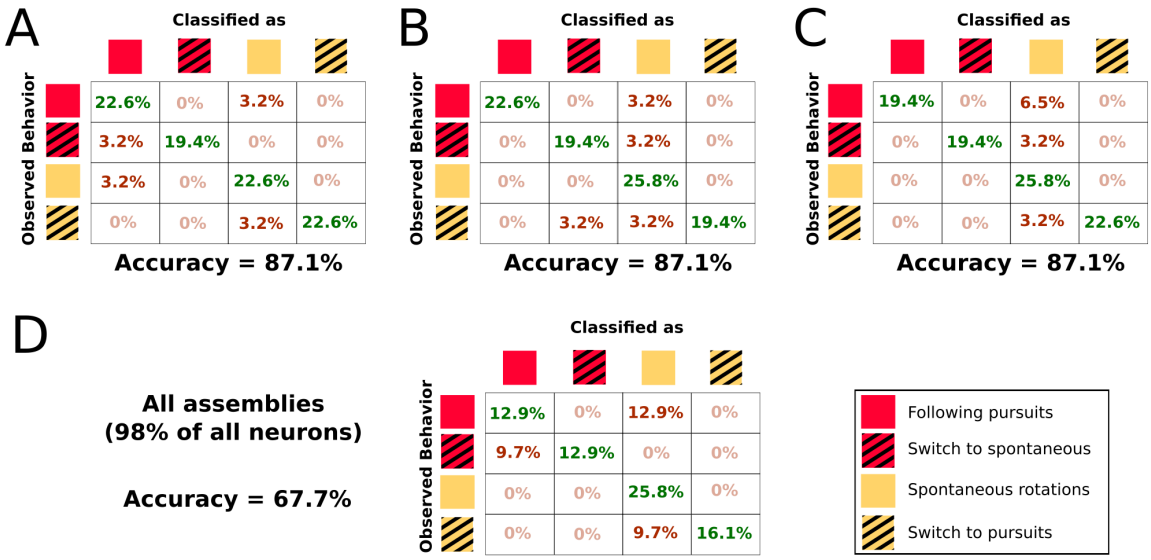

Figure 4.14: **Confusion matrices of the decoder. (A-C)** Confusion matrices of the decoder for the 3 best decoding assemblies. Text in green: the decoder was correct. Text in red: the decoder was wrong. **(D)** Confusion matrix of the decoder for all assemblies together.

assemblies together (Figure 4.14). It was even the only mistake in the assembly C of Figure 4.14. Thus, the specificity for the spontaneous rotations is not very good. This could be explained by the fact that the spontaneous rotations state is the behavioral state that is the longest in the data, and the activity of the neurons might be more diverse because of that. In Figure 4.14A, there was also a few mistakes that classified spontaneous rotations or the switch to spontaneous as pursuits. In Figure 4.14B, some switch to pursuits were wrongly classified as switch to spontaneous. It is interesting to observe that even though the 3 best decoding assemblies showed the same amount of accuracy, the few mistakes were not the same, implying that a different information is extracted from each assembly.

In Figure 4.14A, C and D, the decoder never classified as 5s before the switch to spontaneous a state that was not this switch, and the same is true for the switch to pursuits, meaning that the specificity of the decoder for both perceptive alternations is very good. This implies that there is something in the activity of the neurons that the decoder is able to extract to get the information of an incoming switch, and in which direction of alternation.

The other mistakes observed for every assembly together are either switch to spontaneous classified as pursuits or switch to pursuits classified as spontaneous rotations (Figure 4.14D). This is interesting because the behavior is actually correctly classified: the only difference between 5s before the switch to spontaneous and the pursuits state is the fact that the switch is upcoming or not (same for 5s before the switch to pursuits and

spontaneous rotations). Thus, all assemblies actually classified the behavior per se very well (with no information on the timing of alternation), implying that the two behavioral states are also two neuronal states distributed across the entire brain.

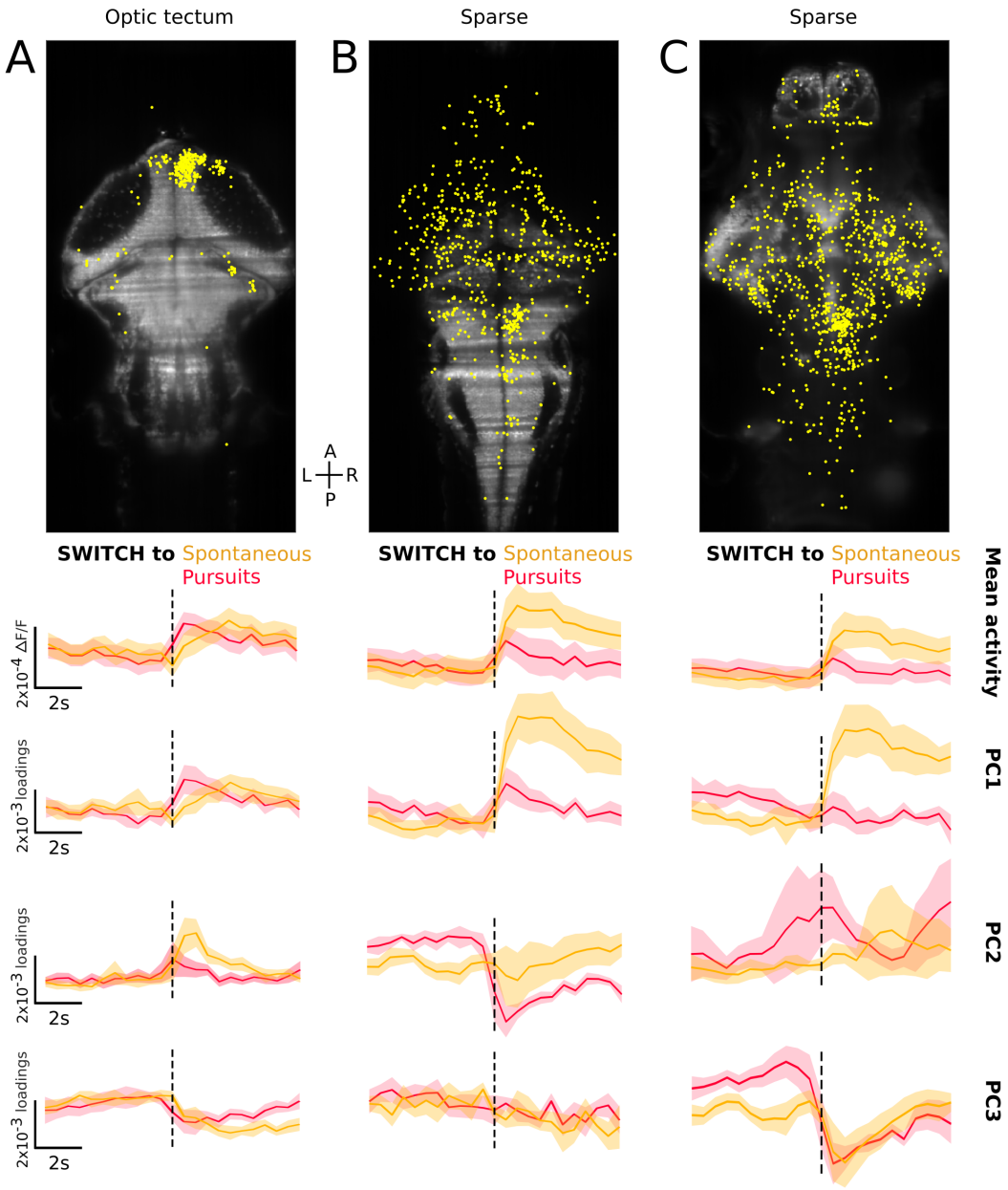

Figure 4.15: **The best 3 decoding assemblies. (A-C)** Location in the brain of the 3 best decoding assemblies (yellow dots), with the indication on top of the main region(s) where the neurons are found. The respective assemblies A, B and C correspond to the same letter in Figure 4.14. The background plane is the plane in which the majority of the neurons of this assembly are found. Just below is the mean ± S.D. activity of the assembly around the switch to pursuits (red) and to spontaneous (yellow). Below the mean activity are the traces (mean loadings ± S.D.) of the first 3 principal components when running PCA on the neuronal activity of the assembly. The vertical black dashed line represents the time of switch.

Looking at the location of the best 3 decoding assemblies, I found that one was located in the optic tectum, and the other two were topographically sparse (Figure 4.15). Their activity was increasing after the switch, but looking only at the mean activity there did not seem to be any major difference between both types of switches. Thus, it is possible that additional information exists in the neuronal activity of the assemblies beyond their mean activity that the decoder could use to infer the behavioral state.

To study this possibility, I ran on each assembly a principal component analysis (PCA) on the activity of its neurons. This method allowed the emergence of principal components (PCs) that best fit the data along different dimensions. The first PCs are representing the data contained in all the neurons of the assemblies in a lower dimension, while keeping as much variation of the neuronal data as possible. For the best 3 predictive assemblies, the explained variance was respectively of 20.4%, 10.9% and 7.3% for PC1, 3.8%, 5.3% and 6.2% for PC2, and 3.3%, 2.9% and 4.7% for PC3. Plotting the first 3 PCs of the assemblies during the switch to spontaneous and the switch to pursuits, I observed that PC1 was nearly perfectly following the mean activity of the assembly (Figure 4.15). However, PC2 was very interesting for the assembly B, with the switch to pursuits having a very different dynamics in PC2 space compared to the switch to spontaneous. For the assembly C, the PC2 and PC3 were displaying before both switches changes in the traces. For the assembly A however, no real difference was found in PC2 or PC3.

As it can be observed in the examples of the assemblies B and C, PCA is extracting relevant information in the neuronal data beyond the mean activity. For example, it can represent the co-varied activity of a subgroup of neurons within an assembly. This suggest that certain assemblies can be activated through different topographic patterns, and each patter could represent a different function of the assembly. The decoder might be able to extract this information and differentiate both switches. However, other explanations are needed for the assembly A: maybe the information exists on later PCs.

4.2.5 Broadening to other larvae

The results presented in this section all come from the same larva, but I analysed also a few others during my PhD. The results are mostly the same in terms of the decoding accuracy of every assembly: between 50% and 70% of accuracy. However, I could not find conserved assemblies across the different larvae. Some general regions were found consistently like the optic tectum, the rhombomeres or the cerebellum but not precise regions. It is possible that the alternations of behavioral states of the different larvae are induced by different mechanisms. Alternatively, the functional connectivity and therefore the identity of the neuronal assemblies could differ between larvae (source of individuality), and therefore, the assemblies that their activity is predictive of the alternations of the behavioral states

would not be the same across larvae.

4.2.6 Additional experiments to study the neuronal mechanisms underlying the alternations of behavioral states

In multiple sparse assemblies, I found a certain fraction of the neurons that were located in the torus semicircularis, for example in the assembly F in Figure 4.7. This region of the brain located laterally below the optic tectum is activated in response to auditory stimulation [Privat et al., 2019]. Thus, I wondered if sounds could change the rate of the perceptual switches. To test this hypothesis, I ran another behavioral experiment, projecting the ambiguous stimulation (F1=10%) for 1 hour, while presenting every 30s a sound stimulus of 300 or 1000 Hz, lasting 1s. For n=5 larvae, the correlation between the sound at 300 Hz and the switch to spontaneous was 0.02 ± 0.02, and for the switch to pursuits it was 0.01 ± 0.02. Between the sound at 1000 Hz and the switch to spontaneous, the correlation was 0.03 ± 0.01, and with the switch to pursuits it was 0.03 ± 0.01 also. I did not find any correlation between the sound presentation and the perceptual alternation rate.

The optic tectum has 3 main types of neurons: glutamatergic, gabaergic and cholinergic. The cholinergic system is known to modulate the attentional [Thiele and Bellgrove, 2018] or internal states of the brain [Lovett-Barron et al., 2017]. Therefore, I wondered whether activating cholinergic neurons could have an influence on the alternation rate of the zebrafish larvae. For this purpose, I performed behavioral experiments while presenting to the larvae the ambiguous moving visual stimulus (F1=10%, see the Results section 4.1.1). In this experiment, I used transgenic larvae expressing ChRimson or ChR2 in cholinergic neurons thanks to the cholinergic promoter acetyltransferase ChAT (lines ChAT:ChRimson bonded to a red fluorescence protein TdTomato to check the presence of the channelrhodopsine, and ChAT:ChR2 bonded to a yellow fluorescence protein EYFP, both lines from the team of Prof. Rainer Friedrich in the Friedrich Miescher Institute for Biomedical Research, Basel, Switzerland). While presenting the ambiguous visual stimulus, I illuminated at random intervals a large portion of the larva's brain, including the optic tectum, via a fiber optic focused on top of the optic tectum of the larvae. The fiber was coupled to a 565nm LED for the ChRimson larvae (ChRimson absorption peak is 590nm) and at 455nm for the ChR2 larvae (ChR2 absorption peak is 470nm). I recorded n=10 transgenic zebrafish larvae expressing paneuronally ChRimson. I found no difference in the behavior with the presence or absence of light (Light ON: pursuits in the stimulus direction 2.2 ± 3.1, pursuits in the opposite direction 24.5 ± 14.2, spontaneous rotations 73.3 ± 14.7 ; Light OFF: pursuits in the stimulus direction 2.2 ± 2.7, pursuits in the opposite direction 26.4 ± 13.1, spontaneous rotations 71.4 ± 13.3). The same

was found for the n=9 ChR2 larvae (Light ON: pursuits in the stimulus direction 1.7 ± 1.8, pursuits in the opposite direction 27.4 ± 17.3, spontaneous rotations 70.9 ± 17.5 ; Light OFF: pursuits in the stimulus direction 1.6 ± 3.1, pursuits in the opposite direction 22.5 ± 15.5, spontaneous rotations 75.8 ± 14.9). Thus, these experiments showed no significant effect of the activation of the cholinergic system on the alternation rate of the behavioral states.

Unpublished work form the lab found that alertness induces synchronous activation of tectal radial glia. This synchronous activation modulates the directional selectivity of tectal neurons. I therefore tested whether the alternations in the behavioral states is associated with the radial glia synchronizations in the optic tectum. Using two-photon calcium imaging in transgenic zebrafish larvae expressing GCaMP6 in radial glia (Her4:GCaMP6f), while presenting the ambiguous visual moving stimulus, I calculated the pairwise correlation values between the activity of the radial glial cells and the 5 seconds before the switch to spontaneous (correlation value: -0.02 ± 0.04 for n=3 larvae) and the same with the 5 seconds before the switch to pursuits (correlation value: 0.002 ± 0.05 for n=3 larvae). The results showed no significant correlation between both events (glia synchronization and alternation in behavioral states).

5

Conclusions and perspectives

5.1 Fourier motion detection in the zebrafish larva

The first part of my PhD was focused on studying how Fourier motion was processed by the zebrafish larva. For this purpose, I monitored the activity of the two main visual centers in the zebrafish brain, the optic tectum and the pretectum, while presenting to the larva visual moving stimuli containing or lacking the first Fourier component.

The zebrafish larva mainly uses Fourier energy to detect visual motion

I created a missing-fundamental stimulus by suppressing the fundamental frequency of a square-wave signal. The features of the missing-fundamental stimulus all move in the same direction as the ones from the square-wave stimulus, except for the Fourier energy that correlates with the direction of the induced eye pursuits. I showed that the presentation of both stimuli induced OKR in opposite directions. Therefore, the larva follows behaviorally the Fourier motion energy and not the other features, as was previously described using the optomotor response (OMR) [Orger et al., 2000].

The activity in the optic tectum represents several features of the presented stimuli

In the optic tectum, I found neurons that responded to several features of the presented static and moving stimuli, including the contrast patterns, spatial frequency, the direction of a moving square-wave stimulus, etc. It responds to the static missing-fundamental stimulus but not to the direction of motion of this stimulus. I did not observe any topographical representation of the different features in the optic tectum, apart from a lateralization of the representation of square-wave motion direction. This is in line with a previous finding showing that the direction-selective neurons are topographically scattered across the tectal circuit [Romano et al., 2015]. Therefore, the optic tectum seems to represent many features of visual motion stimuli. However, it failed to respond to the Fourier motion energy of the missing-fundamental stimulus, most probably because the directional information contained in the stimulus is not coherent (first-order components move in one direction and the second-order ones move in the opposite). These results indicate that the optic tectum is not involved in generating the main properties of OKR. This is in line with the fact that ablation of the optic tectum has been shown to only minimally affect the kinematics of OKR [Roeser and Baier, 2003] and that the optic tectum only plays a modulatory effect on the habituation of OKR and the generation of the motion after effect [Pérez-Schuster et al., 2016].

The activity in the pretectum mainly represents the Fourier energy of the visual stimulus

In contrast to what was observed in the optic tectum, I found that the activity of pretectal neurons mainly represented the eye behavioral state regardless of the type of stimulus presented. In the missing-fundamental stimulus, the Fourier energy is the only feature that correlates with the behavior, so the pretectum mainly computes the Fourier energy of the stimulus to generate OKR and OMR. This is in line with previous results stating that the pretectum is a central region involved in optic flow processing [Matsuda et al., 2021], necessary and sufficient for the generation of OKR [Kubo et al., 2014]. Moreover, I found a spatial organization in the responses to the different motion stimuli in the pretectum. The direction of motion was better represented in the caudal than the rostral part. In the caudal part, each hemisphere responded to a different direction of motion (motion to the left for the left hemisphere and motion to the right for the right hemisphere). During detection of motion to the left (respectively right), the right eye (respectively the left eye) is making pursuits in the temporal-to-nasal direction, and projects to the left hemisphere (respectively the right hemisphere): indeed the retina in zebrafish projects almost exclusively to the contralateral hemisphere of the brain [Burrill

and Easter, 1994]. So my observations (motion to the left for the left hemisphere and motion to the right for the right hemisphere) are in agreement with the results obtained by Chen *et al.* showing that eye pursuits were longer in the temporal-to-nasal direction than the nasal-to-temporal direction [Chen et al., 2016], and Wang *et al.* that showed that pretectum's cells respond more to temporal-to-nasal than nasal-to-temporal monocular moving stimuli [Wang et al., 2019].

Perspectives

In this part of my PhD project, I recorded from only one optical plane in the optic tectum and one plane in the pretectum. It is thus possible that some response types were missed. In the future, it could be possible to use light-sheet microscope to record from the entire tectal and pretectal circuits [Ahrens et al., 2013, Panier et al., 2013], as I did in the second part of my PhD.

I recorded here only in the optic tectum and the pretectum. However, both regions are innervated by the retinal ganglion cells thus it would be very interesting to also record from these neurons, to see what motion information is sent to central regions during the missing-fundamental stimulus presentation, as well as from the other regions innervated by the retinal ganglion cells via the other arborization fields, to get a more general idea of the way the first-order motion component is processed in multiple brain areas.

In this study, I focused on first-order (Fourier) motion. However, even without first-order signals, humans are still capable of perceiving motion: this is what is called non-Fourier (or second-order) motion detection and was thought for a long time to necessitate a cortex. Nevertheless, even without a cortex some animals have been found to be capable of detecting second-order motion. It is the case for flies [Theobald et al., 2008], as well as zebrafish [Orger et al., 2000], that can use second-order motion when this is the only available information. In humans, it is thought that two parallel pathways process the first- and second-order motion [Papathomas and Rosenthal, 1996, Nishida et al., 1997], a model that has been supported also by studies on patients with brain lesions [Vaina and Soloviev, 2004, Rizzo et al., 2008]. Maybe in zebrafish the pretectum mainly responds to the Fourier energy (first-order) of a moving visual stimulus, while for processing second-order motion (associated with local contrast, edges, texture, etc.) the optic tectum takes the relay to control OKR. More experiments are needed to test this hypothesis, for example observing more closely the responses of the optic tectum and pretectum to higher-order features of the signal in combination with pretectal and tectal ablations. Experiments testing the specific involvement of both regions when only second-order motion is present, for example with contrast-defined motion, would also strengthen or infer this hypothesis. The results of my PhD show that the pretectum displays responses

to the Fourier motion independently of the other stimulus' features, while the optic tectum cannot respond in line with the Fourier motion if the non-Fourier features are not coherently moving. Overall, the obtained results suggest that the optic tectum extracts the second-order as well as the first-order information, while the pretectum only process first-order information.

5.2 Neuronal basis of alternations of behavioral states

The second part of my PhD was dedicated to study how alternation of behavioral states are generated in the brain, using a modified version of the missing-fundamental and square-wave stimuli studied in the first part of the thesis. The behavioral output from these two stimuli is eye pursuits in opposite directions, and the idea was to create an intermediate stimulus that would be ambiguous: the larvae would sometimes generate spontaneous alternations between eye pursuits in one or the other direction.

The zebrafish larva does not show visual bistability

To investigate whether zebrafish larva display visual motion bistability, I modified the square-wave stimulus by decreasing the power of the fundamental frequency instead of totally suppressing it, as done for the missing-fundamental stimulus. Testing different power percentages of the fundamental frequency, I observed that when the ambiguity was at its maximum (at 20% of the fundamental frequency), the larvae only showed spontaneous eye rotations as if the larva did not detect visual motion. This suggests that zebrafish and mammals use different visual processing mechanisms. In mammals two percepts of an ambiguous stimulus are first integrated and later compete for perception through a winner-takes-all mechanism [Scocchia et al., 2014]. In zebrafish, the two motions information may be summed up by the sensory circuit rather than inhibiting each other. The latter thus results in no movement detection as the neural responses to opposite directions cancel each other.

Still, when the stimulus is less ambiguous, by setting the first Fourier component at 10% or 40% of its power, I observed an alternation in the behavior between a state of spontaneous rotations and a state of eye pursuits. It thus seems that below some threshold of ambiguity, the larva display an alternation of behavioral states, between a state of "perception" of the motion and a state of "no-perception" of the motion. It is important to note that this alternation in behavior does not appear when presenting to the larva the other types of stimuli: when presenting to the larva the moving square-

wave or missing-fundamental, its behavior will remain in the pursuit mode, and when presenting a static stimulus, its behavior will remain in the spontaneous mode. Hence, an alternation of behavioral states induced specifically by ambiguous stimuli exists in the zebrafish larva. I therefore studied the alternations between "perceptive" and "non-perceptive" states.

Involvement of the neuronal assemblies in the alternation in behavioral states

To study the alternation between the two types of behavioral states, I used a square-wave signal with 10% of the power of the fundamental frequency which induced balanced alternations between pursuits in the Fourier direction and spontaneous eye rotations. While presenting this ambiguous stimulus, I monitored whole-brain activity using light-sheet calcium imaging. Using this paradigm, I found that neuronal assemblies were more active after the alternations of behavioral states than before the alternations. This effect was more pronounced for the switch to spontaneous eye movements. This suggests that the alternation to the "spontaneous mode" is generally more active than the switch to "pursuit mode".

However, the activity of individual assemblies was variable. Certain assemblies showed an increase in activity during or after the switch, some showed no change, and others were more active before the switch and transiently decreased their activity during the switch. The assemblies active around the time of the switch were located in various regions across the brain: the cerebellum, the pallium, the hindbrain, and a lot of them were also topographically sparse. The onset of the activity deviations from baseline of the neuronal assemblies with respect to the time of the switch in behavioral state showed a sequential activation of the assemblies leading to the behavioral switch. This sequence started a few seconds before the switch to 1 second after the switch, suggesting that some assemblies are inducing the activation of others.

Assemblies decoding the behavioral states

Aiming to find the neuronal assemblies that could predict the switch between the two behavioral states, I build a Bayesian decoder. I ran the decoder on individual assemblies and found that a few of them were performing very well. The information about the behavioral state and the impending switch seems to be present in certain assemblies. However, most of the assemblies were not predictive of the switch and just added noise to the decoding. The best 3 decoding assemblies were showing the same level of accuracy (87.1%), but interestingly the decoder did not do the same types of mistake for each

of the 3: a few assemblies are enough to get the majority of information about the behavioral state, but each carries a slightly different information. This suggests that different assemblies may code different aspects of the alternation between behavioral states. A common mistake of the decoder was to classify the 5 seconds before the switch to spontaneous as eye pursuits, or inversely to classify the 5 seconds before the switch to pursuits as spontaneous rotations. It is interesting because with this mistake, the behavior is actually well classified if we do not take into account the information about the upcoming alternation. This implies that when presenting the ambiguous stimulus, there are two general brain activity states across several brain regions representing the two behavioral states: spontaneous rotations or eye pursuits. It is also important to note that the specificity of the decoder to the 5 seconds before both switches was very good (there were not false positives, i.e. no other behavior was classify wrongly as this one). Therefore, these assemblies carry information about the impending alternation between behavioral states.

It was surprising to observe that the best decoding assemblies display a mean activity around the switch that was increasing after the switch, but showed no specific activity before the switch, even though the activity just before the switch was the one taken into account for the decoder. Therefore, I also looked at the activity patterns of the assemblies in their first 3 principal component spaces. The PC1 corresponded globally to the mean activity around the switch, but the PC2 and PC3 showed interesting time series that differentiated, in certain assemblies, the 5 seconds before the switch to spontaneous or before the switch to pursuits. This observation suggests that the neuronal assemblies have activity substates (activation of subgroups of neurons within the same assembly). The activation of the different substates could then be predictive of the switch between behavioral states.

The main results observed in my example larva was found also in the other few larvae that I could record. However, I did not observe common assemblies consistently predictive of the switch across the different larvae. My hypothesis is that different pathways can induce the alternation in behavioral states, and these pathways could have different weights across larvae and represent a neural basis for individuality.

Perspectives

In each recorded larva in the SPIM microscope, I could record approximately 50 000 neurons, corresponding roughly to 50% of the total brain neurons. The main reason why half of the neurons were not accessible was because some part of the larva's brain is between its eyes, and thus not accessible for the laser coming from the side of the larva. To overcome this problem, we worked in the lab on a new version of our SPIM microscope

in which a second laser was added coming from the front of the larva and lighting the part of the brain between the larva's eyes. Experiments in this new setup are still in progress.

Another interesting follow-up analysis on my experiments would be to decipher the two behavioral states of spontaneous rotations and eye pursuits in the brain data. If we can find markers that indicates if the larva is in one or the other state it could help to better determine the timing of the switch, among other things. Indeed, because of the read-out of behavioral state I used, I do not have a very precise timing of the alternation as saccades are separated by approximately 5 seconds. A neuronal read-out of the behavioral state might help us have a more precise temporal resolution about the onset of the alternation between behavioral states.

Ideally, it will be important to test for causality and not just correlation of the activity with the behavioral alternation. The first attempt using auditory stimuli and optogenetic modulation of the cholinergic system did not show any correlations with the alternations, but stimulation of other modulatory pathways could. For example, dopamine, noradrenaline, and serotonine are the neuromodulators involved in top-down attentional control [Thiele and Bellgrove, 2018], that can influence the alternation [Scocchia et al., 2014]. It is also known that the GABA inhibition can modulate the dynamics of bistable perception [Van Loon et al., 2013], so studying in more detail the activation of the inhibitory pathways, and transient changes in excitation/inhibition ratio could be an interesting trail to follow. In the lab, we have recently succeeded in using genetic markers in combination with GCaMP to monitor the activity of excitatory and inhibitory neurons. Moreover, the response of some regions in the larva brain might be interesting to study in more details during the ambiguous stimulation, as for example the habenula, that is known for being involved in attentional processes [Lecourtier and Kelly, 2005] and decision making [Cherng et al., 2020], or the nucleus isthmi, that has been shown to be involved in context-dependent stimulus selection [Fernandes et al., 2021] and sustained attention during prey hunting [Henriques et al., 2019].

It would also be interesting to model the alternation in behavioral states, between a state of winner-takes-all where one direction of motion wins ("perception" state), and a state where the signals are added with none of them taking over the other, resulting in spontaneous behavior ("no-perception" state). Modeling would allow to better understand the phenomena at play during the alternation and predict more precise mechanisms that could be tested experimentally afterwards. According to the results in the first part of my PhD, we could imagine that in the "perception state" the pretectal neurons would respond to the Fourier motion direction and send the appropriate OKR commands, while in the "no-perception state" it would not send them, which would result in spontaneous rotations. However, decoding assemblies were found sometimes in the pretectum, but it

was not the major part. Thus, the dynamics explaining why the pretectum would be able or not to discriminate the Fourier motion direction might come from other regions of the brain.

Bibliography

[Adelson, 1995] Adelson, E. H. (1995). The Checkershadow Illusion.

[Adelson and Bergen, 1985] Adelson, E. H. and Bergen, J. R. (1985). Spatiotemporal energy models for the perception of motion. *Journal of the Optical Society of America A*, 2(2):284.

[Ahrens et al., 2013] Ahrens, M. B., Orger, M. B., Robson, D. N., Li, J. M., and Keller, P. J. (2013). Whole-brain functional imaging at cellular resolution using light-sheet microscopy. *Nature Methods*, 10(5):413–420.

[Anstis, 1970] Anstis, S. (1970). Phi movement as a subtraction process. *Vision Research*, 10(12):1411–IN5.

[Arcaro et al., 2019] Arcaro, M. J., Thaler, L., Quinlan, D. J., Monaco, S., Khan, S., Valyear, K. F., Goebel, R., Dutton, G. N., Goodale, M. A., Kastner, S., and Culham, J. C. (2019). Psychophysical and neuroimaging responses to moving stimuli in a patient with the Riddoch phenomenon due to bilateral visual cortex lesions. *Neuropsychologia*, 128:150–165.

[Aristotle, 1984] Aristotle (1984). *The complete works of Aristotle. Vol.1.* Princeton University Press.

[Azzopardi and Hock, 2011] Azzopardi, P. and Hock, H. S. (2011). Illusory motion perception in blindsight. *Proceedings of the National Academy of Sciences of the United States of America*, 108(2):876–881.

[Barker and Baier, 2015] Barker, A. J. and Baier, H. (2015). Sensorimotor Decision Making in the Zebrafish Tectum. *Current Biology*, 25(21):2804–2814.

[Bernstein and Cooper, 1997] Bernstein, L. J. and Cooper, L. A. (1997). Direction of Motion Influences Perceptual Identification of Ambiguous Figures. *Journal of Experimental Psychology: Human Perception and Performance*, 23(3):721–737.

[Bollmann, 2019] Bollmann, J. H. (2019). The Zebrafish Visual System: From Circuits to Behavior. *Annual Review of Vision Science*, 5(1):269–293.

[Brainard, 1997] Brainard, D. H. (1997). The Psychophysics Toolbox. *Spatial vision*, 10(4):433–6.

[Brown and He, 2000] Brown, R. O. and He, S. (2000). Visual motion of missing-fundamental patterns: motion energy versus feature correspondence. *Vision research*, 40(16):2135–47.

[Brysch et al., 2019] Brysch, C., Leyden, C., and Arrenberg, A. B. (2019). Functional architecture underlying binocular coordination of eye position and velocity in the larval zebrafish hindbrain. *BMC Biology*, 17(1):1–22.

[Burrill and Easter, 1994] Burrill, J. D. and Easter, S. S. (1994). Development of the retinofugal projections in the embryonic and larval zebrafish (Brachydanio rerio). *Journal of Comparative Neurology*, 346(4):583–600.

[Chakrabarti et al., 1983] Chakrabarti, S., Streisinger, G., Singer, F., and Walker, C. (1983). Frequency of gamma-Ray Induced Specific Locus and Recessive Lethal Mutations in Mature Germ Cells of the Zebrafish, BRACHYDANIO RERIO. *Genetics*, 103(1):109–23.

[Chen et al., 2014] Chen, C.-C., Bockisch, C. J., Bertolini, G., Olasagasti, I., Neuhauss, S. C. F., Weber, K. P., Straumann, D., and Ying-Yu Huang, M. (2014). Velocity storage mechanism in zebrafish larvae. *The Journal of physiology*, 592(1):203–14.

[Chen et al., 2016] Chen, C.-C., Bockisch, C. J., Straumann, D., and Huang, M. Y.-Y. (2016). Saccadic and Postsaccadic Disconjugacy in Zebrafish Larvae Suggests Independent Eye Movement Control. *Frontiers in Systems Neuroscience*, 10(October):1–10.

[Chen et al., 2005] Chen, K. J., Sheliga, B. M., Fitzgibbon, E. J., and Miles, F. A. (2005). Initial ocular following in humans depends critically on the fourier components of the motion stimulus. *Annals of the New York Academy of Sciences*, 1039:260–71.

[Chen et al., 2013] Chen, T.-W., Wardill, T. J., Sun, Y., Pulver, S. R., Renninger, S. L., Baohan, A., Schreiter, E. R., Kerr, R. A., Orger, M. B., Jayaraman, V., Looger, L. L., Svoboda, K., and Kim, D. S. (2013). Ultrasensitive fluorescent proteins for imaging neuronal activity. *Nature*, 499(7458):295–300.

[Cherng et al., 2020] Cherng, B. W., Islam, T., Torigoe, M., Tsuboi, T., and Okamoto, H. (2020). The Dorsal Lateral Habenula-Interpeduncular Nucleus Pathway Is Essential for Left-Right-Dependent Decision Making in Zebrafish. *Cell Reports*, 32(11):108143.

[Dehmelt et al., 2019] Dehmelt, F. A., Meier, R., Hinz, J., Yoshimatsu, T., Simacek, C. A., Wang, K., Baden, T., and Arrenberg, A. B. (2019). Spherical arena reveals optokinetic response tuning to stimulus location, size and frequency across entire visual field of larval zebrafish. *bioRxiv*, page 754408.

[Del Bene et al., 2010] Del Bene, F., Wyart, C., Robles, E., Tran, A., Looger, L., Scott, E. K., Isacoff, E. Y., and Baier, H. (2010). Filtering of Visual Information in the Tectum by an Identified Neural Circuit. *Science*, 330(6004):669–673.

[Dieter et al., 2016] Dieter, K. C., Brascamp, J., Tadin, D., and Blake, R. (2016). Does visual attention drive the dynamics of bistable perception? *Attention, Perception, and Psychophysics*, 78(7):1861–1873.

[Dodd et al., 2001] Dodd, J. V., Krug, K., Cumming, B. G., and Parker, A. J. (2001). Perceptually bistable three-dimensional figures evoke high choice probabilities in cortical area MT. *The Journal of neuroscience : the official journal of the Society for Neuroscience*, 21(13):4809–21.

[Duchemin et al., 2022] Duchemin, A., Privat, M., and Sumbre, G. (2022). Fourier Motion Processing in the Optic Tectum and Pretectum of the Zebrafish Larva. *Frontiers in Neural Circuits*, 15(January):1–15.

[Dunn et al., 2016] Dunn, T. W., Mu, Y., Narayan, S., Randlett, O., Naumann, E. A., Yang, C. T., Schier, A. F., Freeman, J., Engert, F., and Ahrens, M. B. (2016). Brain-wide mapping of neural activity controlling zebrafish exploratory locomotion. *eLife*, 5(MARCH2016):1–29.

[Easter and Nicola, 1997] Easter, S. S. and Nicola, G. N. (1997). The development of eye movements in the zebrafish (Danio rerio). *Developmental psychobiology*, 31(4):267–76.

[Easter and Nicola, 1996] Easter, S. S. J. and Nicola, G. N. (1996). The Development of Vision in the Zebrafish. *Developmental biology*, 180(2):646–663.

[Eder and Bading, 2007] Eder, A. and Bading, H. (2007). Calcium signals can freely cross the nuclear envelope in hippocampal neurons: Somatic calcium increases generate nuclear calcium transients. *BMC Neuroscience*, 8:1–11.

[Fernandes et al., 2021] Fernandes, A. M., Mearns, D. S., Donovan, J. C., Larsch, J., Helmbrecht, T. O., Kölsch, Y., Laurell, E., Kawakami, K., dal Maschio, M., and Baier, H. (2021). Neural circuitry for stimulus selection in the zebrafish visual system. *Neuron*, 109(5):805–822.e6.

[Förster et al., 2020] Förster, D., Helmbrecht, T. O., Mearns, D. S., Jordan, L., Mokayes, N., and Baier, H. (2020). Retinotectal circuitry of larval zebrafish is adapted to detection and pursuit of prey. *eLife*, 9:1–26.

[Friedrich et al., 2010] Friedrich, R. W., Jacobson, G. A., and Zhu, P. (2010). Circuit Neuroscience in Zebrafish. *Current Biology*, 20(8):R371–R381.

[Gabriel et al., 2012] Gabriel, J. P., Trivedi, C. A., Maurer, C. M., Ryu, S., and Bollmann, J. H. (2012). Layer-Specific Targeting of Direction-Selective Neurons in the Zebrafish Optic Tectum. *Neuron*, 76(6):1147–1160.

[Gahtan, 2005] Gahtan, E. (2005). Visual Prey Capture in Larval Zebrafish Is Controlled by Identified Reticulospinal Neurons Downstream of the Tectum. *The Journal of neuroscience : the official journal of the Society for Neuroscience*, 25(40):9294–9303.

[Gori et al., 2014] Gori, S., Agrillo, C., Dadda, M., and Bisazza, A. (2014). Do fish perceive illusory motion? *Scientific Reports*, 4:25–28.

[Grama and Engert, 2012] Grama, A. and Engert, F. (2012). Direction selectivity in the larval zebrafish tectum is mediated by asymmetric inhibition. *Frontiers in Neural Circuits*, 6(SEPTEMBER):1–9.

[Grunwald and Streisinger, 1992] Grunwald, D. J. and Streisinger, G. (1992). Induction of mutations in the zebrafish with ultraviolet light. *Genetical research*, 59(2):93–101.

[Grzywacz and Merwine, 2003] Grzywacz, N. and Merwine, D. (2003). Neural basis of motion perception. *Encyclopedia of Cognitive Science*.

[Hamilton, 1822] Hamilton, F. (1822). *An account of the fishes found in the river Ganges and its branches.* Printed for A. Constable and company;, Edinburgh :.

[Hardingham et al., 2001] Hardingham, G. E., Arnold, F. J., and Bading, H. (2001). Nuclear calcium signaling controls CREB-mediated gene expression triggered by synaptic activity. *Nature Neuroscience*, 4(3):261–267.

[Harper and Lawrence, 2010] Harper, C. and Lawrence, C. (2010). *The Laboratory Zebrafish*. CRC Press.

[Hendrickson and White, 1964] Hendrickson, A. E. and White, P. O. (1964). Promax: a quick method for rotation to oblique simple structure. *British Journal of Statistical Psychology*, 17(1):65–70.

[Henriques et al., 2019] Henriques, P. M., Rahman, N., Jackson, S. E., and Bianco, I. H. (2019). Nucleus Isthmi Is Required to Sustain Target Pursuit during Visually Guided Prey-Catching. *Current Biology*, 29(11):1771–1786.e5.

[Howe et al., 2013] Howe, K., Clark, M. D., Torroja, C. F., Torrance, J., Berthelot, C., Muffato, M., Collins, J. E., Humphray, S., McLaren, K., Matthews, L., McLaren, S., Sealy, I., Caccamo, M., Churcher, C., Scott, C., Barrett, J. C., Koch, R., Rauch, G.-J., White, S., Chow, W., Kilian, B., Quintais, L. T., Guerra-Assunção, J. A., Zhou, Y., Gu, Y., Yen, J., Vogel, J.-h., Eyre, T., Redmond, S., Banerjee, R., Chi, J., Fu, B., Langley, E., Maguire, S. F., Laird, G. K., Lloyd, D., Kenyon, E., Donaldson, S., Sehra, H., Almeida-King, J., Loveland, J., Trevanion, S., Jones, M., Quail, M., Willey, D., Hunt, A., Burton, J., Sims, S., McLay, K., Plumb, B., Davis, J., Clee, C., Oliver, K., Clark, R., Riddle, C., Elliott, D., Threadgold, G., Harden, G., Ware, D., Begum, S., Mortimore, B., Kerry, G., Heath, P., Phillimore, B., Tracey, A., Corby, N., Dunn, M., Johnson, C., Wood, J., Clark, S., Pelan, S., Griffiths, G., Smith, M., Glithero, R., Howden, P., Barker, N., Lloyd, C., Stevens, C., Harley, J., Holt, K., Panagiotidis, G., Lovell, J., Beasley, H., Henderson, C., Gordon, D., Auger, K., Wright, D., Collins, J., Raisen, C., Dyer, L., Leung, K., Robertson, L., Ambridge, K., Leongamornlert, D., McGuire, S., Gilderthorp, R., Griffiths, C., Manthravadi, D., Nichol, S., Barker, G., Whitehead, S., Kay, M., Brown, J., Murnane, C., Gray, E., Humphries, M., Sycamore, N., Barker, D., Saunders, D., Wallis, J., Babbage, A., Hammond, S., Mashreghi-Mohammadi, M., Barr, L., Martin, S., Wray, P., Ellington, A., Matthews, N., Ellwood, M., Woodmansey, R., Clark, G., Cooper, J. D., Tromans, A., Grafham, D., Skuce, C., Pandian, R., Andrews, R., Harrison, E., Kimberley, A., Garnett, J., Fosker, N., Hall, R., Garner, P., Kelly, D., Bird, C., Palmer, S., Gehring, I., Berger, A., Dooley, C. M., Ersan-Ürün, Z., Eser, C., Geiger, H., Geisler, M., Karotki, L., Kirn, A., Konantz, J., Konantz, M., Oberländer, M., Rudolph-Geiger, S., Teucke, M., Lanz, C., Raddatz, G., Osoegawa, K., Zhu, B., Rapp, A., Widaa, S., Langford, C., Yang, F., Schuster, S. C., Carter, N. P., Harrow, J., Ning, Z., Herrero, J., Searle, S. M. J., Enright, A., Geisler, R., Plasterk, R. H. A., Lee, C., Westerfield, M., de Jong, P. J., Zon, L. I., Postlethwait, J. H., Nüsslein-Volhard, C., Hubbard, T. J. P., Crollius, H. R., Rogers, J., and Stemple, D. L. (2013). The zebrafish reference genome sequence and its relationship to the human genome. *Nature*, 496(7446):498–503.

[Huang and Neuhauss, 2008] Huang, Y.-Y. and Neuhauss, S. C. F. (2008). The optokinetic response in zebrafish and its applications. *Frontiers in bioscience : a journal and virtual library*, 13:1899–916.

[Hunter et al., 2013] Hunter, P. R., Lowe, A. S., Thompson, I. D., and Meyer, M. P. (2013). Emergent Properties of the Optic Tectum Revealed by Population Analysis of Direction and Orientation Selectivity. *Journal of Neuroscience*, 33(35):13940–13945.

[Intaitė et al., 2019] Intaitė, M., Georgescu, A. L., Noreika, V., von Saldern, M. A., Vogeley, K., and Falter-Wagner, C. M. (2019). Adults with autism spectrum condition have

atypical perception of ambiguous figures when bottom-up and top-down interactions are incongruous. *Autism*, 23(5):1133–1142.

[Jouary, 2015] Jouary, A. (2015). *Visually induced and spontaneous behavior in the zebrafish larva.* PhD thesis, Université Pierre et Marie Curie - Paris VI.

[Kanda et al., 1998] Kanda, T., Sullivan, K. F., and Wahl, G. M. (1998). Histone–GFP fusion protein enables sensitive analysis of chromosome dynamics in living mammalian cells. *Current Biology*, 8(7):377–385.

[Karlsson et al., 2001] Karlsson, J., Von Hofsten, J., and Olsson, P. E. (2001). Generating transparent zebrafish: A refined method to improve detection of gene expression during embryonic development. *Marine Biotechnology*, 3(6):522–527.

[Kawashima et al., 2016] Kawashima, T., Zwart, M. F., Yang, C.-T., Mensh, B. D., and Ahrens, M. B. (2016). The Serotonergic System Tracks the Outcomes of Actions to Mediate Short-Term Motor Learning. *Cell*, 167(4):933–946.e20.

[Kleiner et al., 2007] Kleiner, M., Brainard, D., Pelli, D., Ingling, A., Murray, R., and Broussard, C. (2007). What's new in psychtoolbox-3. *Perception*, 36(14).

[Kondo and Kochiyama, 2018] Kondo, H. M. and Kochiyama, T. (2018). Normal Aging Slows Spontaneous Switching in Auditory and Visual Bistability. *Neuroscience*, 389:152–160.

[Kramer et al., 2019] Kramer, A., Wu, Y., Baier, H., and Kubo, F. (2019). Neuronal Architecture of a Visual Center that Processes Optic Flow. *Neuron*, 103(1):118–132.e7.

[Krekelberg and Albright, 2005] Krekelberg, B. and Albright, T. D. (2005). Motion mechanisms in macaque MT. *Journal of Neurophysiology*, 93(5):2908–2921.

[Kubo et al., 2014] Kubo, F., Hablitzel, B., Dal Maschio, M., Driever, W., Baier, H., and Arrenberg, A. B. (2014). Functional architecture of an optic flow-responsive area that drives horizontal eye movements in zebrafish. *Neuron*, 81(6):1344–59.

[Lecourtier and Kelly, 2005] Lecourtier, L. and Kelly, P. H. (2005). Bilateral lesions of the habenula induce attentional disturbances in rats. *Neuropsychopharmacology*, 30(3):484–496.

[Leopold and Logothetis, 1996] Leopold, D. A. and Logothetis, N. K. (1996). Activity changes in early visual cortex reflect monkeys' percepts during binocular rivalry. *Nature*, 379(6565):549–553.

[Lin and Schnitzer, 2016] Lin, M. Z. and Schnitzer, M. J. (2016). Genetically encoded indicators of neuronal activity. *Nature neuroscience*, 19(9):1142–53.

[Lister et al., 1999] Lister, J. A., Robertson, C. P., Lepage, T., Johnson, S. L., and Raible, D. W. (1999). Nacre Encodes a Zebrafish Microphthalmia-Related Protein That Regulates Neural-Crest-Derived Pigment Cell Fate. *Development*, 126(17):3757–3767.

[Lopes et al., 2015] Lopes, G., Bonacchi, N., Frazao, J., Neto, J. P., Atallah, B. V., Soares, S., Moreira, L., Matias, S., Itskov, P. M., Correia, P. A., Medina, R. E., Calcaterra, L., Dreosti, E., Paton, J. J., and Kampff, A. R. (2015). Bonsai: an event-based framework for processing and controlling data streams. *Frontiers in Neuroinformatics*, 9.

[Lovett-Barron et al., 2017] Lovett-Barron, M., Andalman, A. S., Allen, W. E., Vesuna, S., Kauvar, I., Burns, V. M., and Deisseroth, K. (2017). Ancestral Circuits for the Coordinated Modulation of Brain State. *Cell*, 171(6):1411–1423.e17.

[Martínez and Parra, 2018] Martínez, G. A. R. and Parra, H. C. (2018). Bistable perception: Neural bases and usefulness in psychological research. *International Journal of Psychological Research*, 11(2):63–76.

[Matsuda et al., 2021] Matsuda, K., Kubo, F., and Bene, F. D. (2021). Circuit Organization Underlying Optic Flow Processing in Zebrafish. *Frontiers in Neural Circuits*, 15(July):1–8.

[Mishkin et al., 1983] Mishkin, M., Ungerleider, L., and Macko, K. (1983). Object vision and spatial vision - Two cortical pathways.

[Miura et al., 2006] Miura, K., Matsuura, K., Taki, M., Tabata, H., Inaba, N., Kawano, K., and Miles, F. A. (2006). The visual motion detectors underlying ocular following responses in monkeys. *Vision research*, 46(6-7):869–78.

[Moreno-Bote et al., 2007] Moreno-Bote, R., Rinzel, J., and Rubin, N. (2007). Noise-induced alternations in an attractor network model of perceptual bistability. *Journal of neurophysiology*, 98(3):1125–39.

[Naumann et al., 2016] Naumann, E. A., Fitzgerald, J. E., Dunn, T. W., Rihel, J., Sompolinsky, H., and Engert, F. (2016). From Whole-Brain Data to Functional Circuit Models: The Zebrafish Optomotor Response. *Cell*, 167(4):947–960.e20.

[Neuhauss et al., 1999] Neuhauss, S. C., Biehlmaier, O., Seeliger, M. W., Das, T., Kohler, K., Harris, W. A., and Baier, H. (1999). Genetic disorders of vision revealed by a behavioral screen of 400 essential loci in zebrafish. *The Journal of neuroscience : the official journal of the Society for Neuroscience*, 19(19):8603–15.

[Nikolaou et al., 2012] Nikolaou, N., Lowe, A. S., Walker, A. S., Abbas, F., Hunter, P. R., Thompson, I. D., and Meyer, M. P. (2012). Parametric Functional Maps of Visual Inputs to the Tectum. *Neuron*, 76(2):317–324.

[Nishida et al., 1997] Nishida, S., Ledgeway, T., and Edwards, M. (1997). Dual multiple-scale processing for motion in the human visual System. *Vision Research*, 37(19):2685–2698.

[Orger and Baier, 2005] Orger, M. B. and Baier, H. (2005). Channeling of red and green cone inputs to the zebrafish optomotor response. *Visual Neuroscience*, 22(3):275–281.

[Orger et al., 2000] Orger, M. B., Smear, M. C., Anstis, S. M., and Baier, H. (2000). Perception of Fourier and non-Fourier motion by larval zebrafish. *Nature neuroscience*, 3(11):1128–33.

[Palagina et al., 2017] Palagina, G., Meyer, J. F., and Smirnakis, S. M. (2017). Complex visual motion representation in mouse area V1. *Journal of Neuroscience*, 37(1):164–183.

[Panier et al., 2013] Panier, T., Romano, S. A., Olive, R., Pietri, T., Sumbre, G., Candelier, R., and Debregeas, G. (2013). Fast functional imaging of multiple brain regions in intact zebrafish larvae using Selective Plane Illumination Microscopy. *Frontiers in Neural Circuits*, 7(April):1–11.

[Papathomas and Rosenthal, 1996] Papathomas, T. and Rosenthal, A. (1996). Unified computational model for Fourier and non-Fourier motion. *Proceedings of the IEEE 22nd Annual Northeast Bioengineering Conference*, pages 44–45.

[Parichy, 2015] Parichy, D. M. (2015). Advancing biology through a deeper understanding of zebrafish ecology and evolution. *eLife*, 4:1–11.

[Pérez-Schuster et al., 2016] Pérez-Schuster, V., Kulkarni, A., Nouvian, M., Romano, S. A., Lygdas, K., Jouary, A., Dippopa, M., Pietri, T., Haudrechy, M., Candat, V., Boulanger-Weill, J., Hakim, V., and Sumbre, G. (2016). Sustained Rhythmic Brain Activity Underlies Visual Motion Perception in Zebrafish. *Cell Reports*, 17(4):1098–1112.

[Peyrache et al., 2010] Peyrache, A., Benchenane, K., Khamassi, M., Wiener, S. I., and Battaglia, F. P. (2010). Principal component analysis of ensemble recordings reveals cell assemblies at high temporal resolution. *Journal of Computational Neuroscience*, 29(1-2):309–325.

[Pologruto et al., 2003] Pologruto, T. A., Sabatini, B. L., and Svoboda, K. (2003). ScanImage: Flexible software for operating laser scanning microscopes. *BioMedical Engineering OnLine*, 2(1):13.

[Polonsky et al., 2000] Polonsky, A., Blake, R., Braun, J., and Heeger, D. J. (2000). Neuronal activity in human primary visual cortex correlates with perception during binocular rivalry. *Nature Neuroscience*, 3(11):1153–1159.

[Portugues and Engert, 2009] Portugues, R. and Engert, F. (2009). The neural basis of visual behaviors in the larval zebrafish. *Current opinion in neurobiology*, 19(6):644–7.

[Preuss et al., 2014] Preuss, S. J., Trivedi, C. A., Vom Berg-Maurer, C. M., Ryu, S., and Bollmann, J. H. (2014). Classification of object size in retinotectal microcircuits. *Current Biology*, 24(20):2376–2385.

[Privat et al., 2019] Privat, M., Romano, S. A., Pietri, T., Jouary, A., Boulanger-Weill, J., Elbaz, N., Duchemin, A., Soares, D., and Sumbre, G. (2019). Sensorimotor Transformations in the Zebrafish Auditory System. *Current Biology*, 29(23):4010–4023.e4.

[Qian et al., 2005] Qian, H., Zhu, Y., Ramsey, D. J., Chappell, R. L., Dowling, J. E., and Ripps, H. (2005). Directional Asymmetries in the Optokinetic Response of Larval Zebrafish (Danio rerio). *Zebrafish*, 2(3):189–196.

[Ramirez and Aksay, 2020] Ramirez, A. D. and Aksay, E. R. (2020). Ramp-to-Threshold Dynamics in a Hindbrain Population Controls the Timing of Spontaneous Saccades. *bioRxiv*.

[Randlett et al., 2015] Randlett, O., Wee, C. L., Naumann, E. A., Nnaemeka, O., Schoppik, D., Fitzgerald, J. E., Portugues, R., Lacoste, A. M., Riegler, C., Engert, F., and Schier, A. F. (2015). Whole-brain activity mapping onto a zebrafish brain atlas. *Nature Methods*, 12(11):1039–1046.

[Rinner et al., 2005] Rinner, O., Rick, J. M., and Neuhauss, S. C. (2005). Contrast sensitivity, spatial and temporal tuning of the larval zebrafish optokinetic response. *Investigative Ophthalmology and Visual Science*, 46(1):137–142.

[Rizzo et al., 2008] Rizzo, M., Nawrot, M., Sparks, J., and Dawson, J. (2008). First and second-order motion perception after focal human brain lesions. *Vision Research*, 48(26):2682–2688.

[Robles et al., 2013] Robles, E., Filosa, A., and Baier, H. (2013). Precise lamination of retinal axons generates multiple parallel input pathways in the tectum. *Journal of Neuroscience*, 33(11):5027–5039.

[Robles et al., 2014] Robles, E., Laurell, E., and Baier, H. (2014). The retinal projectome reveals brain-area-specific visual representations generated by ganglion cell diversity. *Current Biology*, 24(18):2085–2096.

[Roeser and Baier, 2003] Roeser, T. and Baier, H. (2003). Visuomotor behaviors in larval zebrafish after GFP-guided laser ablation of the optic tectum. *The Journal of neuroscience : the official journal of the Society for Neuroscience*, 23(9):3726–34.

[Romano et al., 2017] Romano, S. A., Pérez-Schuster, V., Jouary, A., Boulanger-Weill, J., Candeo, A., Pietri, T., and Sumbre, G. (2017). An integrated calcium imaging processing toolbox for the analysis of neuronal population dynamics. *PLoS computational biology*, 13(6):e1005526.

[Romano et al., 2015] Romano, S. A., Pietri, T., Pérez-Schuster, V., Jouary, A., Haudrechy, M., and Sumbre, G. (2015). Spontaneous neuronal network dynamics reveal circuit's functional adaptations for behavior. *Neuron*, 85(5):1070–1085.

[Scocchia et al., 2014] Scocchia, L., Valsecchi, M., and Triesch, J. (2014). Top-down influences on ambiguous perception: the role of stable and transient states of the observer. *Frontiers in human neuroscience*, 8(December):979.

[Semmelhack et al., 2014] Semmelhack, J. L., Donovan, J. C., Thiele, T. R., Kuehn, E., Laurell, E., and Baier, H. (2014). A dedicated visual pathway for prey detection in larval zebrafish. *eLife*, 3:1–19.

[Shapiro and Todorovic, 2017] Shapiro, A. G. and Todorovic, D. (2017). *The Oxford Compendium of Visual Illusions*, volume 1. Oxford University Press.

[Sheliga et al., 2005] Sheliga, B. M., Chen, K. J., FitzGibbon, E. J., and Miles, F. A. (2005). Initial ocular following in humans: A response to first-order motion energy. *Vision Research*, 45(25-26):3307–3321.

[Shemesh et al., 2020] Shemesh, O. A., Linghu, C., Piatkevich, K. D., Goodwin, D., Celiker, O. T., Gritton, H. J., Romano, M. F., Gao, R., Yu, C.-C. J., Tseng, H.-A., Bensussen, S., Narayan, S., Yang, C.-T., Freifeld, L., Siciliano, C. A., Gupta, I., Wang, J., Pak, N., Yoon, Y.-G., Ullmann, J. F., Guner-Ataman, B., Noamany, H., Sheinkopf, Z. R., Park, W. M., Asano, S., Keating, A. E., Trimmer, J. S., Reimer, J., Tolias, A. S., Bear, M. F., Tye, K. M., Han, X., Ahrens, M. B., and Boyden, E. S. (2020). Precision Calcium Imaging of Dense Neural Populations via a Cell-Body-Targeted Calcium Indicator. *Neuron*, 107(3):470–486.e11.

[Simons and Chabris, 1999] Simons, D. J. and Chabris, C. F. (1999). Gorillas in Our Midst: Sustained Inattentional Blindness for Dynamic Events. *Perception*, 28(9):1059–1074.

[Sterzer et al., 2009] Sterzer, P., Kleinschmidt, A., and Rees, G. (2009). The neural bases of multistable perception. *Trends in Cognitive Sciences*, 13(7):310–318.

[Streisinger et al., 1981] Streisinger, G., Walker, C., Dower, N., Knauber, D., and Singer, F. (1981). Production of clones of homozygous diploid zebra fish (Brachydanio rerio). *Nature*, 291(5813):293–6.

[Stuermer et al., 1990] Stuermer, C. A., Rohrer, B., and Münz, H. (1990). Development of the retinotectal projection in zebrafish embryos under TTX-induced neural-impulse blockade. *Journal of Neuroscience*, 10(11):3615–3626.

[Sugita et al., 2012] Sugita, Y., Miura, K., and Kawano, K. (2012). Principal Fourier component of motion stimulus dominates the initial optokinetic response in mice. *Neuroscience Research*, 73(2):133–141.

[Theobald et al., 2008] Theobald, J. C., Duistermars, B. J., Ringach, D. L., and Frye, M. A. (2008). Flies see second-order motion. *Current Biology*, 18(11):R464–R465.

[Thiele and Bellgrove, 2018] Thiele, A. and Bellgrove, M. A. (2018). Neuromodulation of Attention. *Neuron*, 97(4):769–785.

[Thompson et al., 2016] Thompson, A., Vanwalleghem, G., Heap, L., and Scott, E. (2016). Functional Profiles of Visual-, Auditory-, and Water Flow-Responsive Neurons in the Zebrafish Tectum. *Current Biology*, 26(6):743–754.

[Tuthill et al., 2011] Tuthill, J. C., Chiappe, M. E., and Reiser, M. B. (2011). Neural correlates of illusory motion perception in Drosophila. *Proceedings of the National Academy of Sciences of the United States of America*, 108(23):9685–9690.

[Vaina and Soloviev, 2004] Vaina, L. M. and Soloviev, S. (2004). First-order and second-order motion: neurological evidence for neuroanatomically distinct systems. *Progress in brain research*, 144:197–212.

[Van Loon et al., 2013] Van Loon, A. M., Knapen, T., Scholte, H. S., St. John-Saaltink, E., Donner, T. H., and Lamme, V. A. F. (2013). GABA shapes the dynamics of bistable perception. *Current Biology*, 23(9):823–827.

[Wade, 2018] Wade, N. (2018). The age of illusions. *Psychologist*, 31(2):54–59.

[Wang et al., 2019] Wang, K., Hinz, J., Haikala, V., Reiff, D. F., and Arrenberg, A. B. (2019). Selective processing of all rotational and translational optic flow directions in the zebrafish pretectum and tectum. *BMC Biology*, 17(1):1–18.

[Wang et al., 2020] Wang, K., Hinz, J., Zhang, Y., Thiele, T. R., and Arrenberg, A. B. (2020). Parallel Channels for Motion Feature Extraction in the Pretectum and Tectum of Larval Zebrafish. *Cell Reports*, 30(2):442–453.e6.

[Wasmuht et al., 2019] Wasmuht, D. F., Parker, A. J., and Krug, K. (2019). Interneuronal correlations at longer time scales predict decision signals for bistable structure-from-motion perception. *Scientific Reports*, 9(1):1–15.

[Wu et al., 2020] Wu, Y., dal Maschio, M., Kubo, F., and Baier, H. (2020). An Optical Illusion Pinpoints an Essential Circuit Node for Global Motion Processing. *Neuron*.

[Wullimann et al., 1996] Wullimann, M. F., Rupp, B., and Reichert, H. (1996). *Neuroanatomy of the Zebrafish Brain*. Birkhäuser Basel, Basel.

[Yáñez et al., 2018] Yáñez, J., Suárez, T., Quelle, A., Folgueira, M., and Anadón, R. (2018). Neural connections of the pretectum in zebrafish (Danio rerio). *Journal of Comparative Neurology*, 526(6):1017–1040.

[Ye et al., 2019] Ye, X., Zhu, R. L., Zhou, X. Q., He, S., and Wang, K. (2019). Slower and less variable binocular rivalry rates in patients with bipolar disorder, OCD, major depression, and schizophrenia. *Frontiers in Neuroscience*, 13(MAY):1–11.

[Yildizoglu et al., 2020] Yildizoglu, T., Riegler, C., Fitzgerald, J. E., and Portugues, R. (2020). A Neural Representation of Naturalistic Motion-Guided Behavior in the Zebrafish Brain. *Current Biology*, 30(12):2321–2333.e6.

[Yonehara and Roska, 2014] Yonehara, K. and Roska, B. (2014). Neuroscience: Retinal projectome reveals organizing principles of the visual system. *Current Biology*, 24(18):R833–R835.

[Zhou et al., 2020] Zhou, M., Bear, J., Roberts, P. A., Janiak, F. K., Semmelhack, J., Yoshimatsu, T., and Baden, T. (2020). Zebrafish Retinal Ganglion Cells Asymmetrically Encode Spectral and Temporal Information across Visual Space. *Current Biology*, 30(15):2927–2942.e7.